# TUNABLE FEMTOSECOND LASERS WITH LOW PUMP THRESHOLDS

Karen Oppo

A Thesis Submitted for the Degree of PhD
at the
University of St Andrews

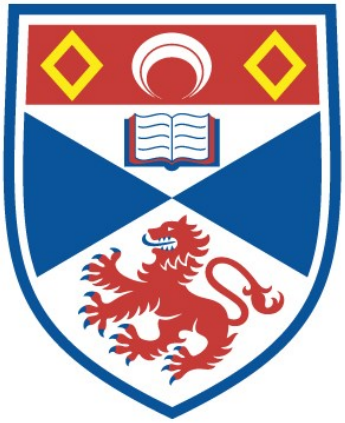

1996

# Tunable Femtosecond Lasers With Low Pump Thresholds.

Thesis submitted for the degree of Doctor of Philosophy

to the University of St. Andrews

by

Karen Oppo, B.Sc.

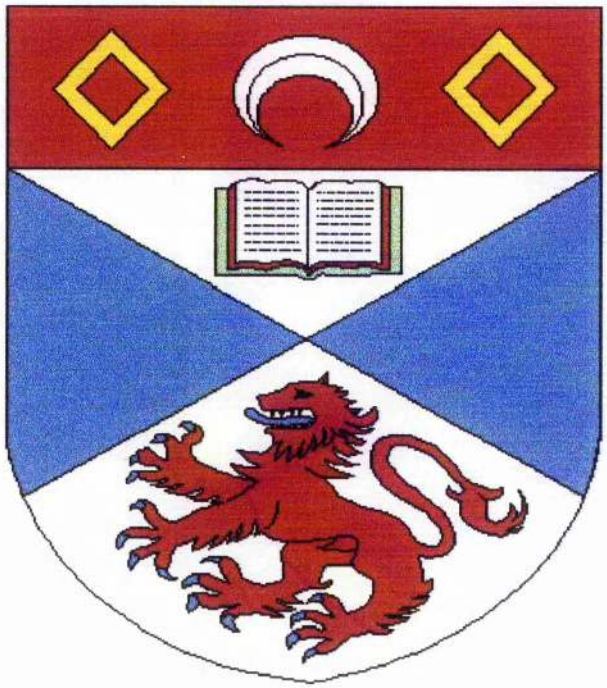

J. F. Allen Physics Research Laboratories
Department of Physics and Astronomy
University of St. Andrews
North Haugh
St. Andrews, Fife
Scotland. KY16 9SS.

April 1996

TL B1000

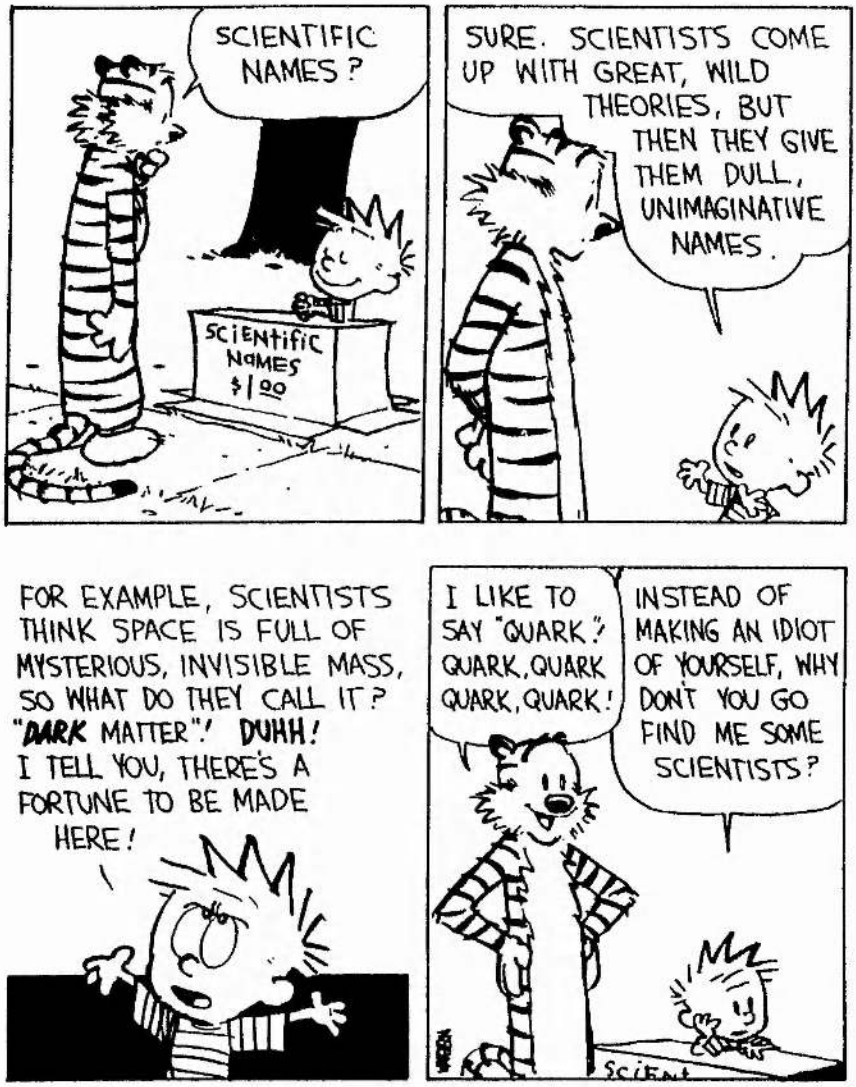
SCIENTIFIC NAMES?
SCIENTIFIC NAMES $1.00
SURE. SCIENTISTS COME UP WITH GREAT, WILD THEORIES, BUT THEN THEY GIVE THEM DULL, UNIMAGINATIVE NAMES.
FOR EXAMPLE, SCIENTISTS THINK SPACE IS FULL OF MYSTERIOUS, INVISIBLE MASS, SO WHAT DO THEY CALL IT? "DARK MATTER"! DUHH! I TELL YOU, THERE'S A FORTUNE TO BE MADE HERE!
I LIKE TO SAY "QUARK"! QUARK, QUARK QUARK, QUARK!
INSTEAD OF MAKING AN IDIOT OF YOURSELF, WHY DON'T YOU GO FIND ME SOME SCIENTISTS?

Dedicated to

my mother

## Declaration.

I, Karen Oppo, hereby certify that this thesis has been composed by myself, that it is a record of my own work, and that it has not been accepted in partial or complete fulfilment of any other degree or professional qualification.

I was admitted to the Faculty of Science of the University of St. Andrews as a candidate for the Degree of Doctor of Philosophy under the ordinance general no.12 on 1st October, 1992.

Signed

Date 15.4.96

## Copyright.

## Certificate.

I hereby certify that the candidate has fulfilled the conditions of the Resolution and Regulations appropriate to the degree of Doctor of Philosophy.

Signature of Supervisor Date 15-04-96

# Abstract.

The work in this thesis is concerned with the development of tunable, femtosecond laser systems, exhibiting low pump threshold powers. The main motive for this work was the development of a low threshold, self-modelocked Ti:$Al_2O_3$ laser in order to replace the conventional large-frame argon-ion pump laser with a more compact and efficient all-solid-state alternative. Results are also presented for an all-solid-state, self-modelocked Cr:LiSAF laser, however most of this work is concerned with self-modelocked Ti:$Al_2O_3$ laser systems.

In chapter 2, the operation of a regeneratively-initiated, and a hard-aperture self-modelocked Ti:$Al_2O_3$ laser, pumped by an argon-ion laser, is discussed. Continuous-wave oscillation thresholds as low as 160mW have been demonstrated, along with self-modelocked threshold powers as low as 500mW.

The measurement and suppression of phase noise on modelocked lasers is discussed in chapter 3. This is followed by a comparison of the phase noise characteristics of the regeneratively-initiated, and hard-aperture self-modelocked Ti:$Al_2O_3$ lasers. The use of a synchronously-operating, high resolution electron-optical streak camera in the evaluation of timing jitter is also presented.

In chapter 4, the construction and self-modelocked operation of an all-solid-state Ti:$Al_2O_3$ laser is described. The all-solid-state alternative to the conventional argon-ion pump laser was a continuous-wave, intracavity-frequency doubled, diode-laser pumped Nd:YLF ring laser. At a total diode-laser pump power of 10W, this minilaser was capable of producing a single frequency output of ~1W, at 523.5nm in a $TEM_{00}$ beam.

The remainder of this thesis looks at the operation of a self-modelocked Ti:$Al_2O_3$ laser generating ultrashort pulses at wavelengths as long as 1053nm. The motive for this work was the development of an all-solid-state, self-modelocked Ti:$Al_2O_3$ laser operating at 1053nm, for use as a master oscillator in a Nd:glass power chain.

# Contents.

## Chapter 3 Measurement and Reduction of Phase Noise on Self-Modelocked Lasers



## Chapter 4 An All-Solid-State, Self-Modelocked Ti:$Al_2O_3$ Laser

# Chapter 1: Introduction.

## 1.1 Broadband tunable solid-state lasers and the production of ultrashort pulses: an overview.

The development of tunable solid-state lasers began over 30 years ago. In 1963, the first broadly tunable "vibronic" transition metal ion laser, a nickel-doped magnesium fluoride laser[1] was reported by Johnson at Bell Labs. However, the discovery of Nd:YAG in 1964[2] and the popularity of dye lasers[3,4] and colour-centre lasers[5] diverted attention away from tunable transition-metal lasers. In the mid 70's, the first femtosecond laser pulses (~300fs) were generated by dye lasers[6,7]. However, these lasers were relatively unstable and difficult to use. Fortunately, in the early 80's there were two important advances in the generation of stable femtosecond pulses. Firstly, a novel passive modelocking technique termed colliding-pulse modelocking (CPM) was invented[8] which produced the first sub-100fs pulses from a dye laser in 1981. The second advance occurred in 1983 when it was shown that the group-velocity dispersion (GVD) inside the laser could be continuously adjusted and optimised by inserting a prism sequence into the laser cavity[9]. However, although pulse durations as short as ~20fs have been reported from a CPM dispersion-compensated rhodamine 6G dye laser[10] its lack of tunability was a serious drawback.

The unreliabilty and narrow tuning range of dye lasers led to a renewed interest in tunable solid-state lasers producing the first demonstration of the alexandrite ($Cr:BeAl_2O_4$) laser in 1979[11] and of the Ti:sapphire ($Ti:Al_2O_3$) laser by Moulton in 1982[12]. During the 1980's a series of broad-bandwidth solid-state laser materials were developed. These new laser materials renewed interest in ultrashort pulse generation since their broad fluorescence emission could potentially support light pulses of a few femtoseonds in duration. Figure 1.1 shows the fluorescence emission spectra for a variety of transition-metal doped laser crystals covering the spectral region from 600-

1600nm. The corresponding laser properties of these crystals are also listed below in Table 1.1.

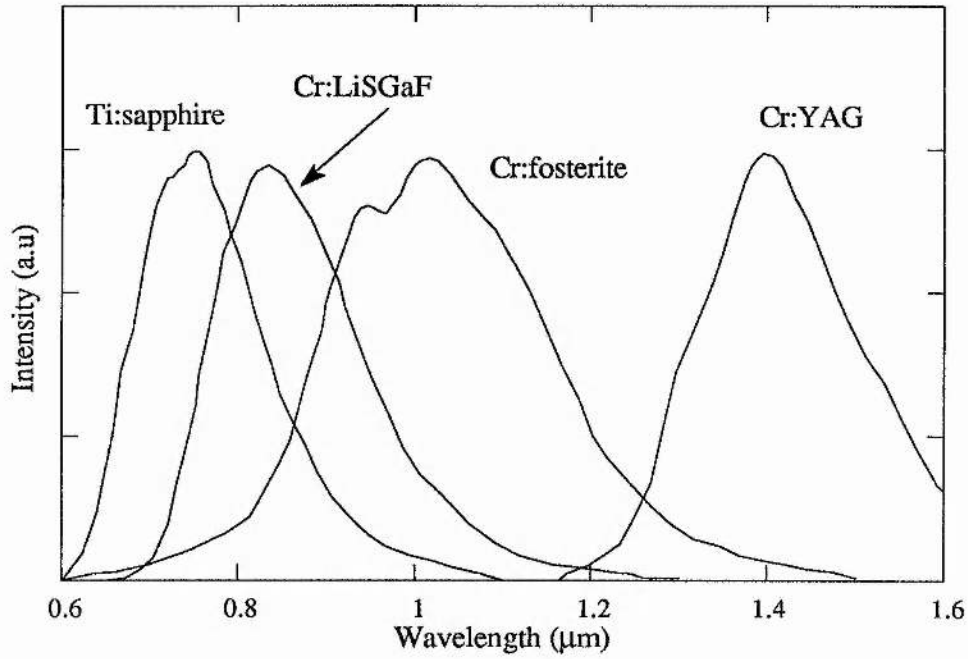


Figure 1.1: Fluorescence emission spectra for a selection of transition metal- doped solid-state laser materials.

| Laser Material | Pump Band $\lambda$ (μm) | Emission Cross-section $\sigma$ (10-19 $cm^2$) | Upper-state lifetime $\tau$ (μs) |
|---|---|---|---|
| Ti:sapphire | 0.45 - 0.60 | 3.8 | 3.2 |
| Cr: LiSGaF | 0.60 - 0.70 | 0.33 | 88 |
| Cr:fosterite | 0.85 - 1.20 | 1.1 | 15 |
| Cr:YAG | 0.88 - 1.10 | 8 | 4 |

Table 1.1:Spectroscopic data for transition metal-doped broadly tunable solid-state laser materials.

The most important of these new transition-metal doped materials was seen to be titanium-doped sapphire. Titanium-doped sapphire is an attractive alternative to organic dyes as an argon-ion pumped gain medium in the near infra-red. One of the most striking features is its tuning range from 660nm - 1180nm, giving a bandwidth of over 400nm, which extends well beyond that of any single dye compound and has the potential of producing pulses as short as 4fs. This feature combined with the fact that near-infrared dye lasers often require constant recharging due to the short chemical lifetimes of the dyes, led to the rapid replacement of dye lasers with Ti:sapphire lasers in many applications. It should also be mentioned that a solid-state gain medium is mechanically stable, making it a good candidate for reliable single-frequency laser operation. On the other hand, a dye jet is prone to hydrodynamic instabilities which lead to frequency fluctuations, and the occasional bubble formation can interrupt lasing.

Over the past few years, various modelocking techniques have been used to generate ultrashort pulses from titanium-doped sapphire. Active modelocking techniques such as acousto-optic modulation[13] led to the generation of pulses in the picosecond domain, and passive modelocking techniques using intracavity dye jets[14] and coloured glass filters[15] as saturable absorbers, resonant passive modelocking (RPM)[16], and coupled-cavity (additive-pulse) modelocking[17,18] have been highly successful in producing pulses as short as 10's of femtoseconds. However, the most important modelocking technique was discovered in 1991 by Spence, Kean and Sibbett[19] and was termed "self-modelocking". Here it was found that the nonlinearity of the gain medium itself was capable of generating ultrashort pulses, without the need for any additional intracavity elements. This breakthrough in the production of femtosecond pulses has led to the demonstration of 8fs pulses from a Ti:sapphire laser which are the shortest pulses generated directly from a laser, to date[20-22].

Subsequent to its demonstration in titanium-doped sapphire, self-modelocking has been demonstrated in a variety of solid-state gain materials such as chromium-doped fosterite[23,24], Cr:LiSAF[25-27], Cr:LiSCAF[28], Cr:LiCAF[29], Cr:LiSGaF[30], Nd:glass[31], Nd:YAG[32], Nd:YLF[33] and $Cr^{4+}$:YAG[34].

## 1.2 Modelocking Techniques.

The mode of operation of a laser can be broadly categorised into two main classes. If the laser output has a relatively narrow optical bandwidth, then the laser is described as being line narrowed or single frequency. However, if the laser output consists of a series of periodic pulses, then the laser is described as being pulsed or modelocked, depending on the exact nature of the output. In this case, the oscillating bandwidths can be relatively large. This section briefly describes the process of modelocking together with some of the techniques used to obtain modelocked laser operation.

The emission profile of a laser is governed by two features. These are the overall emission profile, which determines the frequency range over which laser oscillation can occur, and the longitudinal mode spacing of the laser cavity which determines the actual laser frequencies which will oscillate. The emission profile of the laser will encompass all of the longitudinal modes that experience sufficient gain to lie above threshold. For standing-wave laser resonators, the longitudinal mode spacing is given by the expression: $\Delta\upsilon = c / 2nL$ where nL is the optical length of the cavity, and c is the speed of light. Generally the output of a continuous-wave (cw) laser varies randomly and unpredictably due to the random interference between the longitudinal modes oscillating. If on the other hand these modes are forced to maintain equal frequency spacings and fixed phase relationships, then the output of the laser becomes a periodic sequence of pulses and modelocked laser operation has been achieved.

Ever since its discovery in 1964[35-37], the coupling of the longitudinal modes of a laser resonator has been the most widely used technique for ultrashort pulse generation. It is also interesting to note that the first generation of modelocked lasers generating pulses shorter than 100ps were solid state lasers, such as ruby[38,39] and Nd:YAG[40,41]lasers.

### 1.2.1 Active Modelocking Techniques.

In actively-modelocked lasers the mode coupling that produces modelocked performance is achieved by modulating the cavity gain or loss at a frequency equal to the cavity frequency or one of its harmonics. Loss modulation is accomplished by inserting into the laser cavity an actively driven amplitude (or phase) modulator. In an alternative scheme, the laser gain is modulated by pumping with a modelocked laser source whose cavity repetition time is matched to the cavity repetition time of the laser being pumped. This technique is termed synchronous pumping. These systems are classed as actively-modelocked lasers as the pulse repetition rate is governed by an external frequency source.

In the case of an amplitude modulator, the loss at one point in the cavity is modulated with the same periodicity as the round-trip time of the laser light in the cavity. This is equivalent to introducing an optical shutter into the cavity. Only the light approaching the modulator when its losses are close to their minimum value will see net gain. This in turn leads to the formation of an optical pulse.

In the frequency domain, a cavity resonance oscillating at a frequency $\omega$ will acquire sidebands at frequencies $\omega \pm n\omega_m$ in the presence of an active modulation applied to the resonator. If the applied modulation frequency $\omega_m$ is approximately equal to the resonator frequency, each induced sideband will coincide with one of the other axial modes of the cavity. Each sideband will tend to injection lock with the axial mode it is in resonance with and thus the axial modes will couple together to form a modelocked output.

In 1970 Kuizenga and Siegmann[42] analysed active modelocking in the time domain to form a general analysis for active modelocked operation in homogeneously broadened lasers. In their calculations they assumed a gaussian pulse shape. This pulse was propagated through one round trip of a laser cavity containing an active gain medium and a loss modulator. A self-consistent solution for the pulse characteristics was then sought, one which displayed no net change in one complete round trip of the cavity to the

pulse envelope. This effect models a pulse circulating in an optical cavity once a steady state has been obtained. The results of this analysis included an equation for the expected pulse intensity FWHM from an actively amplitude modulated laser system:

$$\tau_p = \left(\frac{2\sqrt{2}\ln 2}{\pi^2}\right)^{\frac{1}{2}}\left(\frac{g}{\Delta_m}\right)^{\frac{1}{4}}\left(\frac{1}{f_m f_a}\right)^{\frac{1}{2}} \qquad [1.1]$$

where g is the round-trip saturated gain, $\Delta_m$ is the modulation depth, $f_m$ is the modelocked frequency and $f_a$ is the laser bandwidth. It should be noted that the most effective way to shorten the pulse duration is to increase the modulation frequency or the laser bandwidth. The modulation depth will vary with the power applied to the modulator, for an acousto-optic modulator. The pulse duration will therefore decrease, but not very rapidly, with increasing applied modulation power.

In active modelocking, the pulse shaping is produced by an externally driven modulator. The modulator response speed is limited by the drive electronics and is independent on the pulse duration. Also, the pulse repetition frequency is governed by the applied modulation frequency. In contrast, passive modelocking produces much shorter pulses than active modelocking because the peak intensity and saturable absorber action increases as the pulse is shortened. Also, the pulse repetition frequency is only dependent on the round-trip time of the laser cavity. Passive modelocking has been shown to be a powerful technique for femtosecond pulse generation in both dye lasers and solid-state lasers. A combination of both active and passive modelocking is termed hybrid modelocking. A synchronously modelocked dye laser is one example of such a system. In this case the pulse repetition rate is still determined by the active modulation, but the influence of the weak saturable absorber assists with the pulse shaping.

### 1.2.2 Passive Modelocking Techniques.

The technique of passive modelocking provides an alternative approach to the generation of ultrashort pulses. Passive modelocking can result when an element which is a purely passive saturable absorber (i.e, one where the absorption is constant at low optical intensities but decreases (bleaches) at high optical intensities) is placed in the laser resonator. In these systems, the modulation is produced by the modelocked pulses themselves, meaning that it is always synchronised to the circulating radiation and can become stronger as the pulses become shorter. Passive modelocking is usually achieved with the use of organic dyes as the saturable absorber. When the pumping is first turned on, the population inversion increases until the gain exceeds the total saturable and non-saturable losses and laser oscillation builds up from noise. The most intense noise spike will grow to an intensity where it begins to saturate the loss in the saturable absorber. As a result this noise spike then experiences less loss per round trip than the rest of the noise and it can thus grow in preference to the rest of the signal. Under the proper conditions, a single pulse can be selected and the resulting laser output is in the form of a periodic sequence of pulses. Satrurable absorbers can be classed into two types: slow saturable absorbers and fast saturable absorbers.

A slow saturable absorber is a lossy element placed inside the laser cavity which has a long relaxation time compared to the laser pulse duration. The slow saturable absorber absorbs ("eats into') the leading edge of the pulse and assuming the pulse has sufficient energy, the medium becomes bleached part way through the pulse, and the trailing edge is transmitted more or less unchanged. Through time, this leads to pulse asymmetry and a mechanism is therefore needed to attenuate the trailing edge ie: gain saturation of the laser medium. In a laser cavity configuration containing a slow saturable absorber medium, pulse formation is due to the following mechanism which is illustrated schematically in figure 1.2.

Initially the total cavity losses (saturable losses and linear cavity losses) are greater than the saturable gain. When propagating through the saturable absorber

medium, the low intensity leading edge of the pulse is absorbed, experiencing a net loss and is therefore clipped. At the peak of the pulse, the intensity is high enough to bleach the absorber and the losses are driven down below the saturable gain leading to amplification of the peak. If the pulse is of sufficiently high intensity, the gain also becomes saturated and the trailing edge of the pulse also experiences a net loss and is clipped.

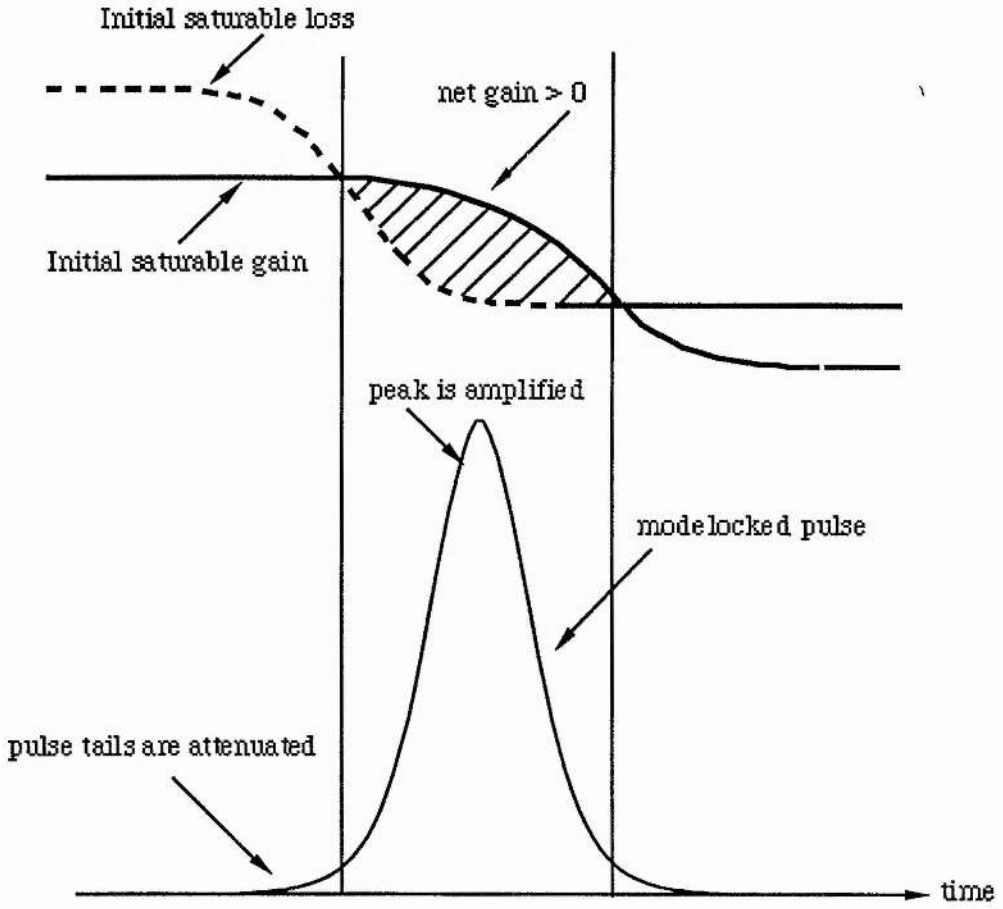


Figure 1.2: Single pass gain and slow saturable absorber saturation in a cw modelocked laser.

To achieve modelocked operation using a slow saturable absorber, certain conditions have to be satisfied. Firstly, the absorber recovery time must be less than the recovery time of the gain medium. Secondly, the recovery time of the gain medium must be comparable with, or not much longer, than the round trip time of the laser cavity so that gain saturation can occur during the passage of a single pulse. To obtain steady-state

modelocking, both the saturable absorption and gain must recover back up to their initial values during the round-trip period of the cavity. These requirements mean that slow saturable absorbers are best used with laser gain media that readily saturate (e.g organic dyes[43] and colour centre crystals[44]).

Most saturable absorbers used to date have been organic dyes which use resonant excitation and an excited state population to produce absorption saturation. The recovery time of the absorber is governed by the relaxation time of the excited state population. Modelocking is therefore only plausible at wavelengths where both the absorber and gain are resonant. However, solid state lasers such as Ti:sapphire, Nd:YAG and Nd:YLF have extremely small gain cross-sections and long gain relaxation times. Thus slow saturable absorber modelocking is difficult in such lasers. Saturable absorber dyes have been used to modelock some solid state systems[45], but their use has been limited by their high insertion loss, by their relative slowness (absorber relaxation times of the order of 1ps) and by the tendency of systems with a long upper-state lifetime to relaxation oscillate rather than modelock. Semiconductor saturable absorbers have been used with success in colour centre lasers[46,47] and resonant passively modelocked (RPM) lasers[48], but pulse shaping still depends upon absorber recovery. For a review of the theory of slow-saturable absorber modelocking see references [49,50,51].

In a fast saturable absorber, the recovery time of the absorber is shorter than the pulse duration. Pulse shortening occurs because the stronger central part of the pulse partially bleaches ("burns through") the saturable absorber and is transmitted with less absorption, whereas the weaker leading and trailing edges of the pulse are preferentially absorbed. However, this pulse-width reduction only occurs over a limited range of input intensities. If the input pulse intensity is too weak, there is no absorption saturation and hence no pulse shortening. Conversely, if the input intensity is too high then the entire pulse burns through the absorber and again there is no pulse shortening.

The following mechanism is responsible for modelocking in a fast saturable absorber and is illustrated in figure 1.3.

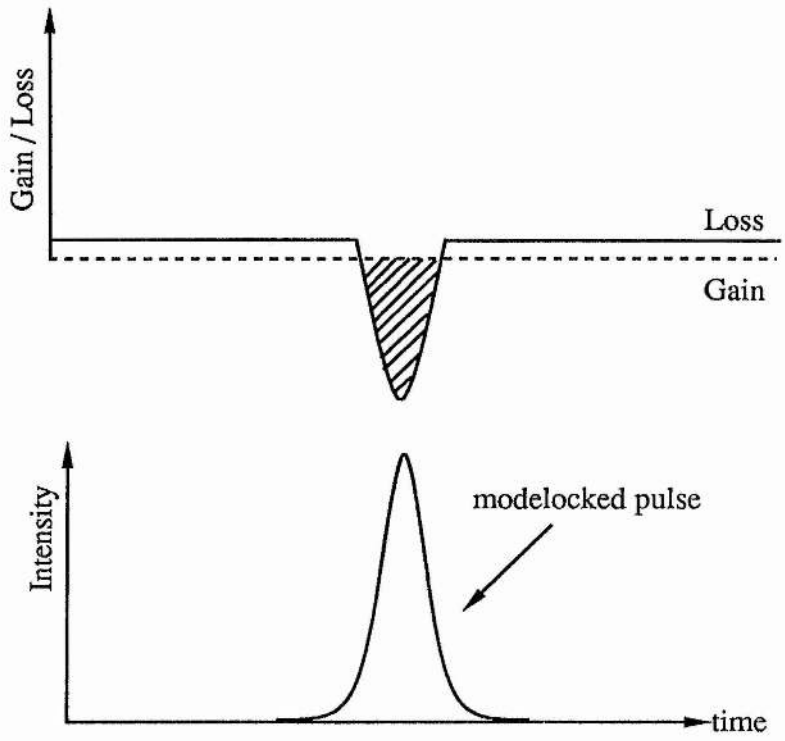


Figure 1.3: Pulse-shaping loss dynamics for fast saturable absorber modelocking.

The leading edge of the pulse is of low intensity, and therefore is unable to saturate the absorber and experiences net loss. The peak of the pulse is of high intensity, leading to saturation of the absorber and therefore experiences no loss. Since the lifetime of the absorber is shorter than the pulse duration, the absorber has recovered before the trailing edge reaches it. Like the leading edge, the trailing edge of the pulse is also of low intensity, and is therefore unable to saturate the absorber and also experiences a loss. All the pulse shaping is carried out in the absorber, therefore there is no requirement for any additional pulse shaping from the gain medium. This means that fast saturable absorbers are best used with gain media that do not saturate.

Passive modelocking in cw lasers, therefore depends on a delicate interplay between certain laser parameters, such as the pulse energy, the gain and absorber recovery times and their saturation energies. For successful passive modelocking the laser must be capable of self-starting from noise or initial fluctuations when the laser is

switched on, and must also be able to sustain pules which are stable against slow, large scale relaxation oscillations.

More recently, an artifical fast saturable absorber modelocking technique was discovered during the development of the soliton laser[52], which led to the development of additive pulse modelocking[53] ( also known as coupled-cavity modelocking) in colour centre lasers[54,55,56]. Subsequent studies extended this modelocking techniques to other solid-state gain media such as Ti:Sapphire[57,58], Nd:YAG[59,60], Nd:YLF[61] and Nd:glass[62]. Additive pulse modelocking (APM) is induced by feeding back into the laser cavity, part of its output after it has been nonlinearly modulated in an external cavity. This pulse shortening mechanism was first proposed by Ouellette and Piche[63] and a comprehensive theory of modelocking based on this principle has been published by Ippen *et al.*[53]. Furthermore, since the APM technique relies on the Kerr effect in an external nonlinear element, this technique has an extremely fast response time and broadband operation is possible over a wide range of wavelengths. Hence unlike saturable absorber dyes and multiple quantum well devices, APM permits the generation of wavelength tunable ultrashort pulses.

Another artifical fast saturable absorber modelocking technique was first demonstrated in 1991 by Spence, Kean and Sibbett[19] and was termed "self-modelocking" (also known as "Kerr-lens modelocking). Self-modelocking has now become the most widely used technique for the production of ultrashort pulses in solid-state gain media.

### 1.2.3 Self Modelocking.

We now understand that self modelocking can be induced in solid-state lasers through the Kerr nonlinearity present in the gain media. It has been known for some time that intense laser beams are subject to self-focussing when they propagate through optical media that have a nonlinear refractive index. Typically in Ti:$Al_2O_3$ lasers the cavity mode is focussed to a beam waist of the order of a few tens of microns in the gain medium. The resulting high intensities mean that for the shortest pulses, spatial nonlinear effects such as self-focussing can become significant. This Kerr self-focussing effect leads to an intensity dependent change in the spatial profile of the oscillating cavity mode. By introducing an intracavity aperture, these spatial effects can be used to create a power dependent loss, in the form of amplitude modulation. This happens because the nonlinear medium acts as an intensity dependent lens producing a smaller beam waist for higher intensities. If an aperture is placed at a suitable location within the laser cavity, where the beam size decreases with increasing intensity, it will have a higher transmission for a high intensity beam than for a low intensity beam. Thus the cavity losses are intensity dependent and the system sees a higher gain with increasing intensity. For properly designed laser cavities, this passive amplitude modulation mechanism favours modelocked operation over cw laser oscillation. Because modelocked operation is induced by the presence of the gain medium itself, the laser is said to "self-modelock" and the presence of amplitude modulation by self-focussing simulates an ultrafast saturable absorber action. Modelocking be self-focussing was first realised when the cavity mode was apertured by the spatial gain profile[19], and subsequently by a hard-aperture placed inside the laser cavity[64,65].

Due to the relatively long gain length and high intracavity powers present in modelocked Ti:$Al_2O_3$ laser systems, there is considerable self-phase modulation (SPM) present. Also, the physical length of the gain medium implies a relatively high amount of normal dispersion since this laser operates at wavelengths in the sub-1μm spectral region. It can therefore be expected that the interaction of SPM and group velocity dispersion

(GVD) will have a considerable influence on the duration and shape of the modelocked pulses. Thus, to generate ultrashort pulses from a laser system, interactions between processes such as gain, GVD, SPM, amplitude modulation, linear loss and phase shift must be carefully balanced.

Unlike slow saturable absorber action, self-modelocking did not spontaneously start from the cw regime in a linear cavity but required an external initiating action. In the first experiments[19] simultaneous oscillation of two transverse modes (eg. $TEM_{00}$ and TEM05) provided appropriate longitudinal mode coupling and efficiently initiated modelocking. Self-modelocking was also initiated by inducing a small but rapid change in the cavity length (mirror tapping)[19,66]. This had the effect of inducing a sufficiently short intensity fluctuation in the cavity so that modelocked operation could build up. Further alternatives are active modelocking[67] regenerative modelocking[68-70], moving mirror[71-74], semiconductor-saturable absorber[75] or dye-saturable absorber modelocking[76,77]. Recently, self-starting of a self-modelocked Ti:sapphire laser was achieved with a unidirectional ring cavity[78], and a linear cavity containing a second folding section containing a highly nonlinear material[79]. Until now it was believed that self-modelocking of Ti:sapphire lasers with a basic linear cavity could not start without a suitable initiating device because the initial pulse shortening force is too weak to initiate self-modelocking from mode-beating or noise.

Recently it has been shown that self-modelocked lasers, with no intracavity elements, except the laser rod and dispersion compensating prisms can be designed to be completely self-starting[80]. For a literature review of the theory of self-modelocking (Kerr-lens-modelocking) see references[81-88].

## 1.3 Pulse Propagation Through Optical Materials.

In this section the effects of dispersion and nonlinearity on the propagation of ultrashort pulses will be described briefly. The concept of dispersion is introduced and a scheme which can be used to provide variable group-velocity dispersion will also be described. Pulse propagation in nonlinear media is outlined and the effects of self-phase modulation and self-focussing are discussed.

### 1.3.1 Linear Pulse Propagation.

In optical materials, the response of the crystal field is dependent on the frequency of the electric field of the light travelling through it. This effect is seen as a frequency dependence on the refractive index of the material. This dependence can be calculated for a given material using the Sellmeier equation:

$$n^2(\lambda) = 1 + \frac{B_1\lambda^2}{\lambda^2 - C_1} + \frac{B_2\lambda^2}{\lambda^2 - C_2} + \frac{B_3\lambda^2}{\lambda^2 - C_3} \quad [1.2]$$

where $B_{1,2,3}$ and $C_{1,2,3}$ are Sellmeier constants derived from experimental data. Equations of this form are valid over a range of wavelengths dependent on the optical material it describes. Dispersion therefore arises from the fact that the speed of light varies with wavelength. When both n and $dn/d\lambda$ decrease with increasing wavelength then this is described as normal dispersion. In normally dispersive media, blue light travels more slowly and refracts more strongly than red light.

In a dispersive medium, each indiviual frequency component within a pulse travels at a unique phase velocity given by $c/n(\lambda)$. Pulse broadening occurs as faster components extend the leading edge of the pulse envelope and slower components retard the trailing edge of the pulse envelope. The instantaneous velocity of the pulse envelope is called the group velocity of the pulse. The pulse envelope will therefore propagate

with a group velocity $v_g$, while the individual optical cycles within the pulse propagate at the phase velocity $v_\phi$. Group velocity dispersion (GVD) in optical systems is often responsible for broadening pulses to durations greater than the transform-limit by introducing a linear phase change or chirp across the pulse.

By assuming that the material has a frequency dependent propagation constant $\beta(\omega)$ and expanding as a Taylor series gives the expression:

$$\beta(\omega) = n(\omega)\frac{\omega}{c} = \beta(\omega_0) + \beta'(\omega-\omega_0) + \frac{1}{2}\beta''(\omega-\omega_0)^2 + \frac{1}{3!}\beta'''(\omega-\omega_0)^3 + \ldots \quad [1.3]$$

The group velocity of the pulse envelope is given by the expression:

$$\beta' = \frac{d\beta}{d\omega} = \frac{1}{c}\left[n + \omega\frac{dn}{d\omega}\right] = \frac{n_g}{c} = \frac{1}{v_g} \quad [1.4]$$

The dispersion parameter $\beta''$ (group velocity dispersion parameter) which is responsible for pulse broadening, can be related to the material dispersion by:

$$\beta'' = \frac{d^2\beta}{d\omega^2} = \frac{d}{d\omega}\frac{1}{v_g} = \frac{4\pi^2 c}{\omega^3}\frac{d^2n}{d\lambda^2} = \frac{\lambda^3}{2\pi c^2}\frac{d^2n}{d\lambda^2} \quad [1.5]$$

If $\beta''$ is zero then an optical pulse will propagate indefinitely without changing its temporal envelope. For many optical glasses $\beta''=0$ at ~1.3μm which is referred to as the "zero dispersion wavelength". When generating ultrashort pulses in the order of 10's of femtoseconds, third order dispersion can be significant and therefore has to be compensated for. The third order dispersion of a material is given by the expression:

$$\beta''' = \frac{-\lambda^4}{4\pi^2 c^3}\left(3\frac{d^2n}{d\lambda^2} + \lambda\frac{d^3n}{d\lambda^3}\right) \quad [1.6]$$

In solid-state modelocked lasers such as Ti:sapphire, the gain medium itself contributes the greatest positive dispersion in the laser cavity. Other intracavity elements

such as acousto-optic modulators and prisms also contribute positive dispersion. To obtain the shortest possible pulses from a laser then the overall cavity group velocity dispersion must be close to zero. A practical method for providing adjustable GVD is a suitably positioned prism sequence as illustrated below. The use of a prism sequence to produce negative dispersion was first described by Fork *et al* [89] and is illustrated below in figure 1.4.

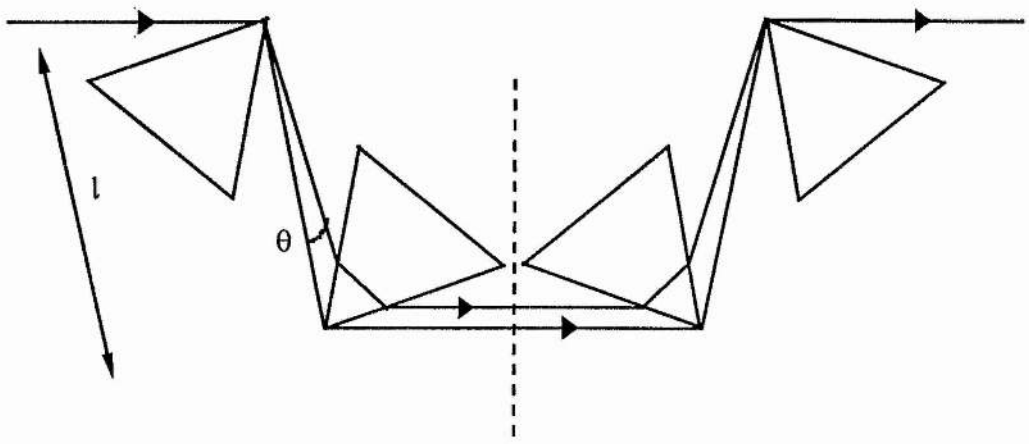


Figure 1.4: Prism sequence used to control group velocity dispersion.

A prism sequence provides a way of introducing group velocity dispersion that is low loss and is both adjustable through both positive and negative values. It can be shown for a single pass of the four prism sequence that:

$$\frac{d^2P}{d\lambda^2} = 4l\left\{\left[\frac{d^2n}{d\lambda^2} + \left(2n - \frac{1}{n^3}\right)\left(\frac{dn}{d\lambda}\right)^2\right]\sin\theta - 2\left(\frac{dn}{d\lambda}\right)^2\cos\theta\right\} \quad [1.7]$$

where P is the optical path length and $l$ is the prism separation.

For most laser configurations, $\theta$ is the order of the angular deviation of the ray bundle so $\cos\theta$ may be approximated to unity and the quantity $l\sin\theta$ is comparable to the beam spot size~2mm, where $l$ is the prism separation.

For overall zero group velocity dispersion, the sum of the dispersion introduced by each individual cavity element, must be zero:

$$\sum \frac{d^2P}{d\lambda^2} = 0 \qquad [1.8]$$

The prism sequence will therefore have a net negative GVD for sufficiently large values of $l$, provided that $d^2n/d\lambda^2$ is not excessively large compared to $(dn/d\lambda)^2$. An arrangement with a negative dispersion equivalent to that for a four-prism sequence can be obtained by using only two prisms and placing a plane mirror at the symmetry plane of the above arrangement.

The third-order dispersion in the cavity can be compensated for by calculating the prism separation $l$ from the expression:

$$\frac{d^3P}{d\lambda^3} \cong 4l\left(\frac{d^3n}{d\lambda^3}\sin\theta - 6\frac{dn}{d\lambda}\frac{d^2n}{d\lambda^2}\cos\theta\right) \qquad [1.9]$$

Besides the gain medium, and an optical intracavity aperture, standard femtosecond self-modelocked resonators contain a pair of prisms for producing net negative group velocity dispersion. While some form of group-velocity dispersion control is necessary for femtosecond modelocking, the prism pair itself also appeared to set a limit to the pulse shortening in sub-100fs systems. Only the use of particular selected prisms allowed the production of sub-20fs pulses in Ti:sapphire lasers[90,91]. An alternative method for controlling group velocity dispersion, without the need of introducing intracavity glass, is by using chirped dielectric mirrors as the source of broadband negative GVD[92,93]. For a literature review of dispersion compensation, and the effects of group velocity dispersion on the output pulse duration of a laser, see references 94-99.

### 1.3.2 Nonlinear Pulse Propagation.

For an optical pulse passing through a nonlinear optical material, such as a laser gain medium like Ti:sapphire, there will be a refractive index change Δn, which is the result of the optical Kerr effect:

$$\Delta n = n_2 I(t) \qquad [1.10]$$

where I(t) is the pulse temporal intensity profile and $n_2$ is the nonlinear refractive index of the material. This change in refractive index leads to a time-dependent phase delay Δϕ(t), which is also dependent on the intensity profile of the pulse:

$$\Delta\varphi(t) = kL\Delta n(t) = \frac{2\pi L}{\lambda} n_2 I(t) \qquad [1.11]$$

where L is the length of material.

This phase delay then results in an instantaneous frequency chirp:

$$\Delta\omega = -\frac{d}{dt}(\Delta\varphi(t)) = -\frac{2\pi L n_2}{\lambda}\frac{dI(t)}{dt} \qquad [1.12]$$

Hence the nonlinear refractive index of the material results in self-phase modulation of the pulse. The increasing index of refraction of the material on the rising edge of the pulse delays the individual oscillations of the electric field, "red-shifting" the leading edge. The trailing edge of the pulse correspondingly "blue-shifts". Hence giving rise to a chirped pulse. It is then the dispersion introduced by an intracavity prism sequence that compensates for the dispersion of the gain medium, and for the chirp introduced by self-phase modulation within the laser gain medium.

This intensity dependent refractive index change also leads to an effect called "self-focussing". Self-focussing is a spatial effect that operates on the transverse profile of a propagating beam. The central portion of the beam will have a higher intensity and therefore experience a larger refractive index then the low intensity edges of the beam. This variation in refractive index across the beam leads to a change in speed of propagation of different parts of the beam. This produces a distortion of the propagating

wavefront which acts as a positive lens, and the beam passing through the nonlinear medium appears to 'self-focus'.

## 1.4 Ultrashort Pulse Measurement.

With the development of passively modelocked lasers, the direct combination of a photodiode and oscilloscope is no longer adequate to temporally resolve the ultrashort pulses generated. The fastest optical detectors have response times ~$10^{-11}$s and so they are unable to measure pulse durations shorter than a few tens of picoseconds. There are two important methods for determining the duration of pulses shorter than ~$10^{-11}$s. Electron-optical streak cameras can be used to measure pulses having durations in the picosecond regime while autocorelation techniques can be used to measure sub-picosecond pulse durations.

### 1.4.1 The Second Harmonic Generation Autocorrelator.

The pulse measurement technique most commonly used today is second-harmonic generation autocorrelation which was first demonstrated in 1966[100]. This technique allows the conversion of the difficult problem of measuring time scales on the order of 100's of femtoseconds into the much easier task of measuring lengths on the order of microns which is now easily measured by high resolution micrometers available today. For example 100fs is the equivalent of an optical path length of 30μm. The experimental arrangement of the real-time autocorrelator used for the work carried out in this project is illustrated schematically in figure 1.5.

The input pulse passes through a Michelson-type delay arrangement and the output of the interferometer if focussed tightly into a second-harmonic generation (SHG) crystal. The pulses from each arm of the Michelson interferometer are spatially collinear and temporally overlapped. The filters prevent unwanted background fundamental light and

ambient lighting saturating the detector, which in this case is a photomultiplier tube. Pulses in one arm of the interferometer has a temporal delay $\tau$ relative to the other arm. The optical delay in the interferometer is varied by translating one of the retroreflectors about a point of coincidence.

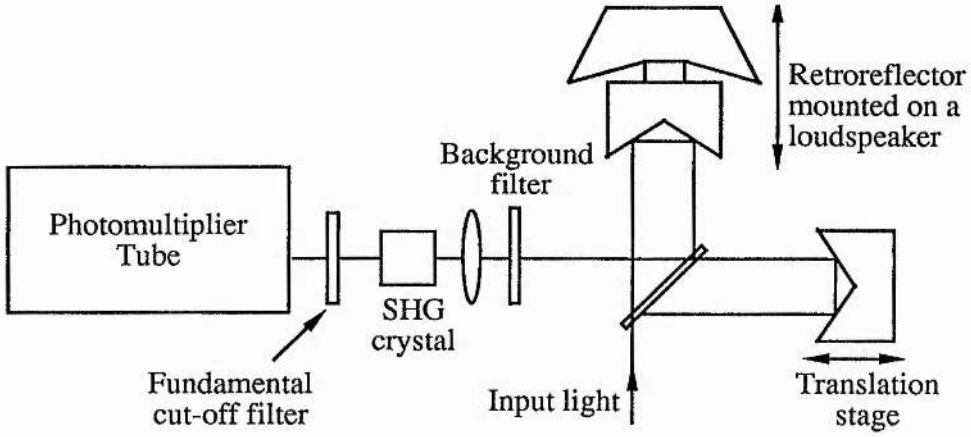


Figure 1.5: Schematic diagram of the second-harmonic generation, real-time autocorrelator.

Real-time monitoring of the autocorrelation function is easily accomplished by mounting one of the retroreflectors on an audio loudspeaker which is made to scan at ~ 20Hz. The second harmonic light generated in the nonlinear crystal is detected by the photomultiplier tube and the resultant electrical signal is integrated over a period which is long compared to the pulse duration. The average power of the second harmonic light of the recombined beam is therefore recorded as a function of the variable delay, and changing the delay of one of the arms of the interferometer varies the degree of overlap of the pulses and hence the amount of second harmonic light generated. The second harmonic signal produced will consist of a background intensity level, due to the separate signals from each arm, plus an enhanced signal where the pulses are overlapped. This enhanced signal, as a function of the relative delay between the two arms of the interferometer, represents the intensity autocorrelation of the pulse.

For collinear autocorrelation, the second-order intensity autocorrelation function is given by the equation:

$$G_2(\tau) = 1 + 2\frac{\int_{-\infty}^{+\infty} I(t)\, I(t-\tau)\, dt}{\int_{-\infty}^{+\infty} |I(t)|^2 dt} \qquad [1.13]$$

where I(t) is the intensity distribution of the pulse and $\tau$ is the time delay. The duration of the pulse $\Delta\tau_p$, is obtained by measuring the full-width half-maximum (FWHM) duration of the autocorrelation function $\Delta t$ and dividing it by a constant k, which depends on the assumed pulseshape

$$\Delta\tau = \frac{\Delta t}{k} \qquad [1.14]$$

The validity of this assumed pulseshape can be verified by measuring the bandwidth of the pulse spectrum and comparing the duration-bandwidth product with the calculated value for the chosen pulse profile. This comparison is only valid for pulses free from any frequency-chirp. Values for the Fourier transform-limited duration-bandwidth product $\Delta\tau_p\Delta\upsilon$ and the constant k for some common pulse shapes are shown in Table 1.2 below.

| Pulse profile | I(t) | $\Delta\tau_p\Delta\upsilon$ | k |
|---|---|---|---|
| $sech^2$ | $sech^2(t/T)$ | 0.315 | 1.543 |
| Gaussian | $\exp(-t^2/T^2)$ | 0.441 | 1.414 |

Table 1.2: Duration-bandwidth products and k factor for some common pulse shapes.

However, the second-order intensity autocorrelation is a symmetric function and cannot provide information on the actual pulseshape. When performed with interferometric accuracy, second-harmonic autocorrelations provide a much more contrasted pattern; the envelope of the constructive interference has a peak to background ratio of 8:1 (3:1 for

intensity autocorrelations). Because the intensity of the second harmonic field is measured, the fourth power of the electric field amplitude is used meaning that interferometric autocorrelations are very sensitive to the exact pulse shape. Unlike intensity autocorrelations where all the phase information is averaged out, various types of chirp produce distinctive patterns in interferometric autocorrelations.

In this case the second-order interferometric autocorrelation function is given by the equation:

$$g_2(\tau) = \frac{\int_{-\infty}^{+\infty} \left| \{E(t)\exp i\omega t + E(t-\tau)\exp i\omega(t-\tau)\} \right|^2 dt}{2^4 \int_{-\infty}^{+\infty} E^4(t)\, dt} \qquad [1.15]$$

Since interferometric autocorrelations resolve individual optical cycles, it is highly sensitive to frequency chirp. For self-phase modulation induced chirp, the frequency sweep is largest over the central part of the pulse and this is evident by a narrowing of the upper and lower envelopes of the interferometric autocorrelation. Any linear chirp causes a loss of coherence between the leading and trailing edge of the pulse leading to a reduction in the visiblity of the interference fringes since the wings of the pulse cannot fully interfere. If the peak wavelength of the pulse is known, then interferometric autocorrelations can be self-calibrating since the fringe separation is one optical cycle. For example, at a wavelength of 800nm the optical period is 2.7 fs. In common with the intensity autocorrelation the pulse duration is determined by dividing the FWHM of the autocorrelation profile by a correction factor specific to a given pulse profile. For a $sech^2$ pulse, the correction factor k = 1.897.

### 1.4.2 The Electron-optical Streak Camera.

Electron-optical streak cameras can be used to measure the duration of laser pulses on a picosecond timescale. A streak image tube basically consists of the photocathode, the mesh electrode, focussing electrodes, deflection electrodes, constant field drift region and a phosphor screen. The Photochron V streak tube which was used for the work desribed in this thesis is illustrated schematically in figure 1.6.

When the camera is in operation, the light signal illuminates the entrance slit and is imaged by a relay lens onto the photocathode. The resulting photo-electrons are then accelerated to 5-10kV by the mesh electrode, and are imaged onto the phosphor screen via the electron-optical lens. Here the photoelectron signal is converted back into an optical signal for recording and analysis.

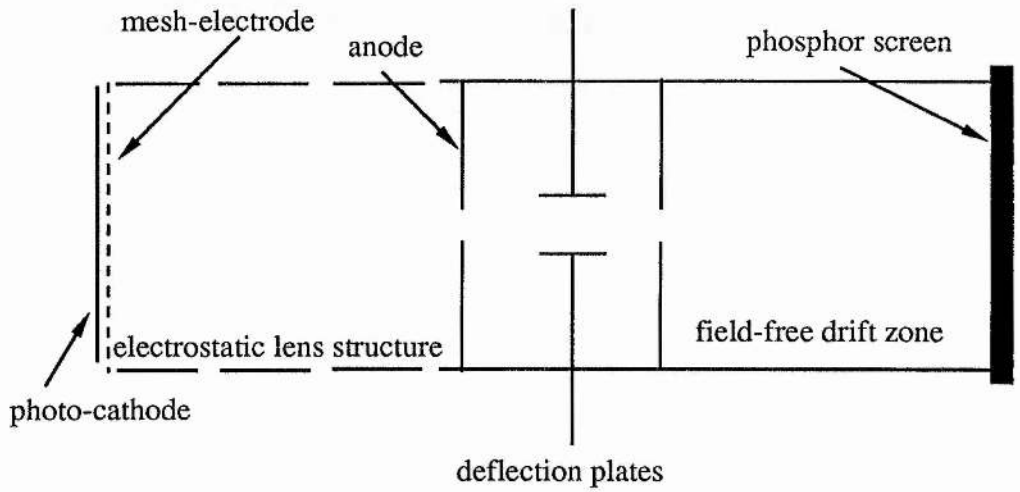


Figure 1.6: Schematic diagram of an electron-optical streak camera.

To resolve the temporal information carried by the photoelectrons, a high frequency, sinusoidal voltage signal is applied to the deflection plates synchronously with the pulses of light incident on the photocathode. This means that the electron beam can be "streaked" repetitively across the phosphor screen, providing a record of the pulse intensity as a function of time.

There are two common methods for deriving the deflection signal for the streak camera. One method is to use a tunnel diode circuit which is designed to oscillate for several periods when triggered. Its oscillation frequency is adjusted to be an exact harmonic of the laser output, so that a photodiode can repeatedly trigger the device into operation. Filtering and limiting is then employed to improve the spectral purity of this reference signal. This technique is illustrated schematically below in figure 1.7 for a laser cavity repetition frequency of 86 MHz

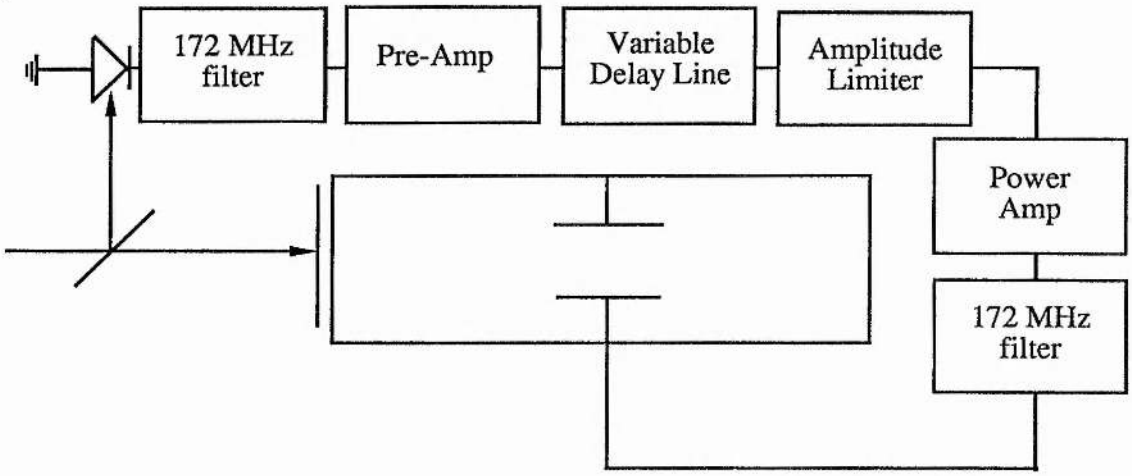


Figure 1.7: Schematic diagram of the passive drive electronics for a synchroscan streak camera.

Another method is to drive the streak camera directly from an ultrastable reference oscillator to which the cavity frequency of the laser is locked. Both of these techniques employ a radio frequency (r.f) resonant circuit to generate large deflection voltages for moderate r.f power levels. When the deflection signal frequency is equal or a multiple of the repetition frequency of the input light signal, and is correctly phased, the streak images are superimposed and become integrated in intensity on the phosphor screen. However, if there is a relatively large variation in the time between the individual light pulses (timing jitter), the synchronisation will be poor. This in turn leads to streak-smearing and severe degradation in the overall temporal resolution of the streak camera.

## 1.5 Conclusions.

This chapter has presented a brief historical introduction to tunable femtosecond lasers and an overview of the most important modelocking techniques in the generation of femtosecond pulse durations. A brief discussion of pulse propagation in both linearly dispersive and nonlinear materials has been given, along with the methods for pulse duration measurements used throughout this work.

This thesis will discuss the operation of tunable, modelocked lasers based on vibronic laser materials covering the near-infra-red wavelength region from 760-1053nm. The emphasis is placed mainly on titanium-doped sapphire, however chapter 5 looks at Cr:LiSAF as a low power alternative to Ti:sapphire.

Chapter 2 begins by describing the construction, operation and performance of argon-ion pumped continuous-wave and self-modelocked Ti:sapphire laser systems. In particular, emphasis is placed on reducing the pump powers required for laser oscillation to levels suitable for pumping with alternative all-solid-state minilasers.

The phase noise characteristics of these self-modelocked Ti:sapphire laser systems are described in chapter 3 along with the results of phase noise reduction techniques. These phase-noise reduction techniques led to the lowest timing jitter figures obtained from an srgon-ion pumped, self-modelocked Ti:sapphire laser. The results of ultrashort pulse measurements using a high resolution streak camera are also described, producing temporal resolutions in the sub-picosecond regime.

In chapter 4, the operation and performance of an all-solid-state, self-modelocked Ti:sapphire laser is described. The pump laser for this system was a diode-laser-pumped, intracavity frequency-doubled, cw Nd:YLF ring laser.

This thesis concludes with a description of a self-modelocked Ti:sapphire laser operating at the upper limit of its spectral bandwidth at 1053nm. Again, emphasis was placed on techniques for the reduction of the pump powers required for laser oscillation. The possibilities of pumping such a system with an all-solid-state minilaser are also discussed.

## 1.6 References.


[1] L.F Johnson, R.E Dietz and H.J Guggenheim "Optical Maser Oscillation from $Ni^{2+}$ in $MgF_2$ involving simultaneous emission of phonons", *Phys. Rev. Lett.*, Vol 11 p.318 (1963).

[2] J.E Geusic, H.M Marcos and L.G Van Uitert "Laser Oscillation in Nd:doped yttrium aluminium, yttrium gallium and gadolinium garnets", *Appl. Phys. Lett.*, Vol.4 p.182 (1964).

[3] P.P Sorokin and J.R Lankard *IBM J. Res .Dev* ., Vol.10 p.162 (1966).

[4] F.P Schafer, F.P.W Schmidth and J. Volze "Organic dye solution laser", *Appl. Phys Lett.*, Vol.9 p.306 (1966).

[5] L.F Mollenauer and J.C White. Eds. *"Tunable Lasers"*, (Topics Appl. Phys.) Vol.59 Berlin, Heidelberg Springer (1987) Chapter 6.

[6] C.V Shank and E.P Ippen "Subpicosecond kilowatt pulses from a modelocked cw dye laser", *Appl. Phys.Lett.*, Vol.24 p.373 (1974).

[7] I.S Ruddock and D.J Bradley "Bandwidth limited subpicosecond pulse generation in modelocked cw dye lasers", *Appl. Phys. Lett.*, Vol.29 p.296 (1976)

[8] R.L Fork, B.I Greene and C.V Shank "Generation of optical pulses shorter than 0.1ps by colliding pulse modelocking", *Appl. Phys Lett.*, Vol.38 p.671 (1981).

[9] R.L Fork, O.E Martinez and J.P Gordon "Negative dispersion using pairs of prisms", *Opt. Lett.*, Vol.9 p.150 (1984).

[10] J.A Valdmanis and R.L Fork and J.P Gordon "Generation of optical pulses as short as 27fs directly from a laser balancing self-phase modulation, group velocity dispersion, saturable absorption and saturable gain" *Opt. Lett.*, Vol.10 p.131 (1985).

[11] J.C Walling, H.P Jenssen, R.C Morris, E.W O'Dell and O.G Peterson "Tunable laser performance in $BeAl_2O_4:Cr^{3+}$" *Opt. Lett.*, Vol.4 p.182 (1979)

[12] P.F Moulton "Spectroscopic and laser characteristics of $Ti:Al_2O_3$" *J. Opt. Soc. Am B.*, Vol.3 p.125 (1986).

[13] J.D Kafka, A.J Alfrey, T. Baer in *Ultrafast Phenomena VI* T. Yajima, K. Yoshihara, C.B Harris and S. Shionaya eds. (Springer-Verlag Berlin 1988). p.64

[14] Y. Ishida, N. Sarukura, H. Nakano in Digest of *Ultrafast Phenomena VII* (Springer-Verlag, Berlin 1990) p.75.

[15] N. Sarukura, Y. Ishida, T. Yanagawa and H. Nakano "All-solid-state cw passively modelocked Ti:sapphire laser using a colored glass filter" *Appl. Phys. Lett.*, Vol.57 p.229 (1990).

[16] U. Keller, W.H Knox and H. Rosko "Coupled cavity resonant passively modelocked Ti:sapphire laser" *Opt. Lett.*, Vol.15 p.1377 (1990).

[17] J. Goodberlet, J. Wang, J.G Fujimoto and P.A Schulz "Femtosecond passively modelocked Ti:sapphire laser with a nonlinear external cavity" *Opt. Lett.*, Vol.14 p.1125 (1989).

[18] D.E Spence and W. Sibbett "Femtosecond pulse generation by a dispersion-compensated, coupled-cavity, modelocked Ti:sapphire laser" *Opt. Lett.*, Vol.8 p.2053 (1991).

[19] D.E Spence, P.N Kean and W. Sibbett "60fs pulse generation from a self-modelocked Ti:sapphire laser" *Opt. Lett.*, Vol.16 p.42 (1991).

[20] F. Krausz, C. Spielmann, P.F Curley, T. Brabec, S.M.J Kelly, A. Stingl, R. Spizocs, E. Wintner and A.J Schmidt "Ultrafast Solid-State Lasers: Status and Prospects" in *Ultrafast Phenomena* Vol.7 of 1994 OSA Technical Digest Series (Optical Society of America, Washington D.C., (1994) paper MA1.

[21] A. Stingl, M. Lenzer, C. Spielmann and F. Krauszand R. Szipocz "Sub-10fs mirror dispersion controlled Ti:sapphire laser" *Opt. Lett.*, Vol.20 p.602 (1995).

[22] J. Zhou, G. Taft, C. Shi, H.C Kapteyn and M. Murnane "Sub-10fs pulse generation in Ti:sapphire: capabilities and limitations" in *Ultrafast Phenomena* Vol.7 of 1994 OSA Technical Digest Series (Optical Society of America, Washington D.C., 1994) paper MA2.

[23] V. Yanovsky Y. Pang, F. Wise and B.I Minkov "Generation of 25fs pulses from a self-modelocked Cr:fosterite laser with optimised group velocity dispersion" *Opt. Lett.*, Vol. 18 p.1541 (1993).

[24] A. Seas, V. Petricevic and R.R Alfano "Self-modelocked chromium-doped fosterite laser generates 50-fs pulses" *Opt. Lett.*, Vol.18 p.891 (1993).

[25] M.J.P Dymott and A.I Ferguson "Self-modelocked diode-pumped Cr:LiSAF laser" *Opt. Lett.*, Vol.19 p.1988 (1994).

[26] M.J.P Dymott and A.I Ferguson "Self-modelocked diode-pumped Cr:LiSAF laser producing 34-fs pulses at 42-mW average power" *Opt. Lett.*, Vol.20 p.1157 (1995).

[27] J.M Evans, D.E Spence, W. Sibbett, B.H.T Chai and A. Miller "50-fs pulse generation from a self-modelocked Cr:LiSrAlF$_6$ laser" *Opt. Lett.*, Vol.17 p.1447 (1992).

[28] H.S Wang, P. LiKamWa, J.L Lefaucheur, B.H.T Chai and A. Miller "CW and self-modelocking performance of a red pumped $Cr^{3+}$:LiSrCaAlF$_6$ laser" *Opt. Commun.*, Vol.110 p.679 (1994).

[29] P. LiKamWa, B.H.T Chai and A. Miller "Self-modelocked $Cr^{3+}$:LiCaAlF$_6$ laser" Opt. Lett., Vol.17 p.1438 (1992).

[30] V.P Yanovsky, F.W Wise, A. Cassanho and H.P Jenssen "Kerr-lens modelocked diode-pumped Cr:LiSGAF laser" *Opt. Lett.*, Vol.20 p.1304 (1995).

[31] U. Keller, T.H Chiu and J.F Ferguson "Self-starting femtosecond modelocked Nd:glass laser that uses intracavity saturable absorbers" *Opt. Lett.*, Vol.18 p.1077 (1993).

[32] K.X Liu C.J Flood, D.R Walker and H.M van Driel "Kerr-lens modelocking of a diode-pumped Nd:YAG laser: *Opt. Lett.*, Vol.17 p. 1361 (1992).

[33] M. Ramaswamy, A.S Gouveianeto, D.K Negus, J.A Izatt and J.G Fujimoto "2.3ps pulses from a Kerr-lens modelocked lamp-pumped Nd:YLF laser with a microdot mirror" Opt. Lett., Vol.18 p.1825 (1993).

[34] A. Sennaroglu, C.R Pollack and H. Nathel "Continuous wave self-modelocked operation of a femtosecond $Cr^{4+}$:YAG laser" *Opt. Lett.*, Vol.19 p.390 (1994).

[35] L.E Hargrove, R.L Fork and M.A Pollack "Locking of He-Ne laser modes induced by synchronous intracavity modulation" *Appl. Phys. Lett.*, Vol.5 p.4 (1964).

[36] M. DiDomenico "Small-signal analysis of internal modulation laser" *J. Appl. Phys.*, Vol.35 p.2870 (1964).

[37] A. Yariv "Internal modulation multimode laser oscillators" *J. Appl. Phys.*, Vol.36 p.388 (1965).

[38] T. Deutsch "Modelocking effects in an internally modulated ruby laser" *Appl. Phys. Lett.*, Vol.7 p.80 (1965).

[39] H.W Mocker and R.J Collins "Mode competition and self-locking effects in a Q-switched ruby laser" *Appl. Phys. Lett.*, Vol.7 p.270 (1965).

[40] M. DiDomenico, H.M Marcos, J.E Geusic and R.E Smith "Generation of ultrashort optical pulses by modelocking the YAlG:Nd laser" *Appl. Phys. Lett.*, Vol.8 p.180 (1966).

[41] L.M Osterink and J.D Foster "A modelocked Nd:YAG laser" *J. Appl. Phys.*, Vol.39 p.4163 (1968).

[42] D.J Kuizenga and A.E Seigmann FM and AM Modelocking of the homogeneous laser" *IEEE J. Quantum. Electron.*, QE-6 p.709 (1970).

[43] J.A Valdmanis, R.L Fork and J.P Gordon "Generation of optical pulses as short as 27fs directly from a laser balancing self-phase modulation, group velocity disperion, saturable absorption and saturable gain" *Opt. Lett.*, Vol.10 p.131 1985.

[44] N. Langford, R.S Grant, C.I Johnston, K. Smith and W. Sibbett "Group velocity dispersion compensation of a passively modelocked ring $LiF^{2+}$ laser" *Opt. Lett.*, Vol.14 p.45 (1989).

[45] Y. Ishida "Generation of 50fs pulses from a pulse compressed cw passively modelocked Ti:sapphire laser" *Opt. Lett.*, Vol.16 p.153 (1991).

[46] C.L Cesar, M.N Islam C.E Soccolich R.D Feldman R.F Austin and K.R German "Femtosecond KCl and RbCl color-centre lasers near 2.8μm with a multiple quantum well saturable absorber" *Opt. Lett.*, Vol.15 p.1147 (1990).

[47] C.E Soccoloch M.N Islam M.G Young and B.I Miller "Bulk semiconductor saturable absorber for a NaCl color-center laser" *Appl. Phys Lett.*, Vol.56 p. 2177 (1990).

[48] U. Keller, T.K Woodwood D.L Sivco and A.Y Cho "Coupled cavity resonant passively modelocked Nd:YLF laser" *Opt. Lett.*, Vol.16 p.390 (1992).

[49] G.H.C New "Pulse evolution in modelocked quasi-continuous lasers" *IEEE J. Quantum. Electron.*, QE-10 p.115 (1974).

[50] H.A Haus "Theory of modelocking with a slow saturable absorber" *IEEE J. Quantum. Electron.*, QE-11 p.736 (1975).

[51] H.A Haus "Parameter ranges for cw passive modelocking" *IEEE J. Quantum. Electron.*, QE-12 p.169 (1976).

[52] L.F Mollenauer and R.H Stolen "The soliton laser" *Opt. Lett.*, Vol.9 p.15 (1984).

[53] E.P Ippen, H.A Haus and L.Y Liu "Additive pulse modelocking" *J. Opt. Soc. Am. B.*, Vol.6 p.1736 (1989).

[54] C.P Yakymyshyn, J.F Pimto and C.R Pollock "Additive pulse modelocked NaCl:OH laser" *Opt. Lett.*, Vol.14 p.621 (1989).

[55] K.J Blow and D. Wood "Modelocked lasers with nonlinear external cavities" *J. Opt. Soc. Am B.*, Vol.5 p.629 (1988).

[56] K.J Blow and D. Wood "Improved modelocking of an F-center laser with a nonlinear non-soliton external cavity" *Opt. Lett.*, Vol.13 p.1026 (1988).

[57] J. Goodberlet, J. Wang, J.G Fujimoto, P.A Schulz "Femtosecond passively modelocked Ti:sapphire laser with a nonlinear external cavity" *Opt. Lett.*, Vol.14 p.1125 (1989).

[58] D.E Spence and W. Sibbett "Femtosecond pulse generation by a dispersion compensated, coupled cavity modelocked Ti:sapphire laser" *Opt. Lett.*, Vol.8 p.2053 (1991).

[59] J. Goodberlet, J. Jacobson, J.G Fujimoto, P.A Schulz and T.Y Fan "Self-starting additive pulse modelocked diode-pumped Nd:YAG laser" *Opt. Lett.*, Vol.15 p.504 (1990).

[60] L.Y Liu, J.M Huxley, E.P Ippen, H.A Haus "Self-starting additive pulse modelocking of a Nd:YAG laser" *Opt. Lett.*, Vol.15 p.553 (1990).

[61] J.M Liu, J.K. Chee "Passive modelocking of a cw Nd:YLF laser with a nonlinear external coupled cavity" *Opt. Lett.*, Vol.15 p.685 (1990).

[62] F. Krausz, C. Spielmann, T. Brabec, E. Wintner and A.J Schmidt "Sub-ps pulse generation from a Nd:glass laser using a nonlinear external cavity" *Opt. Lett.*, Vol.15 p.737 (1990).

[63] F. Ouellette and M. Piche "Pulse shaping and passive modelocking with a nonlinear external cavity" *Opt. Commun.*, Vol.60 p.99 (1986).

[64] L. Spinelli, B. Couillard, N. Goldblatt and D.K Negus "Starting and generation of sub-100fs pulses in Ti:sapphire by self-foccussing" in Digest of *Conference on Lasers and Electro- Optics* (Optical Society of America, Washington D.C 1991) paper CPDP7.

[65] U. Keller, G.W t'Hooft, W.H Knox and J.E Cunningham "Femtosecond pulses from a continuously self-starting passively-modlocked Ti:sapphire laser" *Opt. Lett.*, Vol.16 p.1022 (1991).

[66] L. Spinelli, B. Couillard, N. Goldblatt and D.K Negus in Digest of Conference on Lasers and Electro-Optics (Optical Society of America, Washington D.C 1991) paper CPDP7.

[67] P.F Curley and A.I Ferguson "Actively modelocked Ti:sapphire laser producing transform-limited pulses of 150fs duration" *Opt. Lett.*, Vol.16 p1016 (1991).

[68] L. Turi and F. Krausz "Amplitude modulation modelocking of lasers by regenerative feedback" *Appl. Phys. Lett.*, Vol.58 p.810 (1991).

[69] D.E Spence, J.M Evans, W.E Sleat and W. Sibbett "Regeneratively-initiated self-modelocked Ti:sapphire laser" *Opt. Lett.*, Vol.16 p.1762 (1991).

[70] J.D Kafka, M.L Watts and JWJ Pieterse "Picosecond and femtosecond pulse generation in a regeneratively modelocked Ti:sapphire laser" *IEEE J. Quantum. Electron.*, QE-28 p.2151 (1992).

[71] N.H Rizvi, PMW French and J.R Taylor "Continuously self-modelocked Ti:sapphire laser that produces sub-50fs pulses" *Opt. Lett.*, Vol.17 p.279 (1992).

[72] Y.M Liu, K.W Sun, P.R Pruncal and S.A Lyon "Simple method to start and maintain self-modelocking of a Ti:sapphire laser" *Opt.Lett.*, Vol 17 p.1219 (1992).

[73] W.S Pelouch, P.E Powers and C.L Tang "Self-starting modelocked ring cavity Ti:sapphire laser" *Opt. Lett.*, Vol.17 p.1581 (1992).

[74] M.H Ober, M. Hofer and M.E Fermann "42fs pulse generation from a modelocked fibre laser started with a moving mirror" *Opt. Lett.*, Vol.18 p.367 (1993).

[75] U. Keller, G.W t'Hooft, W.H Knox and J.E Cunningham "Femtosecond pulses from a continuously self-starting passively modelocked Ti:sapphire laser" *Opt. Lett.*, Vol.16 p.1022 (1991).

[76] S. Chen and J. Wang "Self-starting issues of passive self-focussing modelocking" *Opt. Lett.*, Vol.16 p.1689 (1991).

[77] Y. Pang and F. Wise "Use of saturable absorber dyes for self-starting operation of a self-modelocked Ti:sapphire laser" *Optical and Quantum Electronics.*, Vol.24 p.841 (1992).

[78] K. Tamura, J. Jacobson, E.P Ippen, H.A Haus and J.G Fujimoto "Unidirectional ring resonators for self-starting passively-modelocked lasers" *Opt. Lett.*, Vol.15 p.220 (1993).

[79] C. Radzewicz, G.W Pearson and J.S Krasinski, *Opt. Commun.* Vol.96 p.348 (1993).

[80] G. Cerullo, S. De Silvestri and V. Magni "Self-starting Kerr-lens modelocking of a Ti:sapphire laser" *Opt. Lett* ., Vol.19 p.1040 (1994).

[81] T. Brabec, P.F Curley, C. Spielmann, E. Wintner and A.J Schmidt "Hard-aperture Kerr-lens modelocking" *J. Opt. Soc. Am. B.*, Vol.10 p.1029 (1993).

[82] T. Brabec, C. Spielmann, P.F Curley and F. Krausz "Kerr-lens modelocking" *Opt. Lett.*, Vol.17 p.1292 (1992).

[83] G. Cerullo, S. De Silvestri and V. Magni and L. Pallaro "REsonators for Kerr-lens modelocked femtosecond Ti:sapphire lasers" *Opt. Lett.*, Vol.19 p.807 (1994).

[84] O.E Martinez and JLA Chilla "Self-modelocking of Ti:sapphire lasers: a matrix formalism" *Opt. Lett.*, Vol.17 p.1210 (1992).

[85] D. Huang, M. Ulman, L. Acioli, H.A Haus and J.G Fujimoto "Self-focussing-induced saturable loss for laser modelocking" *Opt. Lett.*, Vol.17 p.511 (1992).

[86] S. Gatz and J. Herrmann "Astigmatism and gain-guiding in Kerr-lens modelocked lasers" *Opt. Lett.*, Vol.20 p.825 (1995).

[87] M. Piche "Beam reshaping and self-modelocking in nonlinear laser resonators" *Opt. Commun.*, Vol.86 p.156 (1991).

[88] F. Salin, J. Squier and M. Piche "Modelocking of Ti:sapphire lasers and self-focussing: a gaussian approximation" *Opt. Lett.*, Vol. 16 p.1674 (1991).

[89] R.L Fork, O.E Martinez and J.P Gordon "Negative dispersion using pairs of prisms" *Opt. Lett.*, Vol.9 p.150 (1984).

[90] C.P Huang, M.T Asaki, S. Backus, M.Munane, H.C Kapteyn and H. Nathel "17fs pulses from a self-modelocked Ti:sapphire laser" *Opt. Lett.*, Vol.17 p.1289 (1992).

[91] C. Spielmann, P.F Curley, T. Brabec, E. Wintner and F. Krausz "Generation of sub-20fs modelocked pulses from a Ti:sapphire laser" *Electron. Lett.*, Vol.28 p.1532 (1992).

[92] A. Stingl, C. Spielmann, F. Krausz and R. Szipocs "Generation of 11fs pulses from a Ti:sapphire laser without the use of prisms" *Opt. Lett.*, Vol.19 p.204 (1994).

[93] R. Szipocs, K. Ferencz, C. Spielmann and F. Krausz "Chirped multilayer caotings for broadband dispersion control in femtosecond lasers" *Opt. Lett.*, Vol.19 p.201 (1994).

[94] J.P Gordon and R.L Fork "Optical resonators with negative dispersion" *Opt. Lett.*, Vol.9 p.153 (1984).

[95] O.E Martinez, R.L Fork and J.P Gordon "Theory of passively modelocked lasers including self-phase modulation and group velocity dispersion" *Opt. Lett.*, Vol.9 p.156 (1984).

[96] H.A Haus, J.D Moores and L.E Nelson "Effect of third-order dispersion on passive modelocking" *Opt. Lett.*, Vol.18 p.51 (1993).

[97] B.E Lemoff and C.P.J Barty "Cubic phase free dispersion compensation in solid-state ultrashort pulse lasers" *Opt. Lett.*, Vol.18 p.57 (1993).

[98] J.M Jacobson, K. Naganuma, H.A Haus J.G Fujimoto and A.G Jacobson "Femtosecond pulse generation in a Ti:$Al_2O_3$ laser by using second and third order intracavity dispersion." *Opt. Lett.*, Vol.17 p.1608 (1992).

[99] B. Proctor and F. Wise "Quartz prism sequence for reduction of cubic phase in a modelocked Ti:sapphire laser" *Opt. Lett.*, Vol.17 p.1295 (1992).

[100] M. Maier, W. Kaiser and J.A Giordmaine *Phys. Rev. Lett.*, Vol.17 p.1275 (1966).

# Chapter 2: The Ti:sapphire Laser.

## 2.1 Introduction.

Since its first demonstration in 1982, the Ti:Sapphire laser has become the most popular source of laser radiation in the near-infrared spectral region. The most attractive feature of this laser gain medium is the continuously tunable nature of its output. Early solid-state lasers such as ruby and Nd:YAG operated on transitions between purely electronic levels which are referred to as zero-phonon transitions, and result in narrow bandwidth laser operation. However in the case of vibronic gain media such as Ti:sapphire, vibrational excitations in the crystal result in the laser transitions occuring in broad vibrational sidebands rather than narrow zero-phonon lines. In these media, a direct coupling between the stimulated emission process and non-radiative phonon emission , allows a smooth variation of the energy associated with these processes. It is this property that produces a continuously tunable laser output.

Ti:sapphire lasers are now replacing previously used dye lasers as a more convenient source of near-infrared radiation. The wide wavelength range of Ti:sapphire spans over 400nm, which is approximately four times larger than any single dye compound. Also the solid-state nature of this laser gain medium makes it a much more "user friendly" alternative to dyes, some of which have been identified as having carcinogenic properties. Ti:sapphire lasers are now being used in many areas of research such as high resolution spectroscopy, ultrashort pulse generation and nonlinear optics. Also, the wavelength coverage of Ti:sapphire has been successfully extended by a variety of harmonic generation, frequency mixing and parametric techniques.

In this chapter, a brief outline of the spectroscopic characteristics of titanium-doped sapphire will be given along with crystal growth techniques and laser resonator design. The construction of a Ti:sapphire laser will be described, and results presented for both continuous-wave and self-modelocked operation of this laser.

## 2.2 Spectroscopy and Growth of Titanium-doped Sapphire.

Titanium is a member of the group of transition metals, and such ions have a general electronic configuration given as $1s^2 2s^2 2p^6 3s^2 3p^6 3d^n$. A titanium ion substituted for an $Al^{3+}$ ion in $Al_2O_3$ may be present in either trivalent $Ti^{3+}$ or quadravalent $Ti^{4+}$ form. The $Ti^{4+}$ ion has a closed shell configuration of argon, making this atom optically inert. However, the $Ti^{3+}$ ion electronic configuration is $1s^2 2s^2 2p^6 3s^2 3p^6 3d^1$ which is a closed shell plus one outer 3d valence electron (i.e a single electron outside an Ar core). This gives the $Ti^{3+}$ ion the simplest energy level structure of all the transition metal ions.

The $Ti^{3+}$ ion is the active ion in titanium-doped sapphire and places the laser in the class of 3d transition metal systems. Alone, the single 3d electron has a five-fold degenerate $^2D$ ground state. When placed in a host crystal such as sapphire, the degeneracy is lifted by interactions with other nearby electrons in the host crystal lattice.

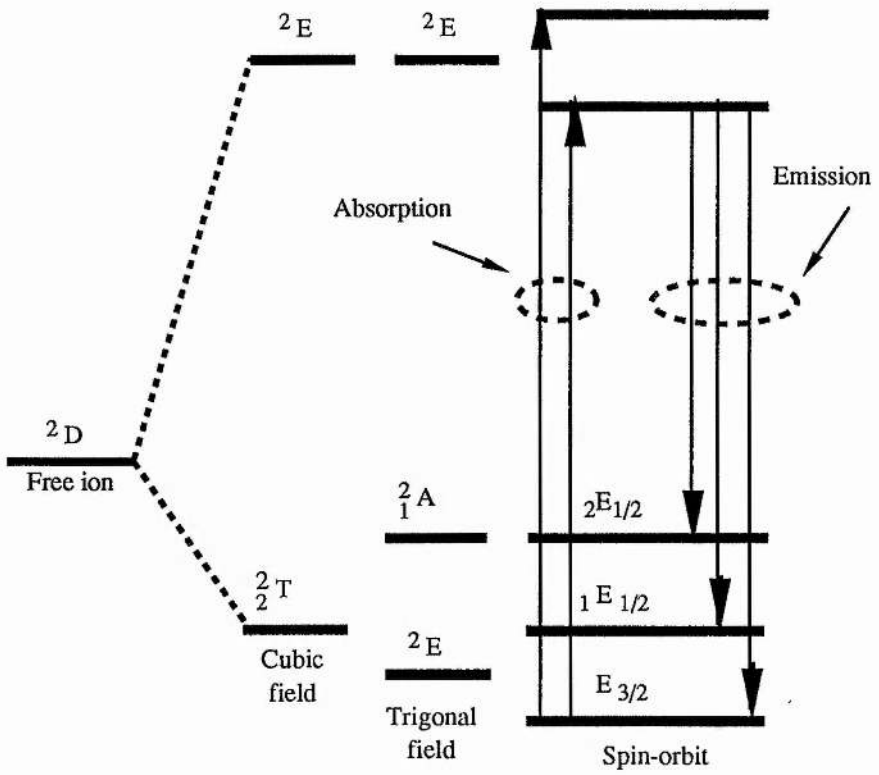


Figure 2.1: Schematic energy level diagram of $Ti:Al_2O_3$.

The dominant interaction splits the energy level of the free ion into a two-fold degenerate $^2E$ excited state, and a three-fold degenerate $^2T_2$ ground state (as shown schematically in figure 2.1). It is between these two levels that laser action occurs in Ti:$Al_2O_3$. Higher lying energy states of the $Ti^{3+}$ ion require promotion of the single d electron out of the 3d shell. The energy required to achieve such a transition is particular to the host medium, and for titanium-doped sapphire this appears to be much larger than the photon energies required for optical pumping and lasing processes. Hence, Ti:$Al_2O_3$ laser performance is not compromised by excited state absorption of either the pump or laser radiation which in 3d transition metal lasers, such as those based on $Cr^{3+}$, causes the medium to absorb the laser radiation that it generates lowering the laser efficiency and its potential tuning range.

The main absorption band of Ti:$Al_2O_3$ is located in the blue-green region of the visible spectrum, and is centred around 490nm as illustrated in figure 2.2.

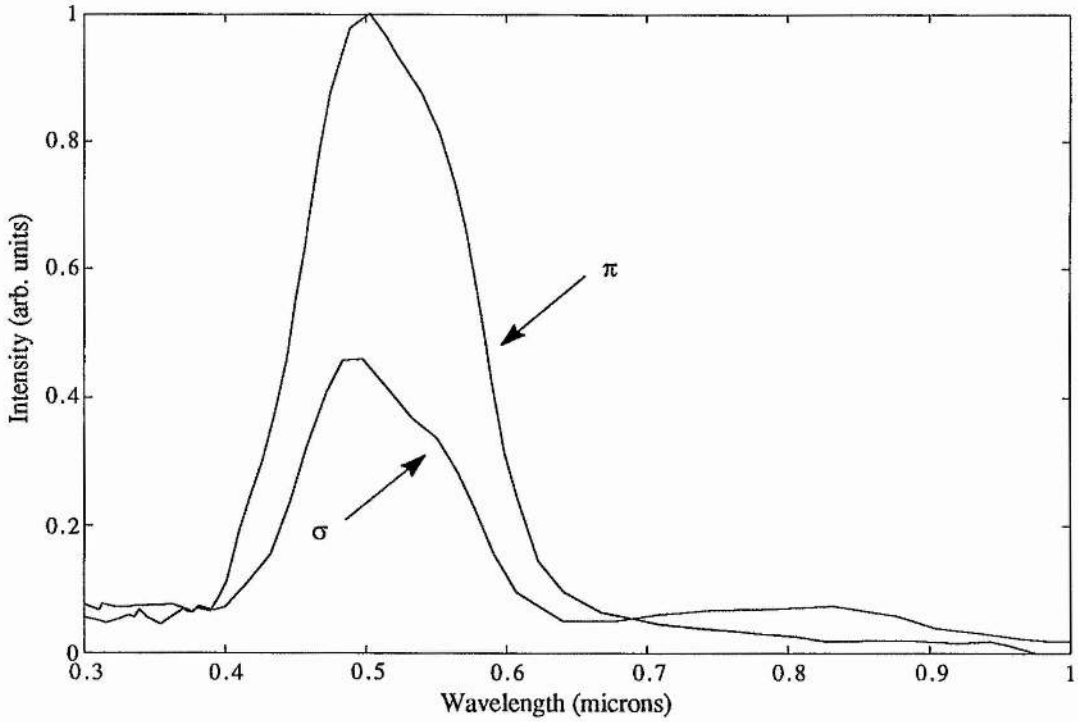


Figure 2.2: Measured absorption spectrum of Ti:$Al_2O_3$[1].

The double-humped structure of this absorption band is due to phonon-coupled excitation (an electronic transition accompanied by the simultaneous emission of lattice phonons), from the $^2T_2$ ground state to the Jahn-Teller split $^2E_g$ ($^2E_{3/2}$) and $^2E_g$ ($^2E_{1/2}$) excited states of the $Ti^{3+}$ ion. These phonon-terminated electronic transitions are also known as vibronic transitions and hence lasers based on them are referred to as vibronic lasers. It is this absorption band that gives $Ti:Al_2O_3$ its characteristic pink colour. A relatively weak absorption band is also observed in the near infra-red spectral region extending from aproximately 650-1600nm. This residual absorption has been attributed to the presence of $Ti^{3+}$-$Ti^{4+}$ pairs within the crystal [2]. As is shown in figure 2.2 the absorption spectrum of $Ti:Al_2O_3$ is polarisation dependent. In the spectral region between 400-630nm, the absorption is stronger for $\pi$ polarised light (light polarised parallel to the c-axis) than for $\sigma$ polarised light (light polarised perpendicular to the c-axis). At the peak of the blue-green absorption band the ratio of the absorption coefficients for the $\pi$ and $\sigma$ polarisations is 2.3. Since this absorption band is used for optical pumping into the upper laser levels, optimum performance of $Ti:Al_2O_3$ lasers is obtained for the $\pi$ polarisation, requiring light propagation perpendicular to the c-axis of the $Ti:Al_2O_3$ rods.

Optical pumping in the blue-green absorption band produces a broad fluorescence band that extends from approximately 600-1200nm and peaks at around 790nm as shown in figure 2.3. However, laser performance is impaired by the weak residual infra-red absorption that peaks between 800 and 850nm causing the laser to re-absorb its emitted radiation. This residual absorption, which has been shown to be due to the presence of $Ti^{3+}$ - $Ti^{4+}$ pairs within the laser crystal, has been the main problem associated with $Ti:Al_2O_3$ laser development. Fortunately, research into new growth techniques has now led to the production of high quality, low residual absorption loss material improving the performance and efficiency of $Ti:Al_2O_3$ lasers.

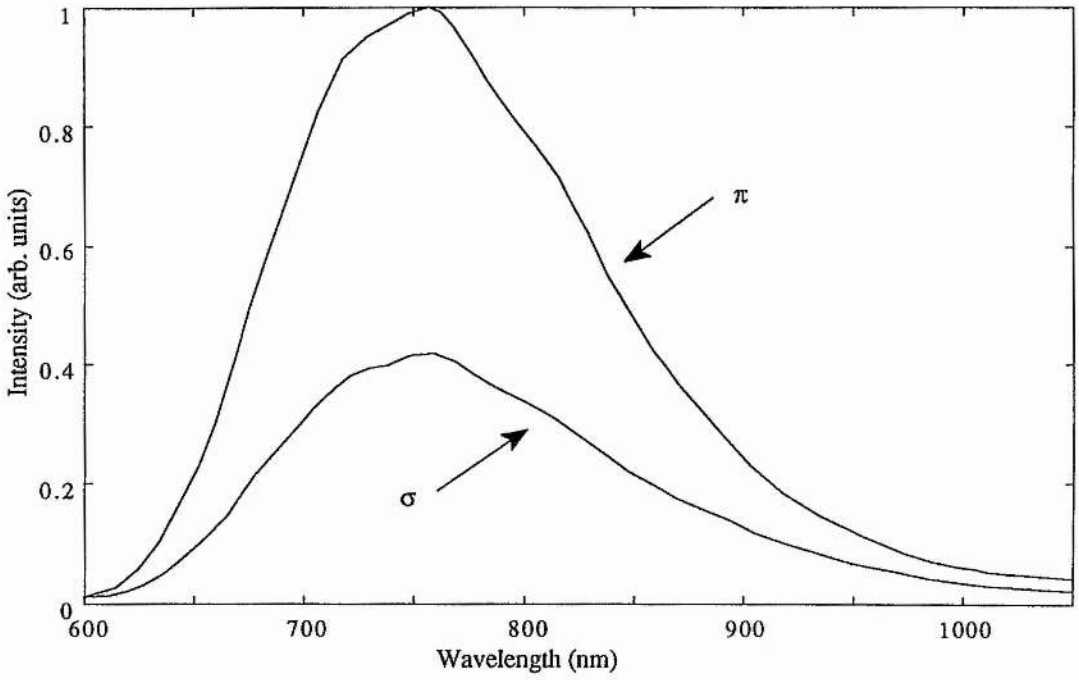


Figure 2.3: Fluorescence spectrum of Ti:$Al_2O_3$ [3].

A useful figure describing the quality of Ti:$Al_2O_3$ crystals for laser applications is the figure of merit defined as[4]:

$$\text{F.O.M.} = \frac{\text{peak } Ti^{3+} \text{ absorption at 490nm}}{\text{peak residual infrared absorption at 850nm}} = \frac{\alpha_{490}}{\alpha_{850}}$$

The higher the FOM, the lower the crystal loss due to residual infra-red absorption and therefore the better the quality of crystal.

Growth of titanium-doped sapphire has been achieved using various techniques such as the heat-exchanger method (HEM)[5], the vertical gradient freeze method[6,7] and the Czochralski method[8]. The crystals used in this work were grown using both the HEM method (Crystal Systems) and the Czochralski method (Union Carbide Corp.). Unlike all other growth techniques, the HEM method is a non-moving growth technique which leads to the production of high quality laser crystals with no lattice distortions. Also using this method the titanium ions are formed in the lattice predominantly as $Ti^{3+}$

ions as the crystal boule is grown under vacuum (or a controlled atmosphere). In moving growth systems such as the Czochralski and vertical-gradient freeze methods, lattice distortions can only be minimised but not avoided. These growth techniques also favour the formation of $Ti^{4+}$ ions under their oxidising system and further treatment of the crystals is necessary to convert the $Ti^{4+}$ ions back to $Ti^{3+}$ ions to improve the quality of the crystals. This is achieved by annealing the crystals at high temperatures (~1600$^0$C) in a reducing atmosphere, such as an Ar-$H_2$ mixture. Although the HEM growth technique inherently produces high quality laser crystals, recent improvements in annealing techniques have now shown that crystals grown by either the HEM or Czochralski method are of comparable high quality.

The dependence of the upper-state lifetime of Ti:$Al_2O_3$ on temperature is illustrated in figure 2.4. The reduction in the upper-state lifetime is characteristic of fluorescence quenching due to non-radiative decay processes. At temperatures below 150K the decay from the upper laser level is purely radiative with a lifetime of ~3.85μs. At room temperature the lifetime is reduced to 3.2μs. Although non-radiative decay is present , it is not sufficient to seriously impair laser performance and therefore only simple water cooling systems are required.

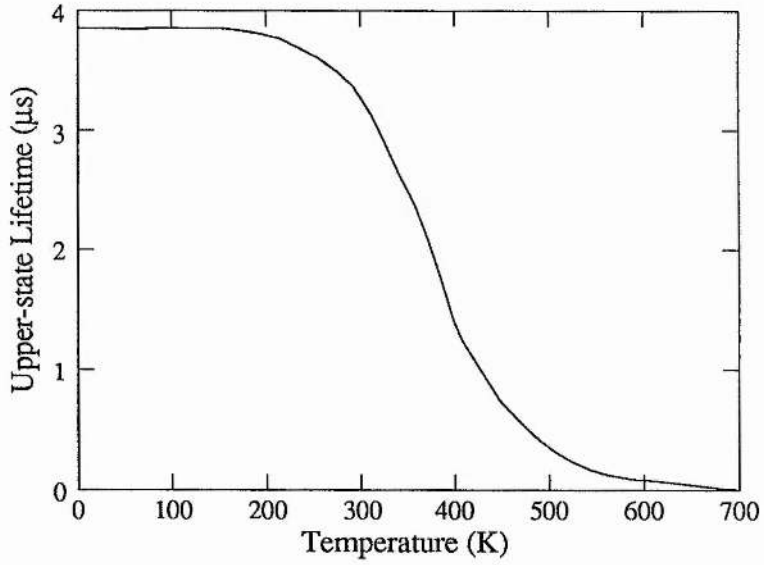


Figure 2.4: Graph showing the temperature dependence of the fluorescence decay time of Ti:$Al_2O_3$[9]

Some important laser properties of $Ti:Al_2O_3$ crystals are given below in Table 2.1.

| Property | Typical Value at 300K |
|---|---|
| Chemical Symbol | $Ti:Al_2O_3$ |
| Thermal Conductivity | 0.33 $Wcm^{-1}K^{-1}$ |
| $Ti^{3+}$ concentration | $1\text{-}5x10^{19}cm^{-3}$ |
| Refractive Index, n | 1.76 |
| Nonlinear Refractive Index, $n_2$ | $3x10^{-16}cm^2W^{-1}$ |
| Absorption Cross-section, $\sigma_{abs}$ | $5\text{-}8x10^{-20}cm^2$ |
| Gain Cross-section, $\sigma_{gain}$ | $3\text{-}4x10^{-19}cm^2$ |
| Absorption Co-efft, $\alpha_{pump}$ | 0.7-3 $cm^{-1}$ |
| Fluorescence Lifetime | 3.2μs |
| Peak Absorption λ | 490nm |
| Peak Emission λ | 790nm |

Table 2.1: Optical properties of $Ti:Al_2O_3$ laser crystals.

## 2.3 Low Threshold Design Considerations for Ti:$Al_2O_3$ Lasers.

The short upper-state lifetime of Ti:$Al_2O_3$ makes direct lamp pumping schemes difficult because of the high pumping rate per unit volume necessary to achieve a population inversion[10]. In order to achieve the highest population inversion the flashlamp pump pulse must be equal to or less than the upper state lifetime. This requirement leads to several problems associated with flashlamp pumped Ti:sapphire lasers. Firstly, the electrical coupling of the lamp becomes less efficient with decreasing pulse duration (typically 100 μsec). Secondly, the emission of the lamp will shift in wavelength away from the visible Ti:sapphire absorption as a result of the necessary increased electrical loading. Finally a lamp operated in such a manner will have a reduced lifetime. The high currents required to obtain sufficient pump energy result in the lamp having a high colour temperature which lies mostly outside the Ti:$Al_2O_3$ pump band. Such high colour temperatures may also lead to degradation of the gain medium.

However the broad absorption peak of Ti:$Al_2O_3$ around 500nm makes argon-ion lasers and frequency-doubled Nd:YAG obvious pump sources for this material. Due to the high damage threshold and thermal conductivity of Ti:$Al_2O_3$, this crystal can withstand pumping at high energy levels without damage or thermal distortions. The use of an efficient, stable and compact diode-pumped, all-solid state laser as a pump source for Ti:$Al_2O_3$, is an extremely attractive alternative to the current high power pump sources. To date, pulsed operation of Ti:$Al_2O_3$ lasers has been reported using frequency doubled modelocked and Q-switched Nd:YLF[11,12], and frequency doubled Q-switched Nd:YAG[13] lasers. However, the relatively high lasing threshold for continous-wave operation of Ti:$Al_2O_3$ has made diode-laser pumping very difficult. Recently, frequency doubled, diode-pumped Nd lasers have achieved average powers suitable for pumping Ti:sapphire lasers, which have been specifically designed for low threshold operation at around 200mW[14].

When designing any laser system, the main objectives are to maximise efficiency while at the same time minimising the laser oscillation threshold. Laser threshold can be minimised by choosing a small beam waist in the gain medium, and pumping only within that region so a high inversion can be easily reached with relatively low pump powers. However, this is difficult to achieve over the total volume of the laser crystal, which may be several millimetres in diameter, so the pump and cavity modes are focussed down into the crystal and then made to overlap[4]. On the other hand, high efficiency comes from having a long gain medium and a high $Ti^{3+}$ ion concentration to achieve maximum absorption of the pump radiation. Unfortunately, it has been shown that highly doped crystals exhibit excess loss at the laser wavelength, so there is inevitably a trade-off between increased efficiency and low threshold.

To effectively minimise the laser threshold, the cavity mode is focussed to a small beam radius w in the laser gain medium, and pumping is only within this mode. As w decreases, the threshold also decreases until the confocal parameter ($b=2n\pi w^2/\lambda$) is approximately equal to the crystal rod length L. When this limit is reached, w is no longer constant along the entire length of the rod, but varies reaching a value of $(2)w^{1/2}$ at either end. Further decrease in the beam waist does not result in a further reduction of the laser threshold, since the resulting high inversion and gain are no longer available over the entire crystal length[15]. The crystal rod length should therefore be no longer than the confocal beam parameter of the laser oscillator.

Optimising the laser performance is therefore achieved by maximising the output power while carefully selecting such constants as the crystal length L, the pump and cavity beam waists, the absorption and emission coefficients ($\alpha_p$ and $\alpha_e$, which are properties of the laser material and are dependent on the active ion concentration), and the cavity output coupling. Numerical modelling of a wide range of crystals with different active ion concentrations suggests that choosing $1.5< \alpha_p L < 2$ provides the best efficiency[14]. Hence this condition can be used to calculate the required pump absorption coefficient $\alpha_p$ for a given crystal length L. The most efficient transfer of pump energy to laser output is acheived using a longitudinal pumping geometry which

provides maximum overlap of the pump and resonator modes. Laser performance can be analysed by using a two-dimensional model for a longitudinally pumped system in which both lasers are assumed to operate in a fundamental Gaussian mode. The cw threshold power $P_{th}$ measured at the output of the pump laser, is approximately given by the following equation[4]:

$$P_{th} = \eta_c \left[\frac{\pi h \upsilon_p}{4\sigma\tau}\right]\left[\frac{(L+T)}{1-\exp(-\alpha l)}\right](w_p^2 + w_L^2)n \quad [2.1]$$

where $\eta_c$ is the coupling efficiency between the pump laser and the crystal, $h\upsilon_p$ is the pump photon energy, $\sigma$ is the emission cross-section, $\tau$ is the upper state lifetime and $w_p$ and $w_L$ are the pump and cavity-mode radii respectively. The round trip cavity losses consist of T (transmission losses), and L (intracavity losses including parasitic absorption). This equation can then be plotted to show the relationship between the laser threshold power and the crystal length for different pump absorption coefficients $\alpha_p$ (see figure 2.5).

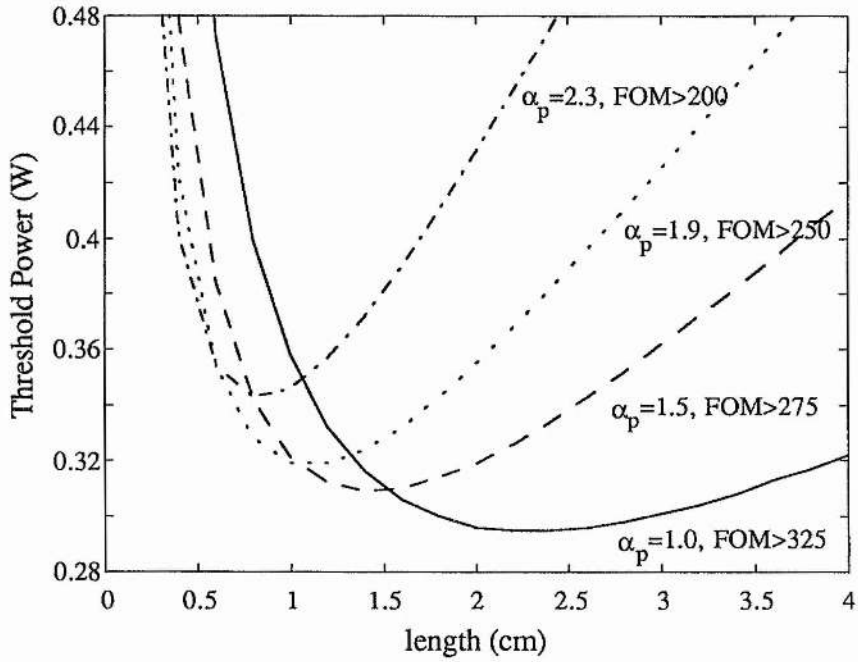


Figure 2.5: Oscillation threshold power as a function of crystal length for various dopant levels.

In the design of a cw low threshold laser the basic philosophy is to use a short, heavily doped crystal with a high FOM in a resonator with a small waist inside the crystal. To date the lowest cw threshold reported is 90mW from a 3.5mm crystal with a pump absorption coefficient of 2.84cm$^{-1}$ [13]. However when designing a low threshold, self-modelocked Ti:sapphire laser we require large enough nonlinearities in the crystal to stimulate fast saturable absorber action. This is guaranteed either by ensuring a large enough nonlinear interaction length, or by having sufficiently high intracavity powers.

## 2.4 The continous-wave Ti:$Al_2O_3$ laser.

The cw Ti:$Al_2O_3$ laser cavity is shown schematically in figure 2.6. The cavity was approximately 1.1m in length and incorporated a 10mm long, Brewster-angled Ti:$Al_2O_3$ rod, which had a pump absorption coefficient of 1.9cm$^{-1}$ (0.1%wt) and a figure of merit (FOM) in excess of 250 (Crystal Systems). The spherical mirrors, $M_1$ and $M_2$, had a radius of curvature of 100mm and were highly reflecting over the 700-850 spectral region and highly transmitting for the 488-514nm $Ar^+$ pump wavelengths. The laser cavity was an astigmatically compensated, four-mirror resonator which required an angle of incidence of ~11.5°. The plane end mirror $M_4$ and the plane output coupler $M_3$ were highly reflecting over the same wavelength range.

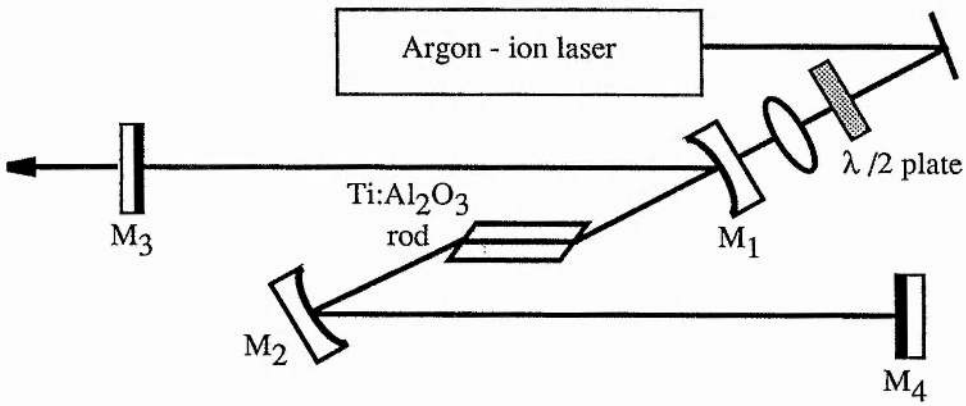


Figure 2.6: Schematic diagram of the cw Ti:$Al_2O_3$ laser cavity.

This laser was longitudinally pumped by a Spectra Physics argon-ion Model 2030 laser operating on the 514nm line and the pump beam was focussed into the crystal with a 100mm focal length lens which was coated with a broadband visible anti-reflection coating. This lens focussed the pump beam to a spot-size of 34μm in diameter, inside the crystal. The laser mode inside the crystal was elliptical in shape with radii 45μm x 27μm. Unfortunately, overlapping an elliptical laser mode with a circular pump mode is inefficient. This could be improved be focussing the pump beam using an appropriately angled mirror. However, this was not physically viable with a restriction on the available space on the optical bench.

The vertically polarised light from the Ar-ion laser had to be rotated so as to enter the Ti:$Al_2O_3$ crystal as $\pi$ polarised light. This was achieved using a multiple-order half-wave plate designed for operation at both 488 and 514nm. It was decided to run the argon-ion laser at 514nm as this is close to the doubled output of a diode-pumped Nd:YAG laser at 532nm. The maximum output power at 514nm was approximately 6W and was dependent on the age of the plasma tube. The electrical to optical efficiency of this laser was about 0.03% and nearly all the energy loss was in the form of heat from the plasma discharge tube, the magnet and the power supply. This means that high pressure water cooling was essential to maintain laser operation and water was supplied to the argon-ion at a flow of approximately 20 litres/min and at a pressure of approximately 70psi.

The Ti:$Al_2O_3$ rod was cooled by a Peltier-effect cooler which was electronically controlled to maintain the temperature of the rod at a constant 15°C. At pump powers >2W it was necessary to also use low pressure water to aid cooling of the crystal.

With an output transmission loss of 1.25%, the cw threshold of this laser was measured to be ~400mW and was reduced to ~350mW when the output coupler was replaced by a plane high reflector. The output power characteristics of the laser were measured for various output couplings and the results are shown in figure 2.7. Using the expression for slope efficiency $\eta_s$ where:

$$\eta_s = \eta_0 (T / T+L) \qquad [2.2]$$

and $\eta_0$ is the intrinsic slope efficiency ( containing the quantum defect and the pump efficiency), T is the magnitude of the output transmissive loss and L represents the sum of all the passive losses present in the laser cavity (this includes the round trip loss incurred at the gain medium and the losses of the cavity mirrors), the intrinsic slope efficiency and total passive losses were estimated for the laser. This was achieved by plotting (slope efficiency)$^{-1}$ as a function of (output coupling)$^{-1}$where the gradient of this graph is equal to $L/\eta 0$, and the y-intercept is equal to the inverse of the intrinsic slope efficiency[16]. From the data obtained from this laser, an intrinsic slope efficiency of 40% was calculated, giving a round-trip loss of ~3%. The quantum-defect limited efficiency value for this laser is approximately 63% (pump wavelength/laser wavelength).

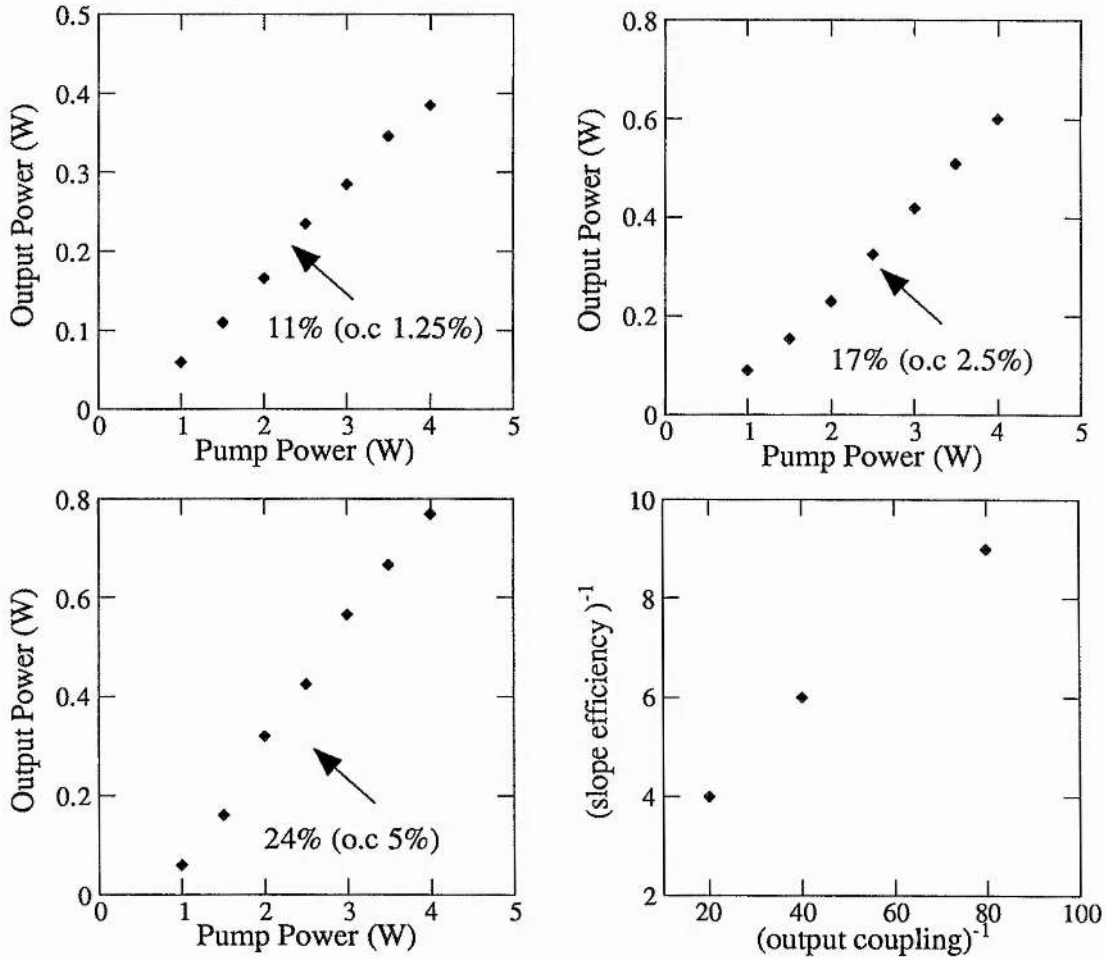


Figure 2.7: Input power versus output power characteristics for the Ti:$Al_2O_3$ laser crystal with pump absorption coefficient $\alpha_p$=1.9cm$^{-1}$.

The crystal length and doping levels were chosen using the design criteria mentioned in Section 2.3. The figure of merit (FOM) was chosen to be as high as possible for the given dopant level, ensuring a high quality crystal. Using the two-dimensional model[4]:

$$P_{th} = \eta_c \left[ \frac{\pi h \upsilon_p}{4\sigma\tau} \right] \left[ \frac{(L+T)}{1-\exp(-\alpha l)} \right] (w_p^2 + w_L^2) n \qquad [2.3]$$

it is possible to plot the oscillation threshold power as a function of crystal length for the cw Ti:$Al_2O_3$ laser described in this section.

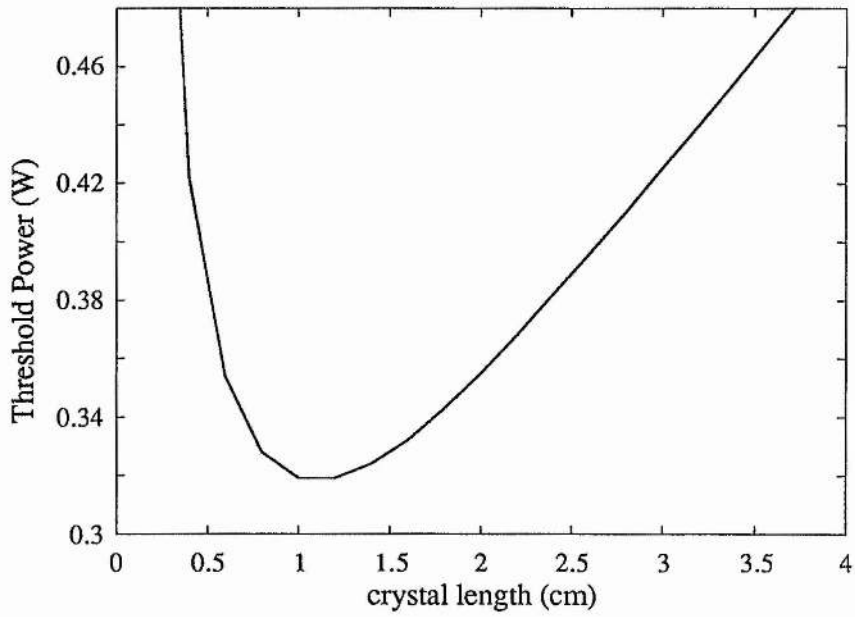


Figure 2.8: Oscillation threshold power as a function of crystal length.

As is shown in figure 2.8, the oscillation threshold power is a minimum for a 10mm long rod, and has a value of 320mW for an output coupling loss of 1.25%, which is comparable to the measured threshold power of 400mW.

As has been shown, oscillation threshold powers at 500mW and below mean that diode-pumped minilasers are now a feasible low power alternative to argon-ion systems. The prospect of employing all-solid-state, cw Ti:$Al_2O_3$ lasers is of great interest for

applications such as space-based remoted sensing. The first all-solid-state Ti:$Al_2O_3$ laser, gain switched by a diode-pumped, Q-switched, frequency-doubled Nd laser was demonstrated by Maker and Ferguson in 1990[17]. The first cw, all-solid-state Ti:$Al_2O_3$ laser system was developed by Harrison[14] and demonstrated the lowest oscillation threshold yet achieved of 120mW. However, such a system employed a short, heavily-doped crystal. In our cw Ti:$Al_2O_3$ laser system, the crystal length and hence doping level were chosen so as to match the confocal parameter of the laser cavity and hence facilitate low-threshold, self-modelocked operation.

## 2.5 The Regeneratively-Initiated, Self-Modelocked Ti:$Al_2O_3$ Laser.

The low-threshold cw Ti:$Al_2O_3$ laser cavity described in the section 2.4 was extended to approximately 1.75m in length and two SF14 prisms were inserted for dispersion compensation. The laser cavity configuration is illustrated schematically in figure 2.9.

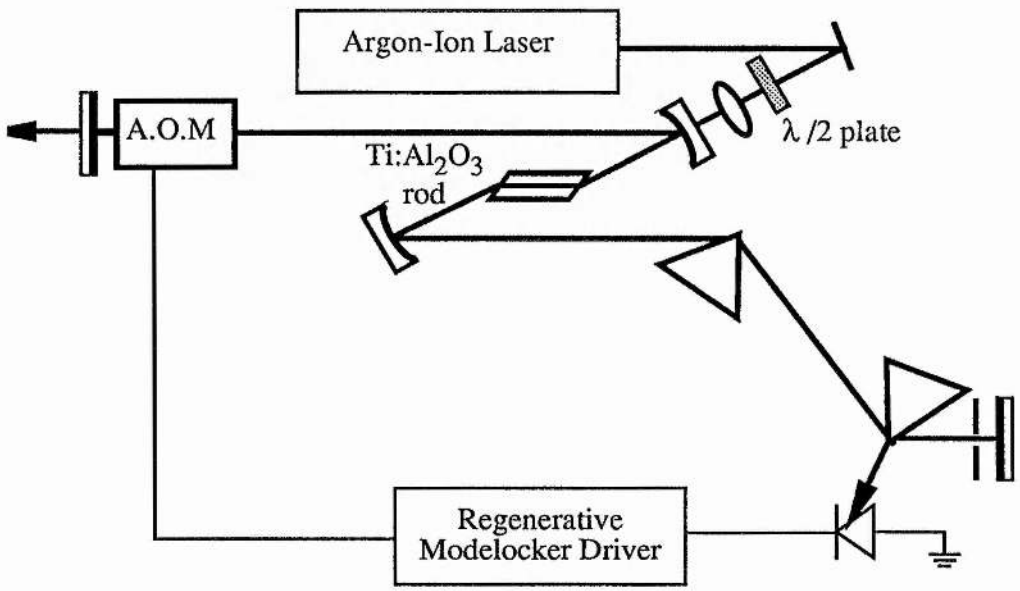


Figure 2.9: Schematic diagram of the regeneratively-initiated, self-modelocked Ti:$Al_2O_3$ laser.

An acousto-optic modulator was placed at the highly-reflecting end mirror and was employed to initiate and stabilise the self-modelocked operation of the laser. Once modelocked, any drifts in the cavity length led to a mismatch between the modulator drive frequency and the cavity repetition frequency which produced instabilities in the output of the laser. In order to overcome this problem, the modulator drive signal was derived from a fast photodiode which monitored the laser output[18]. This scheme was first devised in 1968 by Huggett[19] and is called "regenerative modelocking".

The acousto-optic modulator was a Brewster-angled quartz slab (Brimrose Corporation) and was driven by focussing a weak reflection off one of the prisms onto a fast photodiode (Type BPX65). The output of the photodiode was filtered using a 172 MHz band-pass filter with a bandwidth of approximately 10 MHz. This second harmonic component was amplified using a hybrid RF amplifier (Phillips OM335) and applied to the output of an integrated "divide by 4" circuit to produce an output of 43 MHz. This signal was then filtered and amplified before being applied to the acousto-optic modulator. The typical power of the modulator drive signal was ~500mW. When the laser oscillated, the modebeating on the output was sufficient to drive the modelocker electronics.

Group velocity dispersion was present in the cavity due to the Ti:$Al_2O_3$ rod and the acousto-optic modulator. The calculated cavity dispersion was be approximately $+4300fs^2$. Negative dispersion was introduced into the cavity by the SF14 prism sequence. At a seperation of 320mm, the net cavity GVD was approximately zero, therefore a seperation >320mm introduced net negative GVD. With careful and accurate optimisation of the cavity alignment, the laser could be made to self-modelock, producing pulses with durations in the order of ~100fs.

For pump power levels of ~2W and an output coupling of 2%, this laser routinely generated pulses of 85fs in duration, at a repetition rate of ~86 MHz. These pulses had an average power of ~110mW and were at a wavelength centred around 840nm. Tuning of the laser output was achieved by the translation of a vertical slit positioned between the second prism and the highly-reflecting plane mirror. Figures 2.10a and 2.10b show the

interferometric and intensity autocorrelation data measured from this laser. The spectral data is illustrated in figure 2.10c and implies a bandwidth of approximately 9.4nm. From these experimental results, the duration-bandwidth product is calculated to be ~ 0.34, which implies that the pulses were approximately transform-limited under these self-modelocking conditions (assuming a $sech^2$ pulse profile).

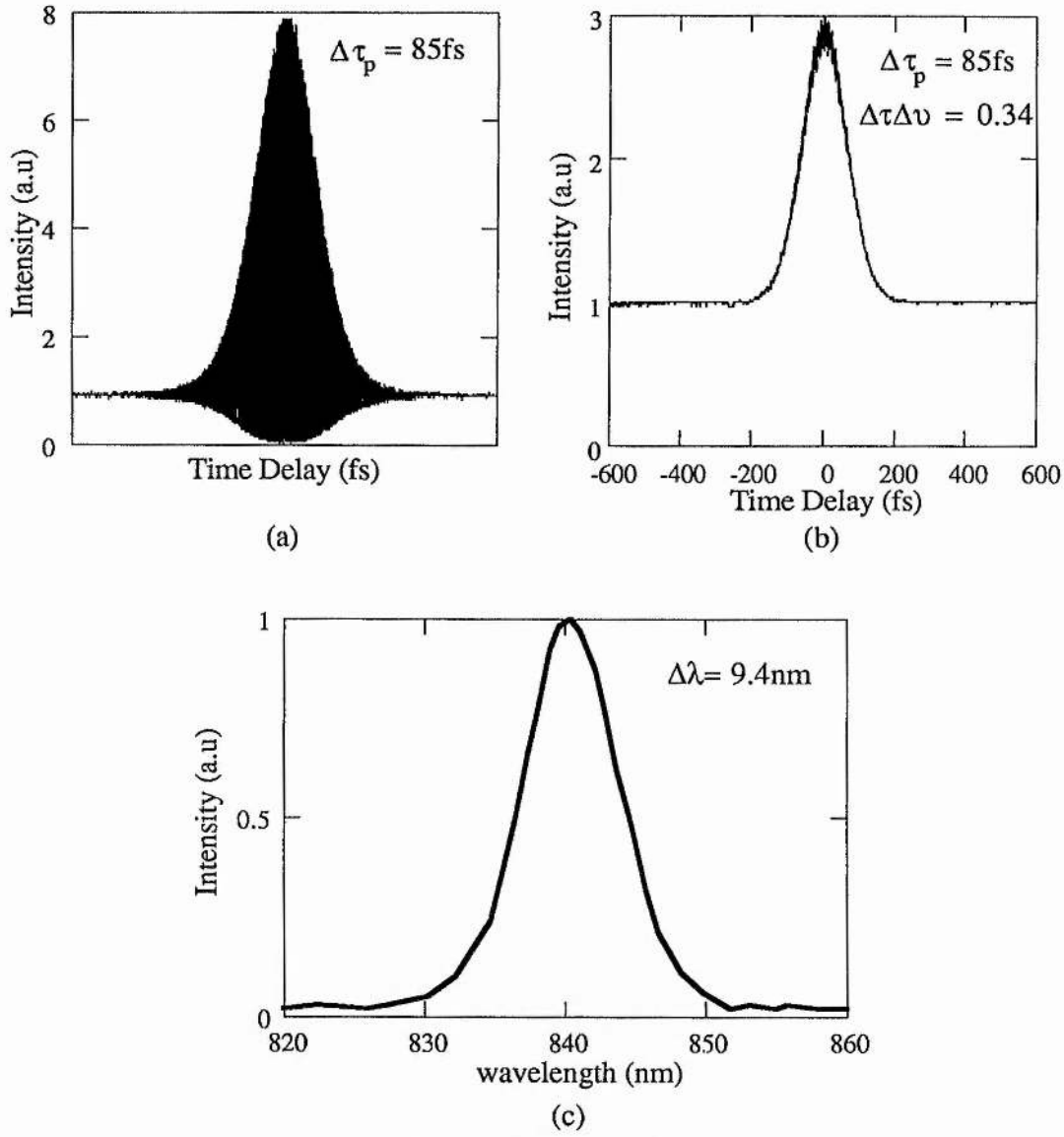


Figure 2.10: (a) interferometric, (b) intensity autocorrelation data and (c) spectral data for the output of a regeneratively-initiated, self-modelocked Ti:$Al_2O_3$ laser at a pumping level of ~ 2W.

The role of the acousto-optic modulator was simply to initiate and stabilise self-modelocked operation of the laser. The signal to the modulator could be blocked without disrupting the self-modelocking process. The laser was capable of generating stable pulse trains for periods of hours without the use of the modulator. However, if the pulse train was disrupted due to external perturbations, self-modelocking was readily initiated by switching on the modulator.

This laser was also capable of generating ultrashort pulses at pump powers as low as 500mW. At a modest pumping level of 1W, the Ti:$Al_2O_3$ laser generated a useful self-modelocked output, with an average power of 50mW. Typically, pulses of the order of 100fs in duration were generated at a repetition frequency of 86 MHz. Figure 2.11a and 2.11b represent the interferometric and intensity autocorrelation data obtained from this laser during low power operation. The intensity autocorrelation implies a pulse duration of 115fs. From the spectral data in figure 2.11c, it can be seen that these pulses were centred at a wavelength around 807nm, with a bandwidth of ~ 6.8nm. The duration-bandwidth product was calculated to be 0.36, implying that these pulses possessed minimal frequency chirp, at these low pump powers. As the pump power was decreased, the pulses inevitably became longer and it became difficult to adjust the prisms and the dispersion in the cavity to compensate for this, without disrupting the self-modelocked operation. The intracavity threshold power for self-modelocked operation was measured to be approximately 2W.

Although this laser was capable of producing stable pulse trains while the acousto-optic modulator was disconnected, the regeneratively-driven modulator was required for initiation of the self-modelocked operation. This means that accurately-aligned electronics are required adding to the complexity of the laser system. In the move towards compact and portable all-solid-state laser systems, it would therefore be an advantage to use a method to obtain self-modelocked operation without the need for any electronics.

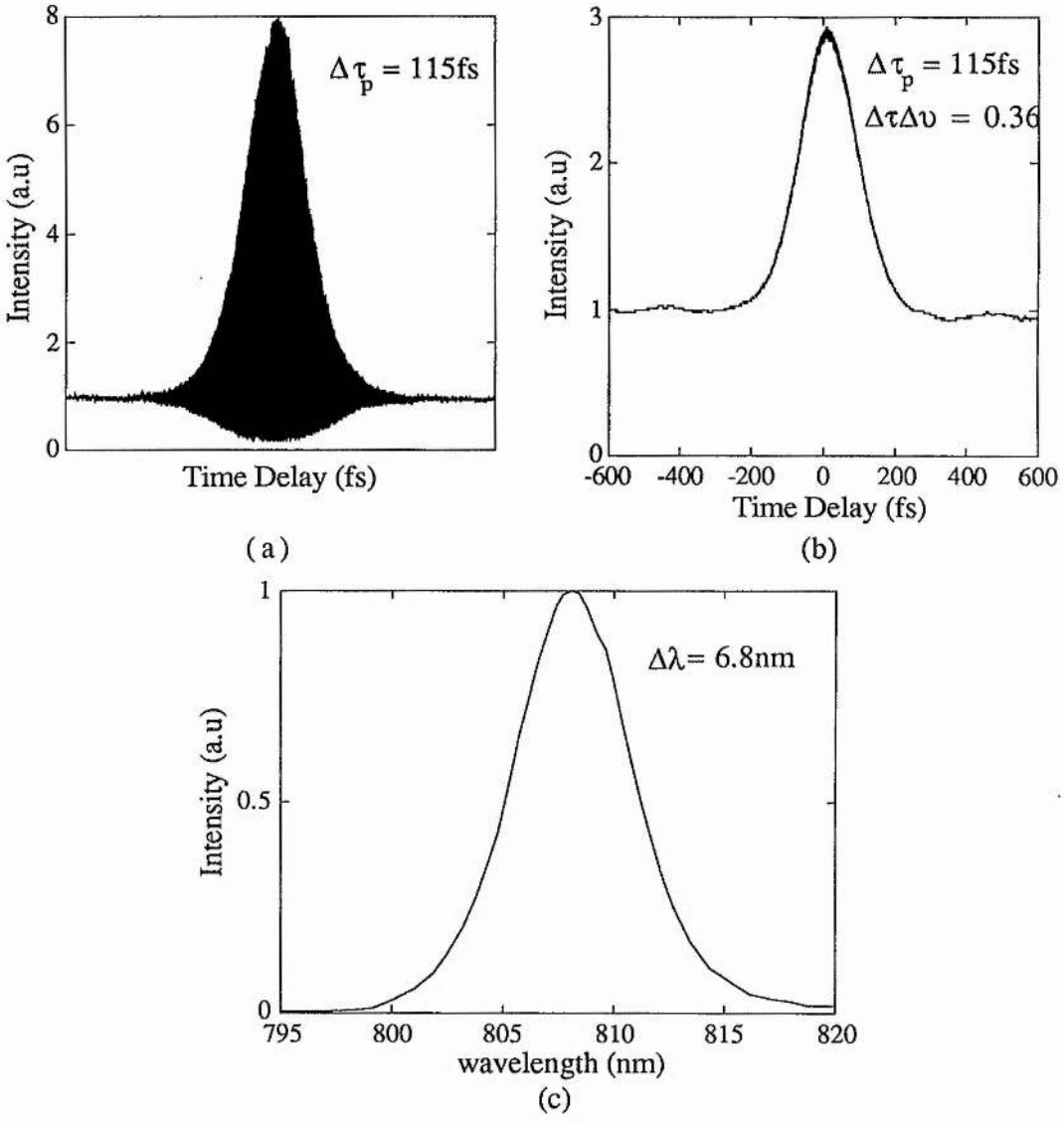


Figure 2.11: (a) interferometric, (b) intensity autocorrelation and (c) spectral data from the output of the regeneratively-initiated, self-modelocked Ti:$Al_2O_3$ laser operating at 1W pump power.

## 2.6 The Hard-Aperture, Self-Modelocked Ti:$Al_2O_3$ Laser.

The technique of self-modelocking (Kerr-lens modelocking) to produce ultrashort pulses, is based on a self-focussing effect in a resonator containing a material with a Kerr nonlinearity. This self-focussing effect modifies the transverse mode of the intracavity beam, and results in either loss or gain modulation. This modulation is provided either by the transverse gain profile of the Kerr medium (soft aperture) of by an intracavity aperture (hard aperture). Self-modelocking in a cavity that incorporates a hard aperture has the advantage of being more reproducible and easier to specify. It also does not suffer from any pump beam instabilities. In the case of soft aperture self-modelocking, the gain aperture is provided by focussing the pump beam into the crystal. Hence any amplitude fluctuations in the pump beam, lead to variations in the gain aperture which can materialise as amplitude noise and phase noise in the modelocked output of the laser.

A formalism has been developed by Cerullo and co-workers[20,21] which accurately predicts the optimum laser cavity design required for successful hard aperture self-modelocking. This feature can be achieved with a careful resonator design that maximises the nonlinear mode variation and dynamic loss modulation caused by a suitably positioned intracavity aperture. The optimum resonator parameters are derived with the help of a theoretical analysis based on a nonlinear ABCD matrix formalism.

In self-modelocked lasers, the cavity losses L can be given to the first order by the expression: $L = L_0 - kP$ [2.4]

where $L_0$ are the total linear losses, k is the nonlinear loss coefficient and P is the intracavity instantaneous power. For the modelocking process to be self-starting, the coefficient k must exceed a suitable value[22,23]. This first order loss variation caused by an aperture is proportional to the small-signal relative spot size variation $\delta$ where:

$$\delta = \left( \frac{1}{\omega} \frac{d\omega}{dp} \right)_{p=0} \quad [2.5]$$

$\omega$ is the spot size at the plane of the aperture and p is the power normalised to the critical power required to produce self-focussing. It has been shown[24] that when $\delta$ is sufficiently large and negative, an aperture placed at this position, will give rise to self-modelocking since the losses decrease with increasing power. This means that when this condition is satisfied, the laser favours self-modelocked operation over cw operation.

In order to optimise $\delta$, it has been shown that the critical cavity parameters are the distance between the folding mirrors z, which strongly influences the optical stability of the resonator, and the distance between the mirror $M_2$ and the face of the gain medium x, which controls the focussing condition without affecting the resonator stability (see figure 2.12). Hence, a self-modelocking laser cavity can be easily designed by plotting $\delta$ as a function of both x and z, and choosing the cavity co-ordinates which provide $\delta$ large and negative.

The hard-aperture, self-modelocked Ti:$Al_2O_3$ laser cavity configuration was similar to the regeneratively-initiated system which was described in section 2.5, and is illustrated in figure 2.12.

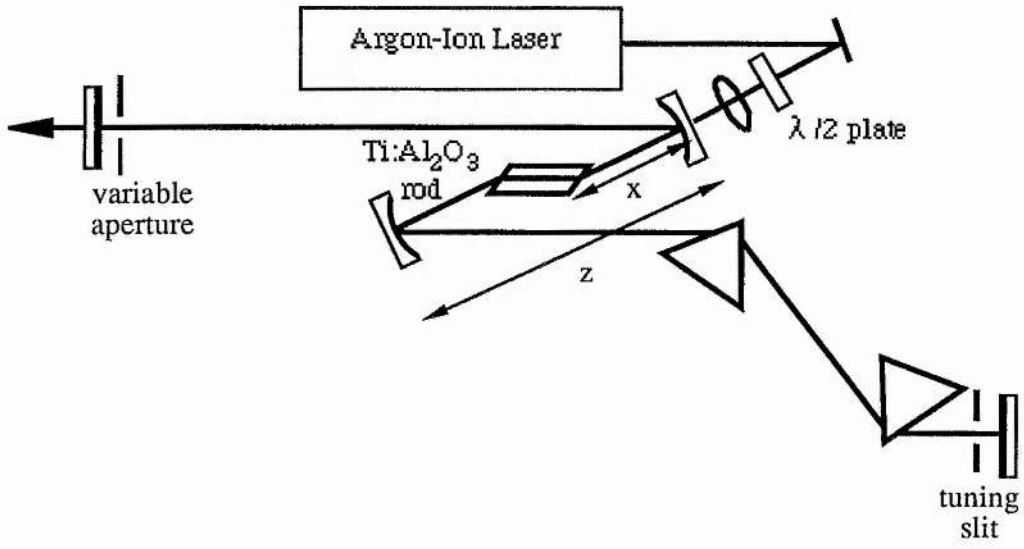


Figure 2.12: Schematic diagram of a hard-aperture, self-modelocked Ti:$Al_2O_3$ laser.

The spherical mirrors had a radius of curvature of 100mm and were highly reflecting over the 700-850nm spectral region and highly transmitting for the 488-514nm $Ar^+$

pump wavelengths. The pump beam was focussed into the Ti:$Al_2O_3$ laser crystal by a 100mm focal length lens which was coated with a broadband visible anti-reflection coating. Two SF14 prisms were inserted for dispersion compensation, and a vertical variable slit was inserted near the plane end mirror to facilitate self-modelocked operation. The cavity was approximately 1.74m in length and was symmetric around the gain medium. In this laser, the gain medium was still a 10mm long Brewster-angled rod, but had a higher absorption coefficient of 2.3$cm^{-1}$ (Crystal Systems). A crystal with a slightly higher doping level was chosen in order to increase the pump absorption and therefore decrease the oscillation threshold. Fortunately, advances in crystal growth techniques meant that the crystal quality was not degraded significantly by the higher dopant level.

In order to verify the quality of this laser crystal, the power characteristics of this laser were evaluated in the cw Ti:$Al_2O_3$ laser configuration, as described in section 2.4 where the cavity was approximately 1.1 m in length, and contained no extra intracavity elements. The output power of the laser was measured as a function of input pump power for a range of output couplings. The results are shown graphically in figure 2.13.

As can be seen in figure 2.13(a), the lowest cw threshold was measured to be ~300mW with an output coupling loss of 1.25%, and this was reduced to ~230mW when the output coupler was replaced by a highly reflecting plane mirror. As would be expected, using a crystal with a higher pump absorption coefficient has resulted in a reduction in the pump power required to achieve laser oscillation. The lowest threshold power obtained from the Ti:$Al_2O_3$ crystal with a pump absorption coefficient of 1.9$cm^{-1}$ was ~400mW (as shown in figure 2.7(a)). Figures 2.13(b) and 2.13(c) show that an increase in the slope efficiency of the laser was achieved by using larger output couplers, however this also led to a corresponding increase in the laser oscillation threshold.

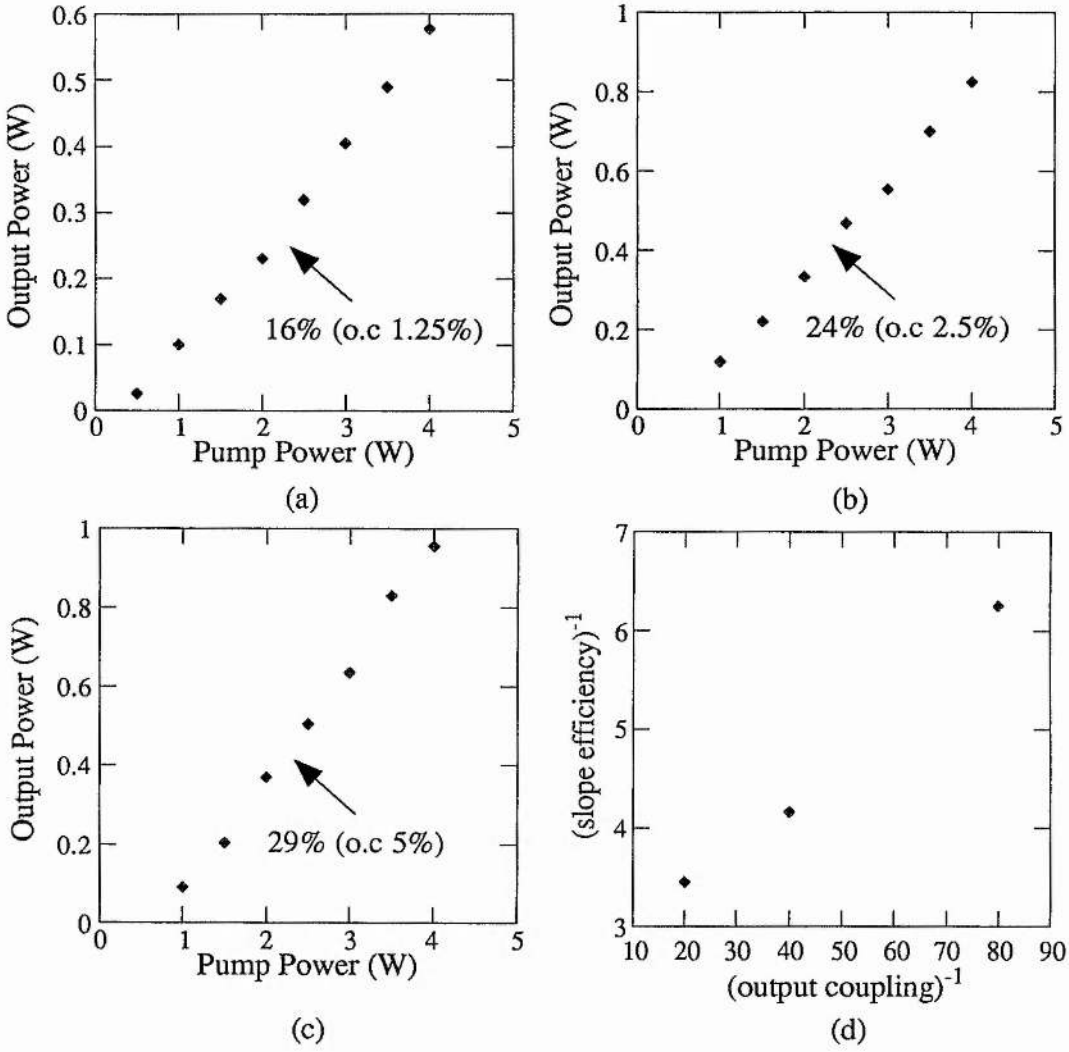


Figure 2.13: Input power versus output power characteristics for the Ti:$Al_2O_3$ laser crystal with absorption coefficient $\alpha_p$=2.3cm$^{-1}$.

From the data shown in figures 2.13 (a)-(d), and using equation 2.2, the intrinsic slope efficiency was measured to be ~42%, and the total passive loss per pass was ~1%. It should be noted that the power characteristics of this laser were only measured for three different output coupling losses. This means that there are only three data points on graph 2.13(d), leading to errors in the evaluation of the best fit line through these data points. Therefore, the measured intrinsic slope efficiency and passive losses of this laser, can only be approximate values. However, these results are comparable with the values obtained for the 1.9cm$^{-1}$ crystal ($\eta_0$~40%, loss per pass~1.5%) confirming that

the laser crystals are of high quality material, and that an increase in dopant level has not led to an increase in the crystal losses.

In order to achieve self-modelocked operation, the cavity was modelled using the model developed by Cerullo[21] and the loss variation at the plane of the aperture was plotted as a function of x and z as illustrated in figure 2.14.

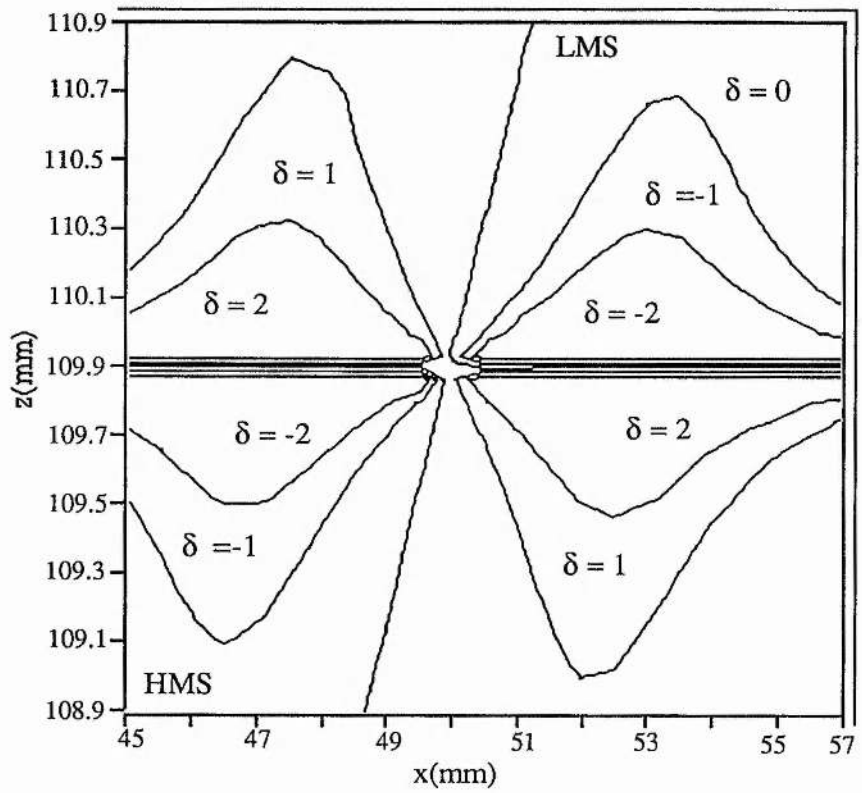


Figure 2.14: Contour plot of the small-signal spot size variation δ plotted as a function of both x and z.

For asymmetric laser resonators, the different stability regions correspond to high misalignment sensitivity (HMS) and low misalignment sensitivity (LMS) as shown. As would be expected it is easier to achieve stable hard-aperture self-modelocking when the cavity is aligned in the LMS region. However, there are benefits in using a symmetric laser resonator design. In a symmetric resonator the HMS and LMS regions become joined and result in a single stability region in terms of z. This means that suitable large and negative values of δ can be achieved without sacrifising the laser stability. Also the

region in the xz plane for which high values of $\delta$ can be obtained progressively broadens as the laser cavity approaches a symmetric configuration.

Figure 2.14 shows a contour plot of $\delta$ plotted as a function of both x and z (where x is the distance from the folding mirror to the crystal face and z is the seperation of the folding mirrors). In this case, the optimum values of x and z required for modelocking are in the region $\delta$=-2 and these values were chosen to be x = 53mm and z = 110mm. In order to achieve hard-aperture self-modelocking, the folding mirrors where positioned as suggested by the model. A vertical slit was placed close to the end mirror as shown in figure 2.12 and was slowly closed until a 10-20% loss in the cw output power was achieved. The pump lens was then adjusted to provide maximum output power. It was then found that gentle tapping on one of the end mirrors initiated self-modelocked operation. The average output power of the laser could then be optimised by careful adjustment of both the slit width and the position of the pump lens. It was found that the tolerance on the position of the folding mirrors with respect to the crystal was only $\pm$ 0.5mm, however the tolerance on the symmetry of the laser cavity was as high as $\pm$ 50mm.

At pump power levels of ~3W with an output coupling of 3.5%, this laser was capable of generating ~80fs pulses with an average output power of 150mW. Figures 2.15a and 2.15b show the interferometric and intensity autocorrelation data for a typical output pulse and imply a pulse duration of ~80fs. The spectral data are shown in figure 2.15c and show that the pulses were centred around a wavelength of 780nm and had a bandwidth of ~9.2nm. From these data, the duration-bandwidth product was calculated to be ~0.34 indicating that the pulses were approximately transform-limited under these self-modelocking conditions (assuming a $\text{sech}^2$ pulse profile). The self-modelocked operation of this laser was found to be highly stable and only minor day-to-day adjustments of the cavity were required to maintain the output power level.

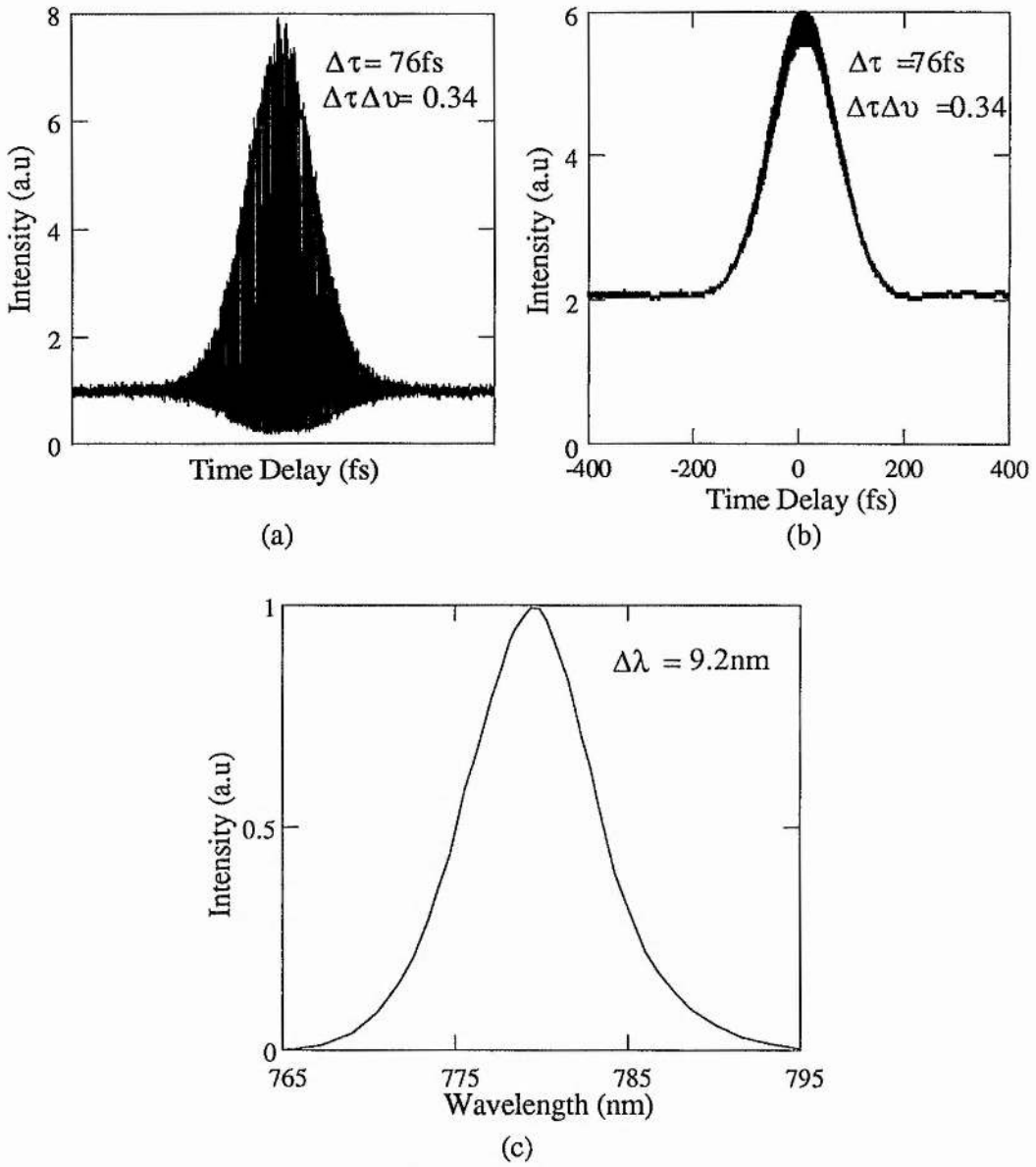


Figure 2.15: (a) Interferometric and (b) intensity autocorrelation profiles and (c) spectral data for the output pulses of the hard-aperture, self-modelocked Ti:$Al_2O_3$ laser at a pump power level of 3W.

Hard-aperture self-modelocked operation of this laser was also observed at pump power levels as low as 1.5W. Under these conditions, this laser was capable of producing 100fs pulses with an average output power of 50mW, with an output coupling of 1.5%. Figures 2.16a and 2.16b show the interferometric and intensity autocorrelation data obtained from this laser while operating at this low pumping level. The spectral data illustrated in figure 2.16c show that the pulse bandwidth was ~ 6.3nm and was

centred at a wavelength around 786nm. These data imply a duration-bandwidth product of ~0.33 meaning that the output of the laser was approximately transform-limited under these self-modelocking conditions. It was observed that the intracavity threshold power for hard-aperture self-modelocking was ~3W.

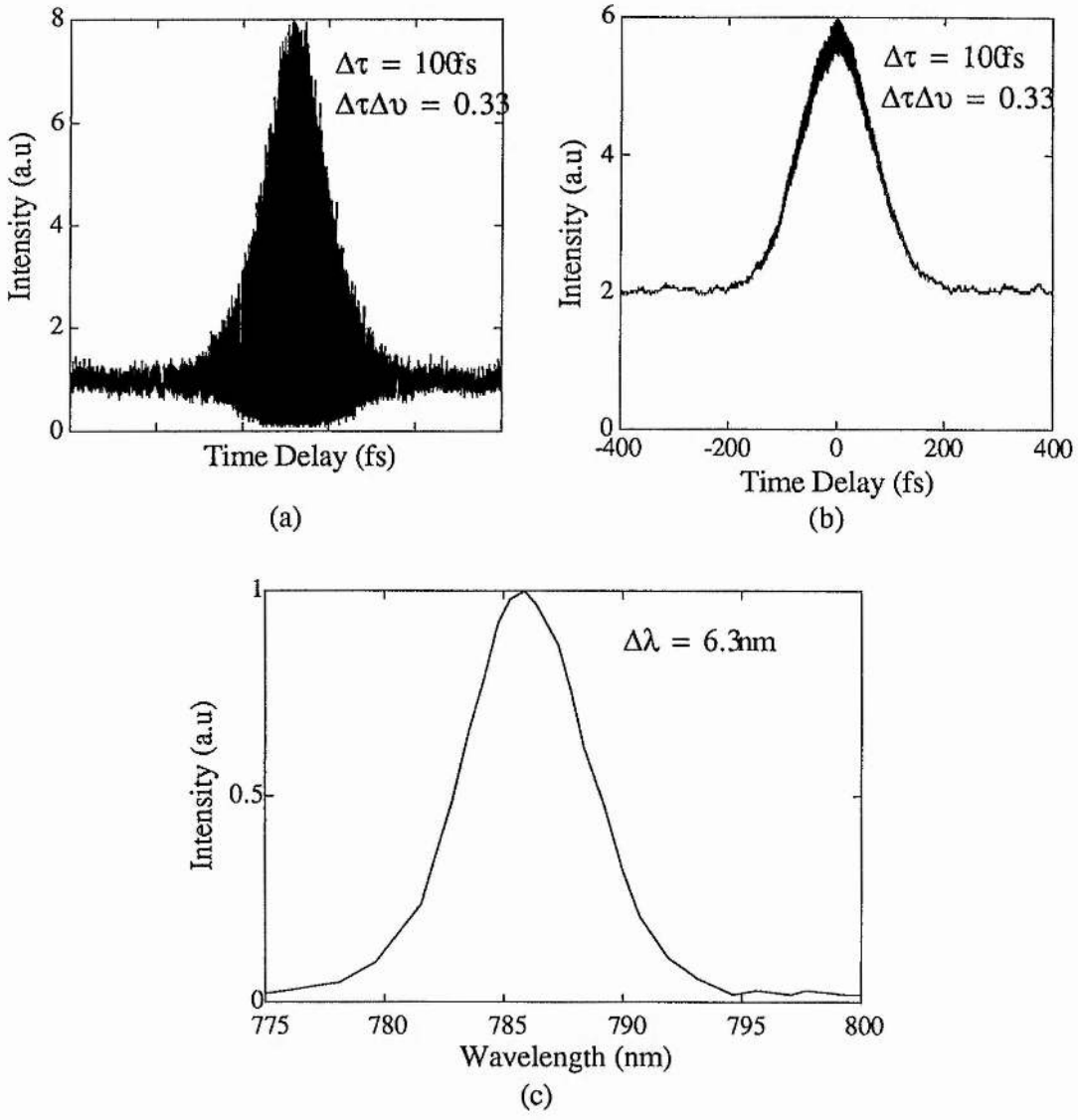


Figure 2.16: (a) Interferometric (b) intensity autocorrelation profiles and (c) spectral data for the output pulses from the hard-aperture, self-modelocked Ti:$Al_2O_3$ laser operating at a pump power level of 1.5W.

In the lasers discussed so far, losses from the surface of the laser crystal were minimised by cutting the crystal faces at Brewster's angle. However this has the effect of increasing the pump and cavity mode spot sizes within the crystal by a factor equal to the refractive index. Therefore, in a further attempt to reduce the oscillation threshold of the self-modelocked Ti:$Al_2O_3$ laser, the brewster-angled rod in the hard-aperture, self-modelocked laser was replaced by a plane-parallel cut Ti:$Al_2O_3$ laser crystal. The Ti:$Al_2O_3$ laser crystal (Union Carbide) was a 15mm long rod with plane-parallel facets which were anti-reflection coated at 800nm to reduce cavity losses. The pump absorption coefficient was ~2.3$cm^{-1}$ which gave a pump absorption at 514nm of ~98%. Unfortunately, a 5% reflection loss of the pump radiation was measured at the input surface of the rod, but this loss could be greatly reduced by anti-reflection coating the crystal face for the pump wavelength. The angle of incidence of the curved mirrors was kept as small as possible so as not to introduce astigmatism. The cavity mode inside the crystal was circular and the radius was measured to be ~21μm. This gives a cavity mode area of ~1.4$nm^2$ compared to an area of ~3.8$nm^2$ for the Brewster-angled rod (ellipse with radii 45μm and 27μm). This reduction in cavity mode area should therefore lead to a reduction in the cw oscillation threshold power of the laser. There is also improved mode-matching with the pump beam which is focussed to a waist inside the crystal of radius ~17μm.

For a short, symmetric resonator which was ~ 1.1m in length containing no extra intracavity elements, and with no output coupling loss, the lowest cw oscillation threshold obtained was 160mW. This is significant improvement on the results obtained from the Brewster-cut rod which demonstrated a cw oscillation threshold of 230mW.

The cw output power of this laser was measured as a function of input pump power for different output coupling losses, and the results are shown below in figure 2.17. As is shown in figure 2.17(a), by introducing an output coupling loss of 1.25%, the cw oscillation threshold rose from 160mW to 240mW. Figures 2.17(b) and 2.17(c) show that although the plane-cut rod exhibits an overall lower oscillation threshold than

the brewster-angled rod, this in turn leads to a decrease in the overall slope efficiency of the laser.

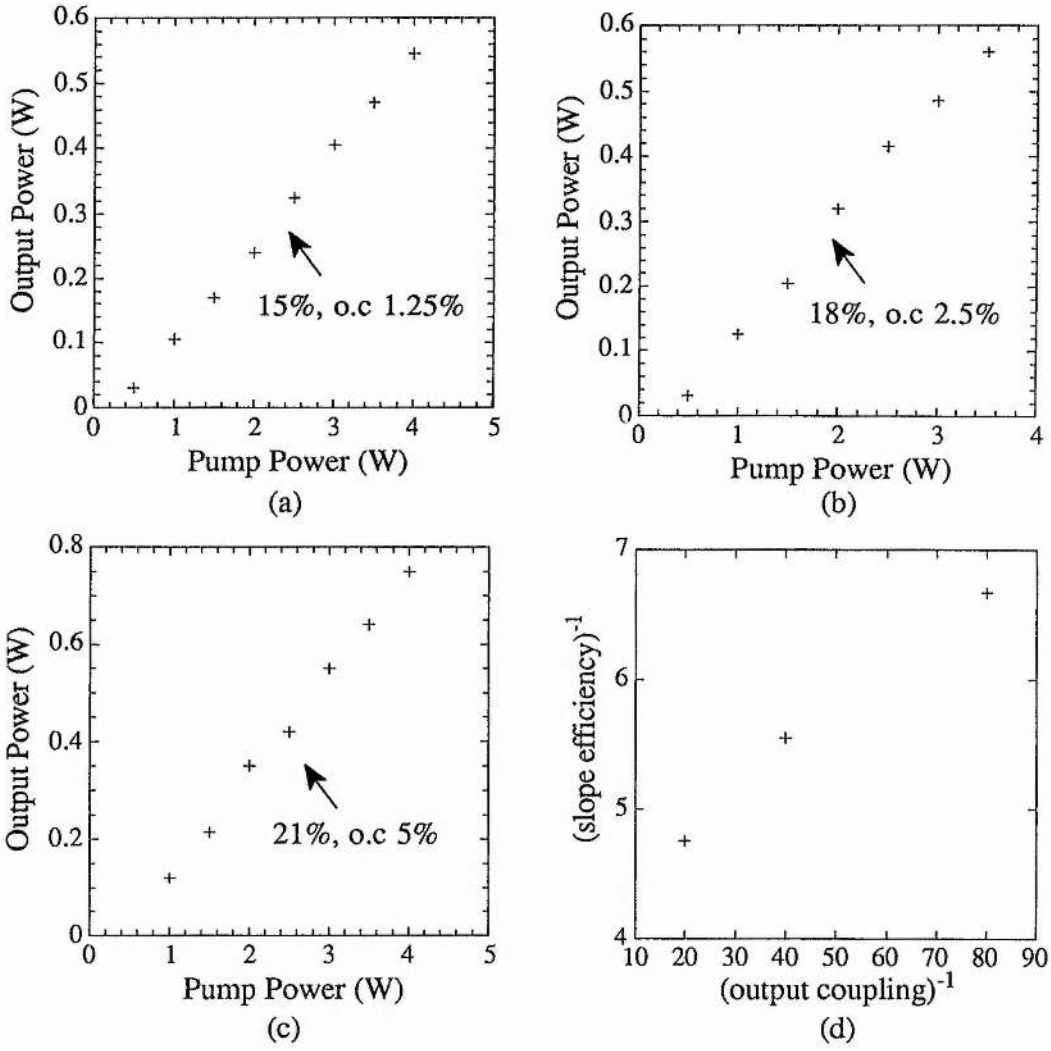


Figure 2.17: Output power characteristics of the plane-parallel Ti:$Al_2O_3$ laser rod for various output coupling losses.

Figure 2.18 illustrates the comparison between the power characteristics obtained for the brewster-cut rod and the plane-cut rod. It can be seen from this graph that at high pump powers, the Brewster-cut rod is more efficient with a larger output power. However, when pumping close to the threshold limit, it is more beneficial to incorporate the plane rod into a laser resonator design. There is an obvious trade-off between oscillation threshold power and laser slope efficiency.

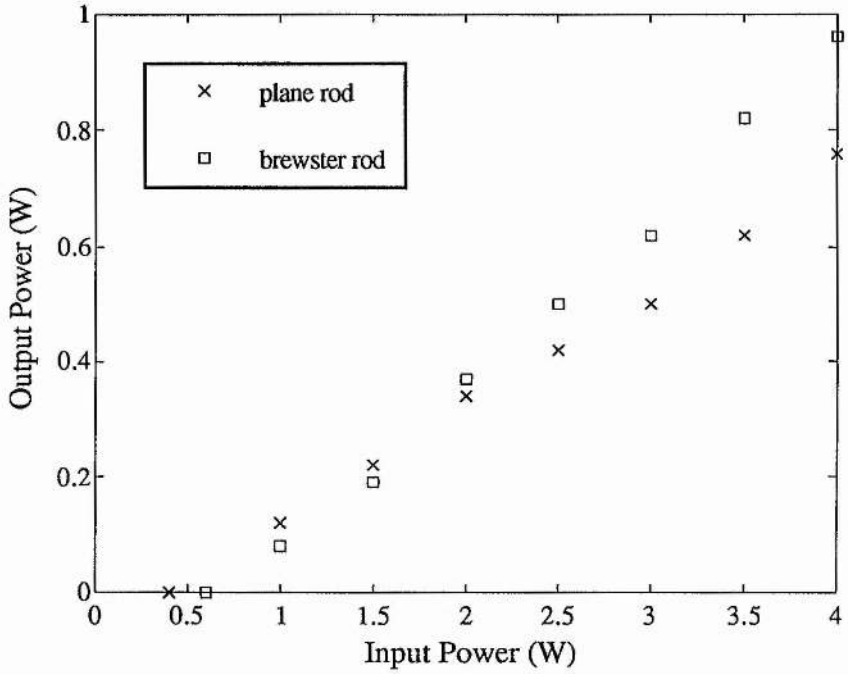


Figure 2.18: Input power versus output power for the Brewster-cut rod and the plane-cut rod for an output coupling loss of 5%.

In order to characterise the plane-cut rod in a self-modelocked configured laser cavity, the resonator was lengthened to ~1.75m and an adjustable, vertical slit was placed close to the output coupler (as shown in figure 2.12). Careful alignment of the focussing mirrors and slit width facilitated self-modelocked operation of this laser. At a pump power of 3W, and an output coupling of 1.25%, this laser produces 80fs pulses with an average output power of 100mW. Figure 2.19a and 2.19b show the interferometric and intensity autocorrelation data obtained for these pulses. Figure 2.19c shows the spectral data measured from the output of the laser and implies that the pulses were centred around 795nm with a bandwidth of 8.9nm. These data give a calculated duration-bandwidth product of 0.34 implying that the pulses were transform-limited under these self-modelocked conditions (assuming a $\text{sech}^2$ pulse profile).

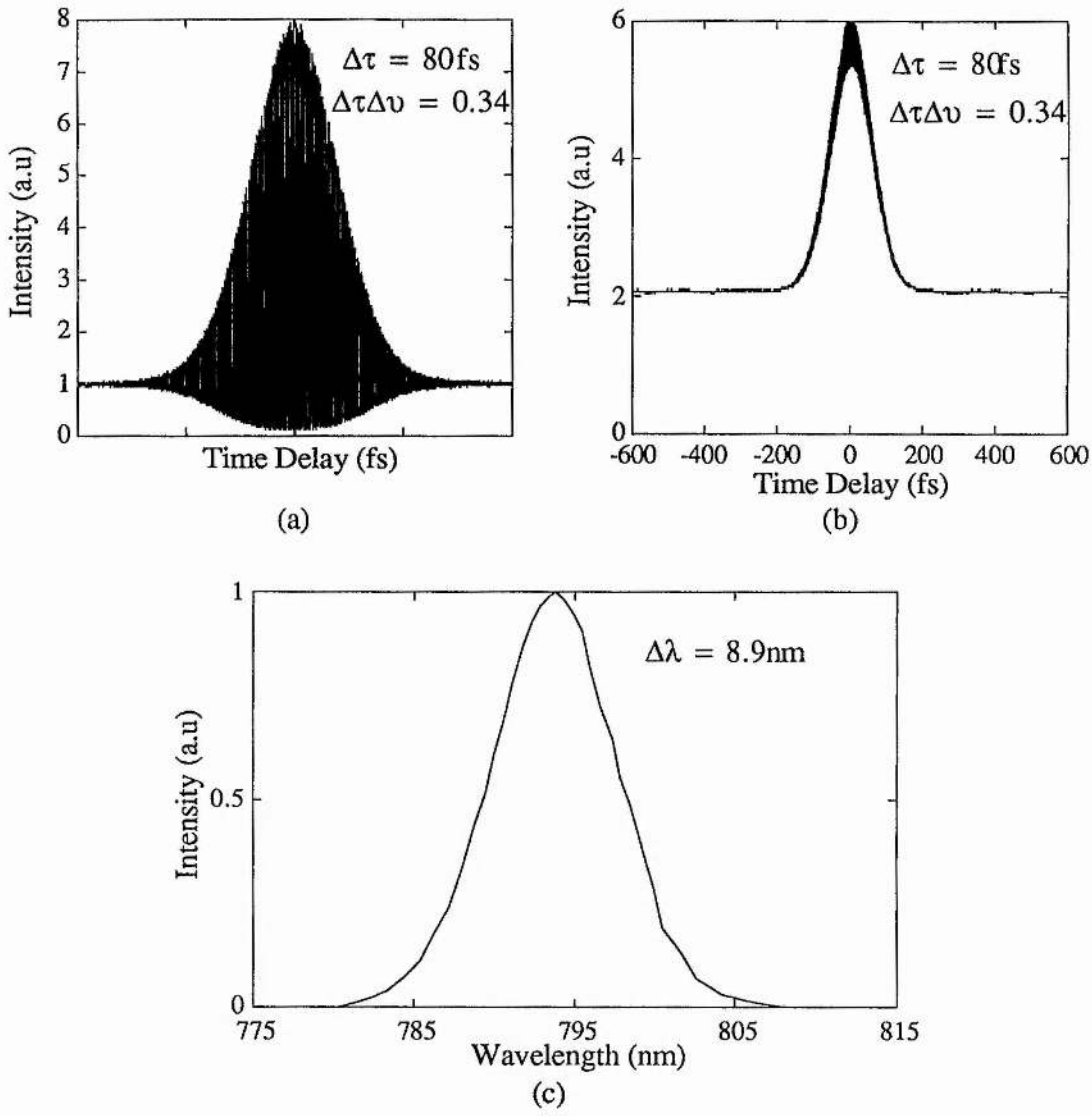


Figure 2.19: (a) Interferometric (b) intensity autocorrelation profiles and (c) spectral data from the output of the hard-aperture self-modelocked Ti:$Al_2O_3$ laser incorporating the plane-cut crystal.

Unfortunately, it was found that the self-modelocked operation of this laser was highly unstable and was not observed at pump powers less than 3W. The problems occurred in self-modelocking this laser may be attributed to the birefringent nature of the crystal. If the c-axis of the laser crystal is not exactly parallel with the cavity polarisation, then the rod itself acts as a birefringent plate between two polarisers. This leads to preferential wavelength selection and holes in the output spectrum of the laser appearing. i.e the laser is no longer continuously tunable. This means that any misalignment of the

laser rod could lead to unstable self-modelocked operation as these pulses have bandwidths in the order of ~10nm. Another factor may have been the anti-reflection coatings on the facets of the laser crystal. These coatings were narrowband coatings at 800nm, however the quality of these coatings was dubious and it is possible that there were wavelength dependent reflection changes across the crystal face.

## 2.7 Conclusions.

In this chapter, a brief description of the important growth techniques and spectroscopy of laser quality Ti:$Al_2O_3$ material has been given. This was followed by a discussion of its laser properties and the design considerations involved in the construction of a Ti:$Al_2O_3$ oscillator. The continous-wave operation of a few Ti:$Al_2O_3$ lasers has been characterised. For a brewster-angled laser rod, a laser oscillation threshold power as low as 230mW has been demonstrated, and output powers up to 1W at wavelengths around 800nm. For a plane-parallel laser rod, a laser oscillation threshold power as low as 160mW has been demonstrated. Such low threshold powers mean that it is possible to pump cw Ti:$Al_2O_3$ lasers with all-solid-state laser systems such as frequency-doubled Nd:YAG and Nd:YLF lasers. Although lower threshold powers can be achieved by using shorter, heavily doped laser crystals, the aim of this work was to demonstrate low power operation of a self-modelocked Ti:$Al_2O_3$ laser system.

The performance characteristics of a regeneratively-initiated self-modelocked Ti:$Al_2O_3$ laser have also been discussed. At pump powers of ~2W, this laser has been shown to produce ultrashort pulses of ~85fs in duration at wavelengths around 850nm. This laser was also capable of generating ultrashort pulses of ~100fs in duration at pump power levels as low as 500mW. The operation of a hard-aperture, self-modelocked Ti:$Al_2O_3$ laser has also been discussed which generated pulses of ~80fs at pump powers of ~3W at wavelengths around ~780nm. It was also possible to generate ultrashort pulses of ~100fs in duration at pumping levels as low as 1.5W.

## 2.8 References.


[1] D.E Spence "Modelocked Vibronic Lasers for the 700nm-1000nm Region" PhD Thesis, University of St. Andrews 1992.

[2] R.L Aggrawal, A. Sanchez, M.M Stuppi, R.E Fahey, A.J Strauss, W.R Rappoport, C.P Khattak "Residual Infrared Absoprtion in As-Grown and Annealed Crystals of Ti:$Al_2O_3$", *IEEE J. Quantum. Electron.*, QE-24 p.1003 (1988).

[3] P.F Moulton "Spectroscopic and laser characteristics of Ti:$Al_2O_3$", *J. Opt. Soc. Am. B* Vol.3 p.125 (1986).

[4] A. J Alfrey "Modelling of Longitudinally Pumped Cw Ti:$Al_2O_3$ Laser Oscillators", *IEEE J. Quantum. Electron.*, QE-25 p.760 (1989).

[5] W.R Rappaport, C.P Khattak "Titanium sapphire laser characteristics", *Appl. Optics* , Vol.27 p.2677 (1988).

[6] R.E Fahey, A.J Strauss, A. Sanchez and R. L Aggrawal, in "Tunable Solid State Lasers II", Springer Series in Optical Sciences Vol.52, A.B Budgor, L.Esterowitz and L. G De Shazer, eds., Springer-Verlag, New York p.82(1987).

[7] A. J Strauss, R. E Fahey, A. Sanchez and R. L Aggrawal, Proc. SPIE Vol.681 p.62 (1987).

[8] P. Lacovara, L. Esterowitz "Growth, Spectroscopy, and Lasing of Titanium-Doped Sapphire", *IEEE J. Quantum. Electron.*, QE-21 p.1614 (1985).

[9] P. Albers, E. Stark and G. Huber "Continous-wave laser operation and quantum efficiency of titanium-doped sapphire", *J. Opt. Soc. Am. B.*, Vol.3 p.134 (1986).

[10] P. Lacovara, L. Esterowitz and R. Allen "Flashlamp-pumped Ti:sapphire laser using fluorescent conversion" *Opt. Lett .*, Vol.10 p.273 (1985).

[11] G. T Maker and A.I Ferguson "Ti:sapphire laser pumped by a frequency-doubled diode-pumped Nd:YLF laser", *Opt. Lett .*, Vol.15 p375 (1990).

[12] G.P.A Malcolm and A.I Ferguson, "Ti:sapphire laser pumped by a frequency-doubled, diode-pumped Nd:YLF laser", *Opt. Commun,.* Vol.82, p.299 (1991).

[13] T.R Steele, D.C Gerstenberger, A. Drobshoff and R.W Wallace, "Broadly tunable high poweer operation of an all-solid-state titanium-doped sapphire laser system", *Opt. Lett.*, Vol.16 p.399 (1991).

[14] J. Harrison, A. Finch, D.M Rines and P.F Moulton, "Low threshold, cw, all-solid-state Ti:$Al_2O_3$ laser", *Opt. Lett.*, Vol.16 p.581 (1991).

[15] A. Sanchez, A.J Strauss, R.L Aggrawal and R.E Fahey "Crystal growth, spectroscopy and laser characteristics of titanium-doped sapphire" *IEEE J. Quantum. Electron .*, QE-24 p.995 (1988).

[16] S. A Payne, L.L Chase, L.K Smith, W.L Kway and H.W Newkirk "Laser performance of $LiSrAlF_6:Cr^{3+}$", *J. Appl. Phys.*, Vol.66 p.1051 (1989).

[17] G.T Maker and A.I Ferguson "Ti:sapphire laser pumped by a frequency-doubled diode-pumped Nd:YLF laser" *Opt. Lett.*, Vol.15 p.375 (1990)

[18] D.E Spence, J.M Evans, W.E Sleat and W. Sibbett "Regeneratively-initiated self-modelocked Ti:sapphire laser" *Opt. Lett.*, Vol.16 p.1762 (1991).

[19] G.R Huggett *Appl. Phys. Lett.*, Vol.13 p.186 (1968).

[20] V. Magni, G. Cerullo and S. De Silvestri "ABCD matrix analysis of propagation of gaussian beams through Kerr media" *Opt. Commun.*, Vol.96 p.348 (1993).

[21] G. Cerullo, S. De Silvestri, V. Magni and L. Pallaro "Resonators for Kerr-lens modelocked femtosecond Ti:sapphire lasers" *Opt. Lett.*, Vol.19 p.807 (1994).

[22] E.P Ippen, L.Y Liu and H.A Haus "Self-starting condition for additive-pulse modelocked lasers" *Opt. Lett.*, Vol.15 p.183 (1990).

[23] F. Krausz, T. Brabec and C. Spielmann "Self-starting passive modelocking" *Opt. Lett.*, Vol.16 p.235 (1991).

[24] G. Cerullo, S. De Sivestri and V. Magni "Self-starting Kerr-lens modelocking of a Ti:sapphire laser" *Opt. Lett.*, Vol.19 p.1040 (1994).

# Chapter 3: Measurement and Reduction of Phase Noise in Self-Modelocked Ti:Sapphire Lasers.

## 3.1 Introduction.

The output pulses in any practical modelocked laser exhibit some random changes in the pulse properties rather than being perfect periodic replicas of each other. Distinctive types of noise can arise from fluctuations in the pulse intensity (amplitude noise), the pulse repetition time (phase noise), and fluctuations in the pulse duration. The development of modelocked lasers with very low timing jitter (phase noise) is important for applications in electro-optic sampling[1], time-domain spectroscopy and synchronous streak camera measurements[2,3]. It is therefore clear that the knowledge and characterisation of these pulse fluctuations is of particular relevance as regards some applications of such pulses.

Extensive experimental studies involving the characterisation and improvement of timing jitter in a variety of modelocked laser sources have been reported [4-8]. In recent theoretical treatments[9] the noise characteristics of modelocked lasers have been studied where Haus and Mecozzi[10] in particular, considered in detail the timing jitter of passively modelocked lasers such as the self-modelocked Ti:$Al_2O_3$ laser. An important application of the Haus-Mecozzi theory is the calculation of the expected spectra of the laser timing jitter based only on the effects of quantum-mechanical spontaneous emission.

In this chapter, comparisons of the phase noise characteristics of regeneratively-initiated, self-modelocked Ti:$Al_2O_3$ lasers and hard-aperture, self-modelocked Ti:$Al_2O_3$ lasers are discussed. The use of a synchronously-operating, high resolution electron-optical streak camera in the evaluation of pulse timing jitter is also demonstrated.

## 3.2 Techniques for the Measurement of Noise.

The study of phase noise described here, has been based upon the measurements and analyses of the output intensity power spectra of the lasers under investigation. Such power spectra are readily obtained by directing the laser output onto a suitably fast photodiode and analysing the resultant electrical power spectrum of the laser intensity using a microwave spectrum analyser. Such analyses have previously been used to characterise the phase stability of microwave synthesisers, and were first used by von der Linde[4] to characterise noise in modelocked lasers.

The power spectrum of a real modelocked laser pulse train can be shown to be an infinite series of delta functions spaced at the laser repetition frequency, with associated amplitude noise and phase noise sidebands (as illustrated in figure 3.1).

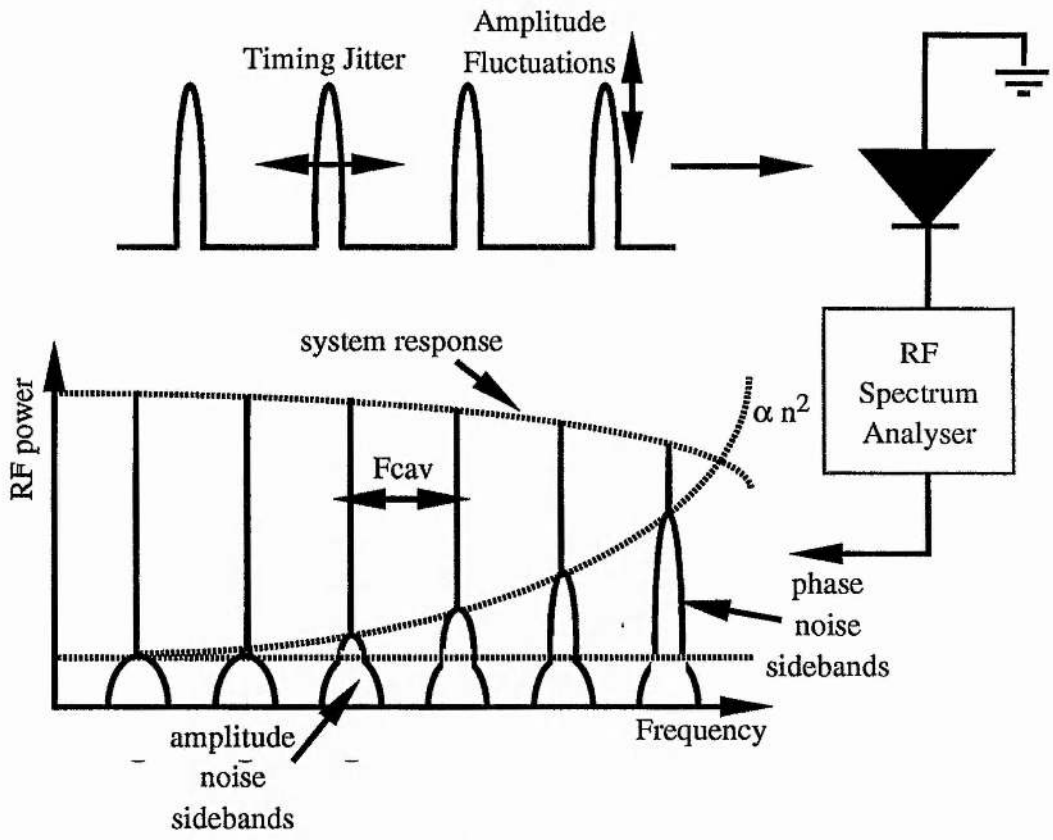


Figure 3.1: Schematic diagram showing the detection of a laser pulse train, and the resulting RF power spectrum [4].

It is important to point out that the power in the phase noise sidebands is proportional to $n^2$ (square of the harmonic number), whereas the amplitude noise sidebands remain constant with increasing harmonic number, n. For sufficiently low harmonics, the amplitude noise components generally dominate and conversely, at higher harmonics the phase noise components are dominant. The $n^2$ dependence of the phase noise is significant as it allows us to distinguish the amplitude noise from the phase noise on a modelocked pulse train. This means that it is possible to determine the phase fluctuations of the laser by comparing the frequency domain spectra of the low order harmonics (dominated by amplitude fluctuations), with those of the higher harmonics (indicating the phase noise).

Spectrum analysers measure the power spectral density P(f) of the laser output, integrated over the analyser resolution bandwidth, B. The frequency structure of the timing fluctuations in a pulse sequence can be more compactly presented as a log-log plot of the single sideband noise spectral density L(f)[1] as a function of frequency. This parameter which was originally used to measure the phase stability of microwave oscillators, is defined as the ratio of the power in one phase modulation sideband, in a one Hertz integration bandwidth, to the total carrier power, at an offset f Hz away from the oscillation frequency ("carrier"). L(f) has units of dBc per Hz.

The phase noise spectral density, L(f) for a given harmonic n, can be calculated from the expression:

$$L_n(\Delta f) = 10 \log_{10}\left[\frac{P(nf_0+\Delta f)}{1.2BP_c}\right] \qquad [3.1]$$

where $f_0$ is the laser repetition frequency, and $\Delta f$ is the frequency offset from the carrier. The factor 1.2 is included to normalise the filter response of the spectrum analyser to a rectangular function and accounts for the equivalent noise bandwidth of the device. If the power spectra of the fundamental and a high harmonic are recorded on the spectrum analyser, the corresponding functions $L_1(f)$ and $L_n(f)$ can be calculated from the above equation. The noise sidebands at the nth harmonic are given by $L_n(f)$ which is the

number of decibels below the carrier (nth harmonic) of the noise sideband at a frequency offset f for a given resolution bandwidth B. $L_{1(f)}$ is then determined by $L_n(f)$ divided by the resolution bandwidth B (more accurately the equivalent noise bandwidth) and the square of the laser harmonic $n^2$.

Once these functions have been determined, the phase noise spectrum, $L_J(f)$ and amplitude noise spectrum $L_A(f)$ can be obtained from the following equations where:

$$L_J(f) = 10\log_{10}\left[\frac{10^{L_n(f)/10} - 10^{L_J(f)/10}}{(n^2-1)}\right] \quad [3.2]$$

$$L_A(f) = 10\log_{10}\left[\frac{n^2 10^{L_1(f)/10} - 10^{L_n(f)/10}}{(n^2-1)}\right] \quad [3.3]$$

$$= 10\log_{10}\left[10^{L_1(f)/10} - 10^{L_J(f)/10}\right]$$

It is then possible to calculate the rms values of the pulse timing jitter $\sigma_J$, within a frequency range $f_{low} \le f \le f_{high}$ which is defined as:

$$\sigma_J = \sqrt{\langle J(t)^2 \rangle} = \frac{1}{2\pi f}\sqrt{\frac{P_{sb}}{P_c}}$$

$$\text{where } P_{sb} = \int_{f_{low}}^{f_{high}} \frac{2P_J(f)}{B}\,df$$

$$\text{which gives } \sigma_J(f_{low}, f_{high}) = \frac{1}{2\pi f_0}\sqrt{2\int_{f_{low}}^{f_{high}} 10^{L_J(f)/10}\,df} \quad [3.4]$$

where J(t) is the timing fluctuations of the laser pulse train. (Note that the rms phase noise is given by $\phi_{rms} = 2\pi f_0 \sigma_J$).

Similarly, if A(t) is the normalised pulse intensity fluctuations, then the rms values of the amplitude noise $\sigma_A$ are given by:

$$\sigma_A(f_{low}, f_{high}) = \sqrt{2 \int_{f_{low}}^{f_{high}} 10^{L_A(f)/10} df} \qquad [3.5]$$

In practice, the lower frequency limit is set by the measurement acquisition time which in turn depends on the sensitivity of the detection system, while the higher frequency limit is usually set by the bandwidth of the detection system.

In general, actively modelocked lasers such as an acousto-optically modelocked argon-ion laser and a synchronously modelocked dye laser exhibit phase noise which results primarily from the active modulation[4]. The low frequency phase noise of a synchronously-modelocked dye laser has been shown to be an exact replica of the noise on the pump laser, and the timing jitter on an acousto-optically modlocked argon-ion laser has been attributed to plasma current fluctuations resulting from power supply noise. On the other hand, assessments of passively modelocked laser systems have revealed that the predominant phase noise components arise from cavity length variations, which in turn can lead to large timing fluctuations. Slow fluctuations in temperature can lead to cavity length changes in the order of microns per hour, which corresponds to frequency fluctuations of hundreds of Hertz. Mirror mount instabilities, mechanical perturbations, and acoustic noise also lead to laser frequency fluctuations. A small and slow change in the laser cavity length leads to significant variation in the phase of the laser pulse train as the phase change accumulates over many round-trip times of the cavity. Periodic changes in cavity length L, will therefore lead to a modulation of the cavity, f. For small differences in cavity length, the maximum frequency deviation $\delta f$ is related to the maximum change in the effective cavity length of $\delta L$ by:

$$\frac{\delta f}{f} = \frac{\delta L}{L} \qquad [3.6]$$

Assuming that this frequency deviation is small compared to the laser cavity repetition frequency, then the corresponding phase modulation $\delta\phi$ is given by:

$$\delta\varphi = \frac{\delta f}{f_m} = \left(\frac{\delta L}{L}\right)\left(\frac{f}{f_m}\right) \qquad [3.7]$$

To find the maximum timing variation of the pulse $\delta t$, we substitute the equation:

$$\delta\vartheta = 2\pi f \delta t \text{ which gives } \delta t = 2\pi f_m \frac{\delta L}{L} \qquad [3.8]$$

This implies that the rms timing variation of the pulse train will therefore be:

$$\sigma_J(f_m) = \frac{\delta_t}{2\sqrt{2}} = \frac{\delta L}{4\sqrt{2}\,\pi\, L\, f_m} \qquad [3.9]$$

It is interesting to use the above equation to estimate the timing jitter which would result from a cavity length change of 10nm at a frequency 100Hz. For a cavity length of 1.75m, the resulting rms timing jitter is 1.6ps. In reality, the cavity length changes are distributed over the entire frequency spectrum, but it is evident that a substantial amount of timing jitter can result from small, low frequency changes in the length of the laser cavity. Additional amplitude and phase noise can result from amplitude fluctuations of the pump laser, particularly those which arise from plasma current fluctuations resulting from power supply noise.

It is also possible to obtain a measure of the relative timing jitter on a laser output by monitoring the pulse train on a synchronously-operating electron-optical streak camera. The precise synchronisation of the deflecting signal to the frequency of the laser is vital if the streak images are to be integrated on the phosphor screen without loss of temporal resolution. Synchronisation is degraded by the presence of phase noise between the pulse train and the deflection voltage applied to the streak camera, and so all phase noise sources need to be identified and their influence minimised. This therefore implies that by lowering the timing jitter on the laser pulse train, higher temporal

resolutions will be obtainable from the streak camera until the physical temporal resolution of the camera is reached.

### 3.2.1 Phase-Noise Measurements on a Regeneratively-Initiated, Self-Modelocked Ti:$Al_2O_3$ Laser.

The phase noise characteristics of the regeneratively-initiated, self-modelocked Ti:$Al_2O_3$ laser described in section 2.5 were determined using the spectrum analysis method described. When the phase noise measurements were recorded, the self-modelocked Ti:$Al_2O_3$ laser was typically pumped at powers of ~ 3W, and generated 100fs pulses with an average power of 200mW. The Ti:$Al_2O_3$ crystal was thermoelectrically cooled to provide temperature stability and all the optical components in the laser cavity were mounted using precision optical mounts (Newport ULTRAlign$^{TM}$) which have high rigidity and excellent long term stability. The output pulse train of the laser was directed onto a silicon avalanche photodiode (Telefunken BPW 28) which had a 3dB bandwidth of ~2 GHz. This photodiode was biased at 130V using a mains power supply which had a high degree of smoothing. The diode signal was then sent to a Hewlett Packard 71000 series RF spectrum analyser which had a frequency range from 50 kHz- 22 GHz and 10 Hz resolution bandwidth. The spectrum analyser was used to record several power spectra for the laser, each one having progressively smaller span down to a span of 1kHz and 10 Hz resolution bandwidth. These measurements were made for the laser cavity frequency and for selected higher harmonics. The data were then downloaded from the spectrum analyser to a computer for processing. The computer provided plots of the calculated phase noise spectrum and associated pulse timing jitter figures.

Using a BPW28 photodiode and a Hewlett Packard 71000 series RF spectrum analyser, noise data for the regeneratively-initiated self-modelocked laser were obtained from the laser cavity frequency of 86 MHz and the 10th harmonic. There was no

advantage to be had in recording higher harmonics because of the relatively large timing jitter on the laser output pulse train. The power spectra obtained from the spectrum analyser are shown in figure 3.2a for spans of 10 kHz and 1 kHz, with resolution bandwidths of 30 Hz and 10 Hz respectively.

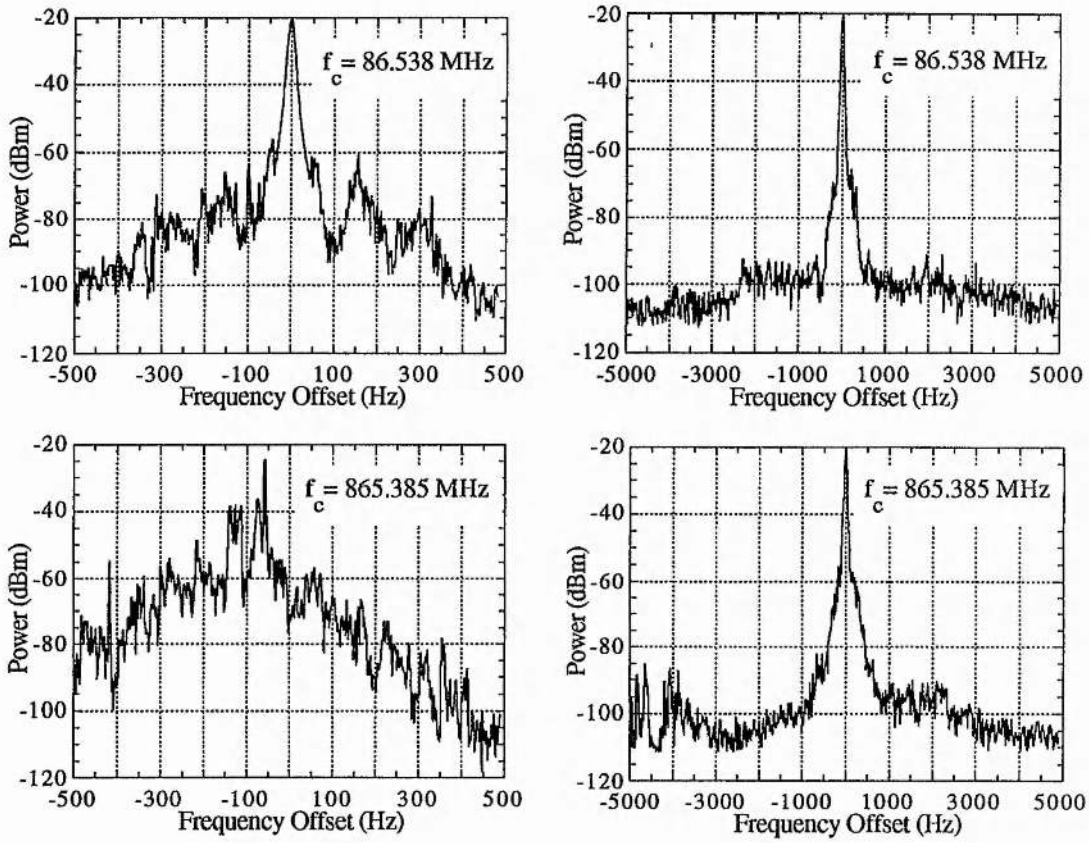


Figure 3.2a: Noise power spectra recorded from the regeneratively-initiated self-modelocked Ti:$Al_2O_3$ laser.

From these noise power spectra, it can be seen that most of the noise is concentrated at frequencies below a few kHz. This is characteristic of passively-modelocked laser systems where most of the phase noise is generated from acoustic and mechanical noise from the surrounding enviroment. The asymmetry of the noise spectra is due to frequency drift of the unlocked laser cavity during the acquisition time of the data. This in turn leads to inaccuracies in calculating the corresponding timing jitter

figures, meaning that these figures will give an upper limit to the actual phase noise present on the pulse train.

Using the data shown in figure 3.2a, the single-sideband phase noise and amplitude noise spectra were obtained and are shown in figures 3.2b and 3.2c. The pulse timing jitter figures calculated from these data were: 6.3ps (50-500 Hz) and 797fs (500 Hz-5 kHz). At frequencies above 5 kHz, the noise on the laser output had dropped to a level which represented the noise floor of the measurement system (~-130 dB).

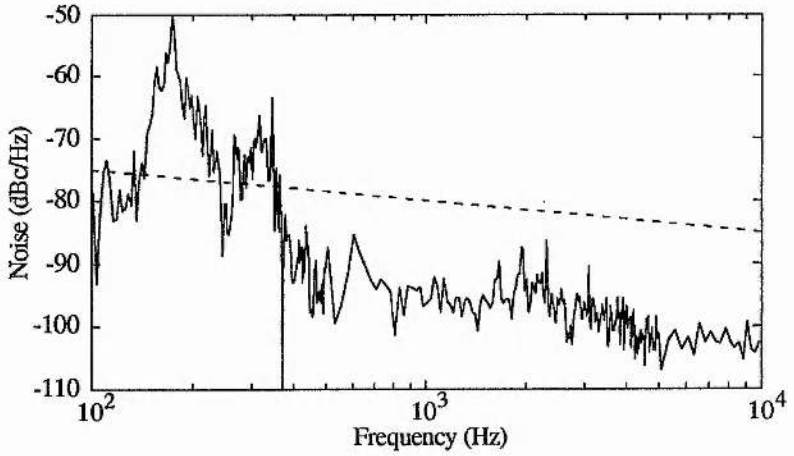


Figure 3.2b: Amplitude noise sideband of the regeneratively-initiated self-modelocked Ti:$Al_2O_3$ laser, from analysis of the laser cavity frequency and 10th harmonic.

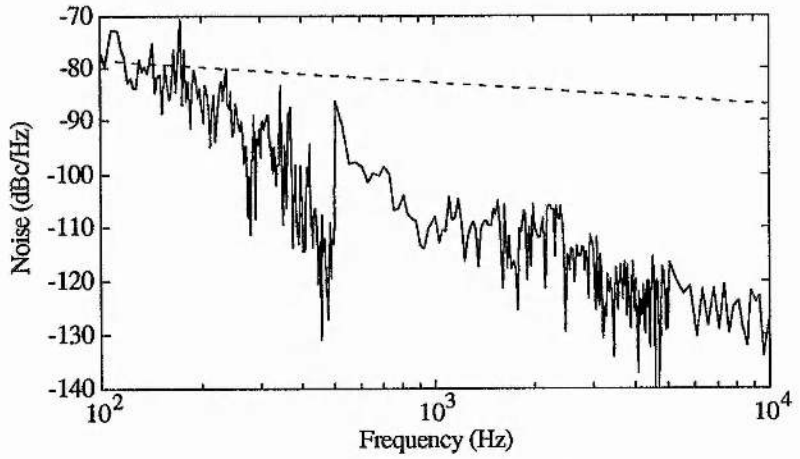


Figure 3.2c: Phase noise sideband of the regeneratively-initiated self-modelocked Ti:$Al_2O_3$ laser, from analysis of the laser fundamental frequency and 10th harmonic.

The straight dotted line present in figures 3.2b and 3.2c represents the small-signal limit of the measurement system. The small-signal approximation is only valid when the noise content of the sideband is sufficiently small so that no secondary sidebands are generated. When this limit is broken, the noise measurement technique becomes highly inaccurate.

### 3.2.2 Phase Noise Measurements on a Hard-aperture, Self-Modelocked Ti:$Al_2O_3$ Laser.

Measurements of the phase noise were also taken for the hard-aperture self-modelocked system previously described in section 2.6. When the noise measurements were recorded, this laser was typically operating at pump powers of ~3W, generating 80fs pulses with an average output power of 150mW. Again, data were obtained for the laser cavity frequency of 86 MHz and the 10th harmonic. The power spectra obtained are shown in figure 3a for spans of 10 kHz and 1 kHz, with resolution bandwidths of 30 Hz and 10 Hz respectively.

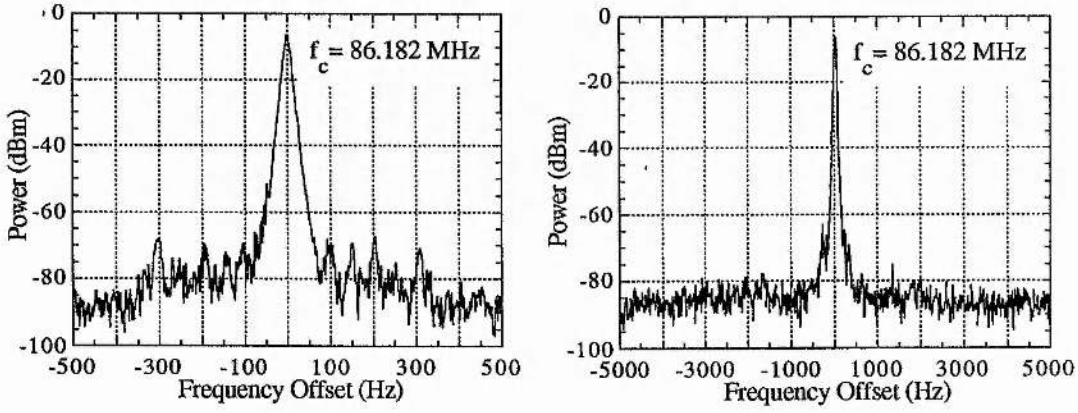

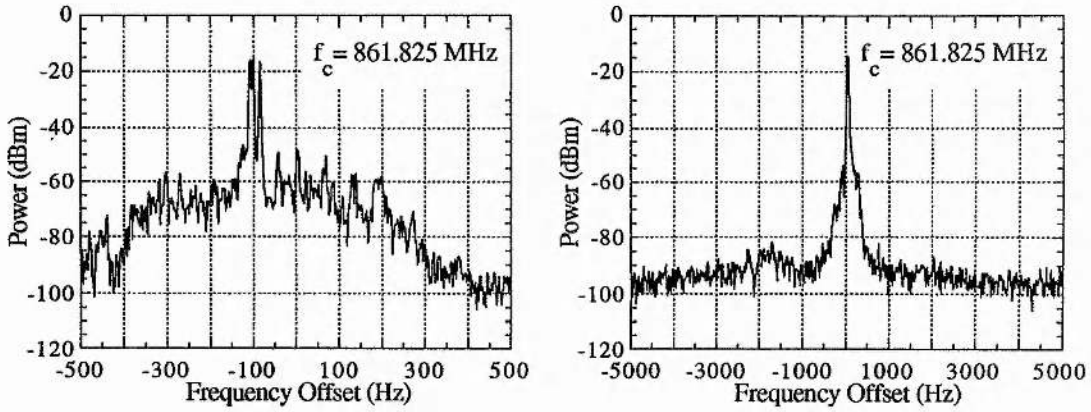


Figure 3.3a: Noise power spectra from the hard-aperture, self-modelocked Ti:$Al_2O_3$ laser.

Using these data, the single-sideband amplitude noise and phase noise spectra were obtained and are shown below in figures 3.3b and 3.3c respectively. The corresponding pulse timing jitter figures were calculated to be : 3.8 ps (50-500 Hz) and 231 fs (500 Hz-5 kHz). Again, the noise on the laser output has dropped below the noise floor of the measurement system at frequencies higher than 5 kHz.

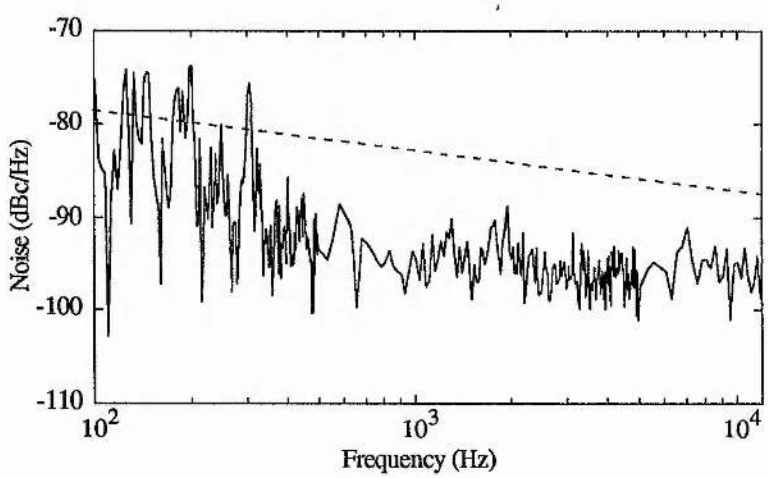


Figure 3.3b: Amplitude noise sideband of the hard-aperture self-modelocked Ti:$Al_2O_3$ laser, from analysis of the laser fundamental frequency and 10th harmonic.

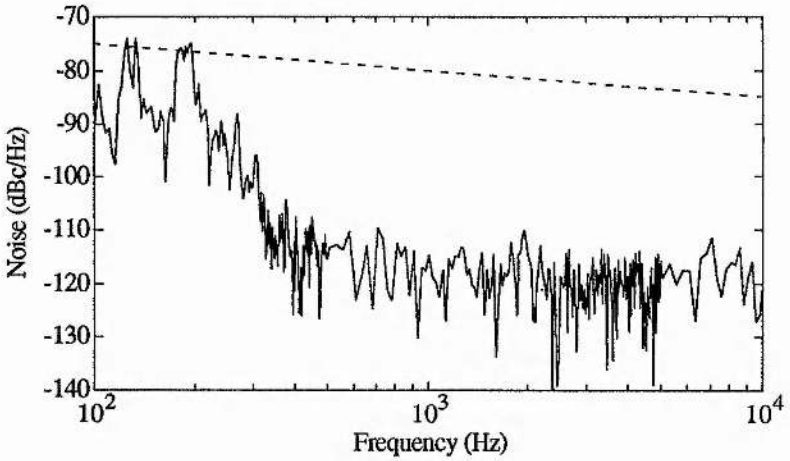


Figure 3.3c: Phase noise sideband of the hard-aperture self-modelocked Ti:$Al_2O_3$ laser, from analysis of the laser fundamental frequency and 10th harmonic.

The timing jitter figures obtained from this system were significantly better than the timing jitter figures obtained from the regeneratively-initiated, self-modelocked Ti:$Al_2O_3$ laser system. This may be due to the fact that the hard-aperture modelocked system does not rely on the use of an acousto-optic modulator and the associated electronics. Also, in "soft-aperture" self-modelocking, an aperture is created by tight focussing of the pump beam inside the laser crystal. This means that any amplitude fluctuations in the pump beam will lead to instabilities in the gain aperture which may manifest as amplitude noise on the modelocked pulse train. This amplitude noise is in turn converted into phase noise via the acousto-optic modulator drive electronics. Also, any beam-pointing instabilities from the argon-ion pump laser will manifest as phase noise on the output pulse train of a regeneratively-initiated, self-modelocked Ti:$Al_2O_3$ laser. In the case of hard-aperture self-modelocking, the necessary loss modulation required to initiate the generation of ultrashort pulses, is created by the insertion of a variable slit inside the laser cavity. Due to its fixed width and physical rigidity, this slit leads to an inherently more stable form of self-modelocked laser operation.

## 3.3 Techniques For Reducing Phase Noise.

For a passively modelocked laser, the pulse repetiton rate is determined purely from the cavity length, and so any length fluctuations lead to phase noise on the modelocked pulse train. In theory, any instability in the laser repetition rate, due to changes in the cavity length, can be corrected for by the movement of one of the end mirrors. In practice the degree of compensation is limited to the maximum distance that this mirror can travel, and the speed and accuracy of its movement. Commercially available piezo-electric translators (PZT) are well suited to correct for both frequency drift and timing jitter. In this way the pulse timing fluctuations can be reduced by using a phase-lock loop arrangement[11,12]. In this arrangement, a fast photodiode is used to monitor the laser pulse train, and the phase of one of the frequency components is compared with the output of an ultrastable electronic reference oscillator. This in turn leads to the generation of a phase error signal which is amplified, and then supplied to a PZT attached to one of the cavity end mirrors. The mirror will then move in step with any error signal leading to the stabilisation of the pulse repetition frequency.

The first attempts to reduce the phase noise of modelocked lasers was applied to actively modelocked lasers. In 1985, Cotter[13] used a phase-lock loop feedback system to reduce the phase noise on an actively-modelocked argon-ion laser. In this system, a photodide was used to monitor the pulse train and the phase of its fundamental frequency was compared with that of an ultrastable reference oscillator to generate a phase error signal. This error signal was then amplified and filtered and used to alter the phase of the modelocked driver via a voltage-controlled phase shifter. In this manner the loop continually adjusts the phase of the laser pulse train to equal that of the ultrastable reference oscillator. In Cotter's work, the phase noise on an actively-modelocked argon-ion laser was reduced from 20ps to sub-picosecond fluctuations. This technique was also successfully implemented by Rodwell[11] to reduce the phase noise on an actively-modelocked Nd:YAG laser from 20ps to 0.3ps

### 3.3.1 Reduction of Phase Noise on the Regeneratively-Initiated, Self-Modelocked Ti:$Al_2O_3$ Laser.

To reduce the phase noise on the output of our self-modelocked Ti:$Al_2O_3$ laser, we used a technique based on cavity-length stabilisation. Similar feedback techniques to those described were used to control the laser cavity repetition rate via a PZT mounted on one of the end mirrors. This technique has previously been employed in the phase noise reduction on passively-modelocked dye lasers and coupled-cavity modelocked colour centre lasers[14]. The electronic arrangement used to phase-lock the self-modelocked Ti:$Al_2O_3$ laser cavity is illustrated below in figure 3.4.

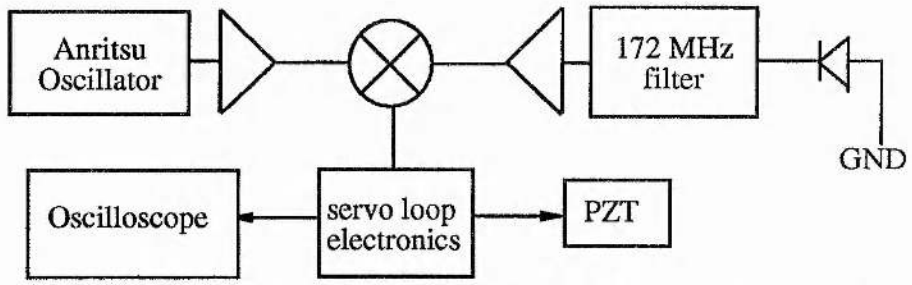


Figure 3.4: Schematic diagram of cavity locking electronics used on the regeneratively-initiated, self-modelocked Ti:$Al_2O_3$ laser operating at a pulse repetition rate of ~86 MHz.

The cavity repetition frequency was monitored using a fast photodiode (silicon PIN photodiode type BPX65). The diode signal was filtered using a 5 MHz bandpass passive filter tuned to 172 MHz, the second harmonic of the laser cavity frequency. This filtered signal was pre-amplified using a hybrid rf amplifier (Philips OM335) which typically provided a gain of 27 dB. The second rf amplifier was again a wide-band device (Motorola CA2832) which provided approximately 30 dB of gain. This signal was then compared to the signal from the ultrastable reference oscillator (Anritsu MG3632A). The phase comparator was a high level double-balanced mixer of the diode ring type (Mini-Circuits SRA-1MH) with a specified drive power of +13 dBm local oscillator and +9 dBm RF. The mixer was typically operated at input powers approximately 3 dBm above these levels in order to minimise loop jitter derived from the

200μV dc offset of the device. The mixer output signal was then amplified with variable gain and time constant before reaching a final voltage amplification stage to produce an output signal suitable to drive the PZT. The PZT provided ~15μm movement for a voltage change of 120V and had an unloaded resonant frequency of ~20 kHz.

The laser cavity configuration used for the experiment is illustrated schematically in figure 3.5. A plane mirror was attached to the PZT using cyanoacrylate adhesive. This mirror was made as small and light as possible so as not to significantly reduce the resonant frequency of the PZT.

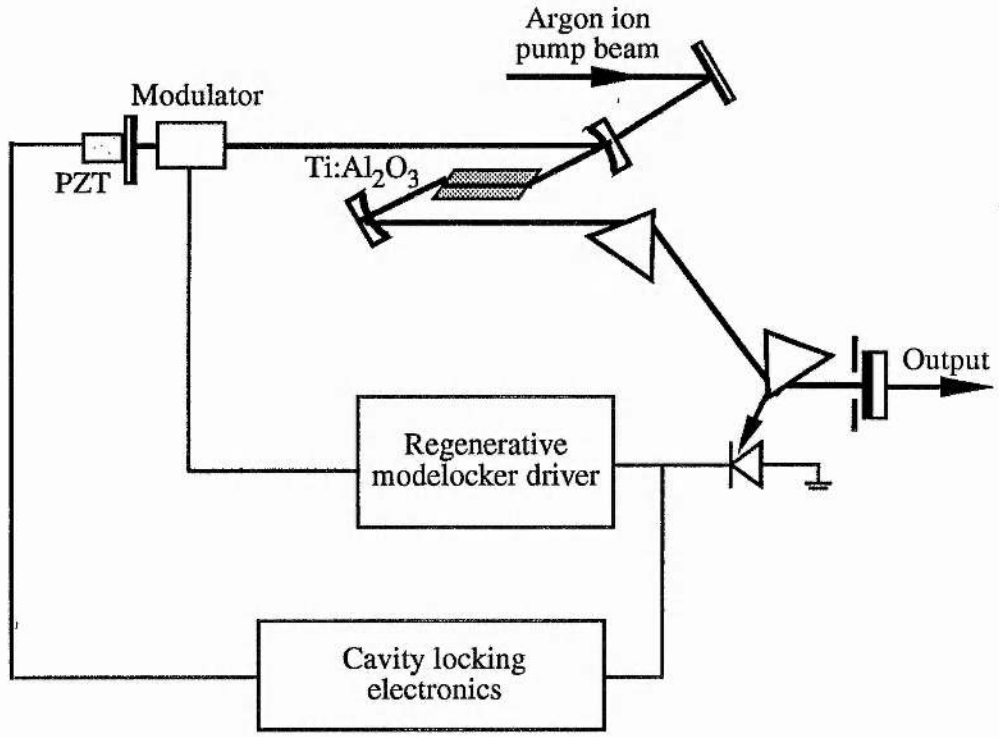


Figure 3.5: Schematic diagram of the regeneratively-initiated, self-modelocked laser.

The cavity was frequency-locked by matching the output of the reference oscillator to the second harmonic of the cavity repetition frequency and the loop was closed with the variable gain set to minimum. The gain was then slowly increased to a maximum value consistent with stable laser operation. The noise measurements for the phase-locked cavity were measured by recording the power spectra for the fundamental laser frequency

and 20th harmonic. The spectrum analyser power spectra obtained for these harmonics, for spans of 1 kHz and 10 kHz are shown below in figure 3.6a.

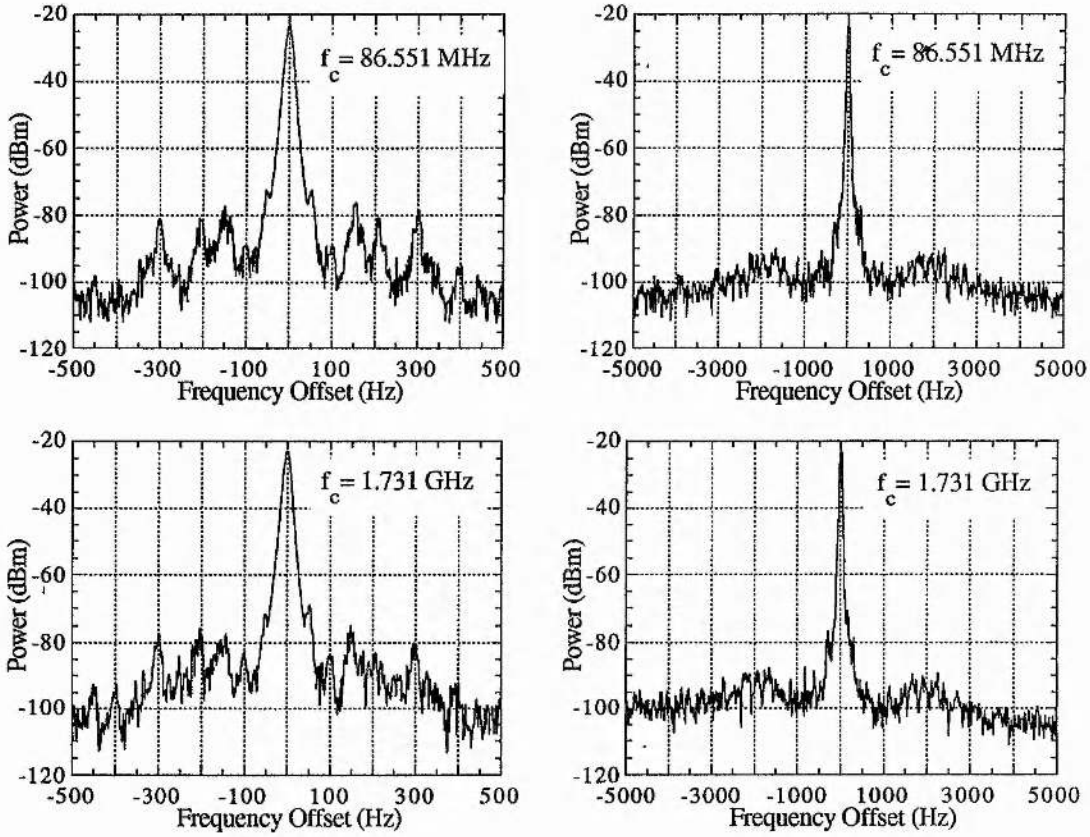


Figure 3.6a: Noise power spectra of the cavity length stabilised, regeneratively-initated self-modelocked Ti:$Al_2O_3$ laser, for the fundamental laser frequency and the 20th harmonic, when phase-locked to the 2nd harmonic.

From these results, it can be seen that there is very little difference in the noise content of the laser signal at the laser fundamental frequency compared to the 20th harmonic. This implies that the phase-noise reduction technique has been successful. By comparing the noise power spectra at the high harmonics for the unlocked (see figure 3.2a) and phase-locked laser cavities, it is apparent that the phase noise has been dramatically reduced. The structure on the noise power spectra occurs at multiples of 50 Hz, and is likely to be due to mains-induced fluctuations from the argon-ion power supply.

The corresponding phase and amplitude noise spectra are also shown below in figures 3.6b and 3.6c, and the calculated pulse timing jitter figures were: 479fs (50-500 Hz), 154fs (500 Hz-5 kHz). Again, these figures are an indication of the effectiveness of the cavity-locking electronics, as these timing jitter figures are dramatically lower than those obtained from the unlocked laser cavity (6.3ps (50-500 Hz) and 797fs (500 Hz-5 kHz)).

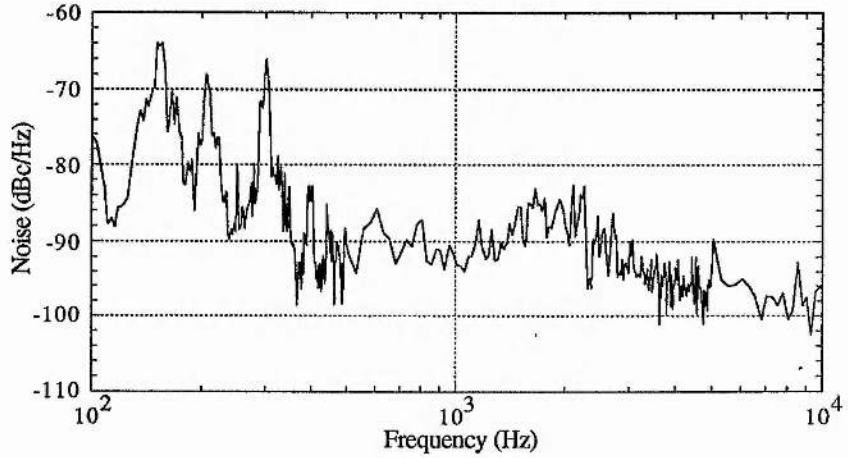


Figure 3.6b: Amplitude noise sideband of the cavity length stabilised, regeneratively-initiated, self-modelocked Ti:$Al_2O_3$ laser, when locked to the 2nd harmonic.

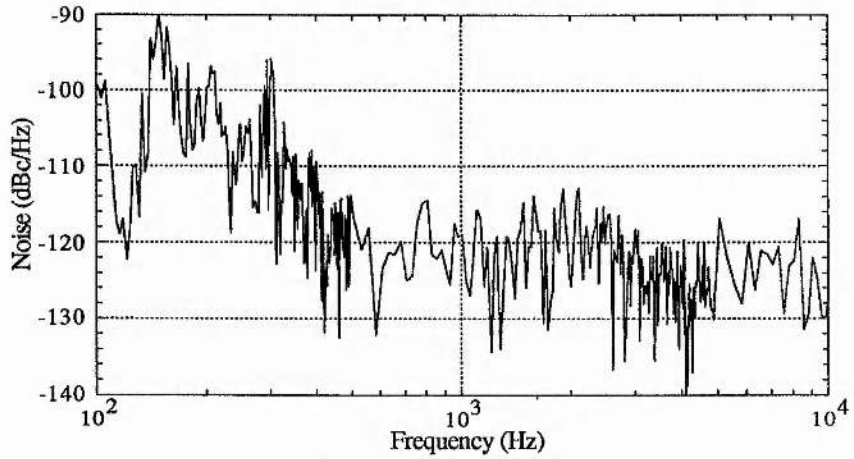


Figure 3.6c: Phase noise sideband of the cavity length stabilised, regeneratively-initiated, self-modelocked Ti:$Al_2O_3$ laser, when locked to the 2nd harmonic.

By comparison of the phase noise sideband from the unlocked laser cavity (see figure 3.2c) and that from the frequency-locked laser cavity (see figure 3.6c, above), the low

frequency noise level has dropped from approximately -80 dBc/Hz to -100 dBc/Hz. This is in keeping with the reduction in the respective timing jitter figures obtained.

In an attempt to increase the sensitivity of the phase-lock loop to the timing jitter on the laser output, it was decided to use the 10th harmonic of the laser frequency to drive the mixer. This was achieved by replacing the 173 MHz filter with an equivalent filter tuned to 866 MHz. When the laser was phase-locked to the reference oscillator at 866 MHz, the power spectra of the fundamental laser frequency and 30th harmonic were recorded on the spectrum analyser and are reproduced in figure 3.7a.

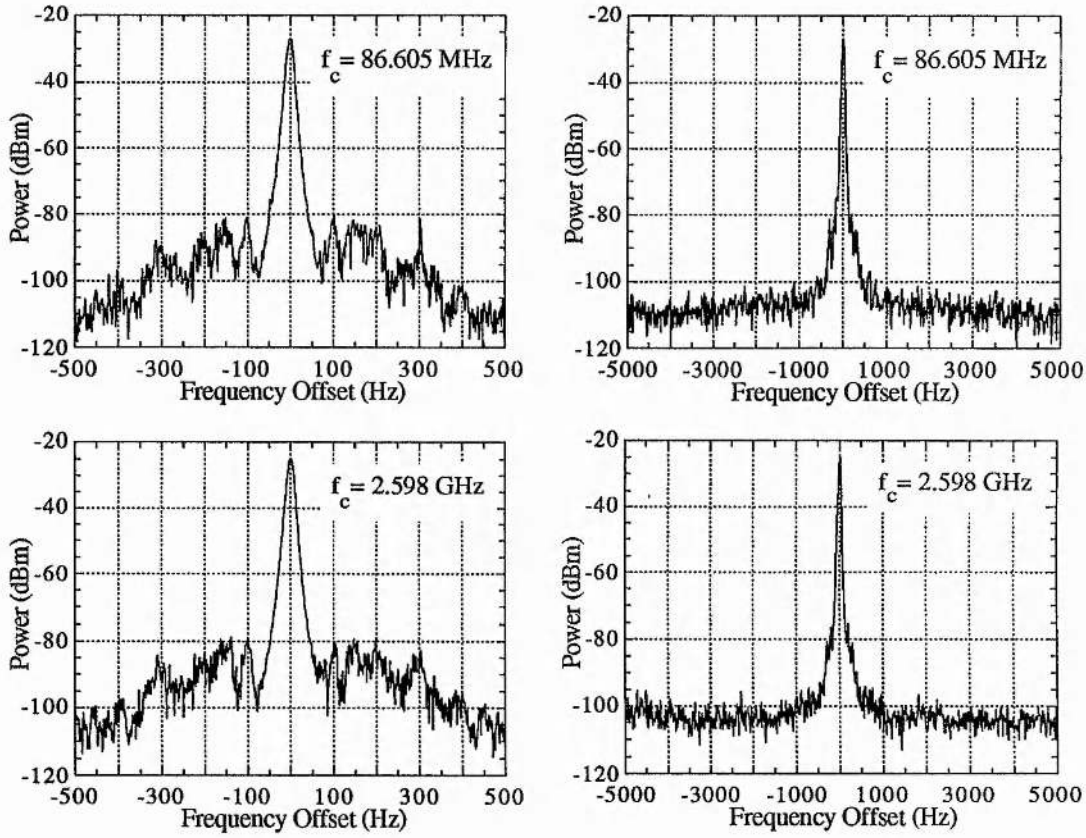


Figure 3.7a: Noise power spectra of the regeneratively-initiated, self-modelocked laser locked to the 10th harmonic, for the fundamental laser frequency and the 30th harmonic.

By comparing figures 3.7a and 3.6a, it can be seen that the noise content of the laser output at the 30th harmonic, is as good as the 20th harmonic when locked to the 2nd

harmonic. As expected, this means that phase-locking the laser cavity to the 10th harmonic leads to a further reduction in phase noise on the laser output.

From the noise power spectra obtained for the laser fundamental frequency and the 30th harmonic, the corresponding amplitude noise and phase noise spectra were calculated and are shown below in figures 3.7b and 3.7c, respectively. The resulting pulse timing jitter figures were calculated to be: 303fs (100-500 Hz), 93fs (500 Hz- 5 kHz).

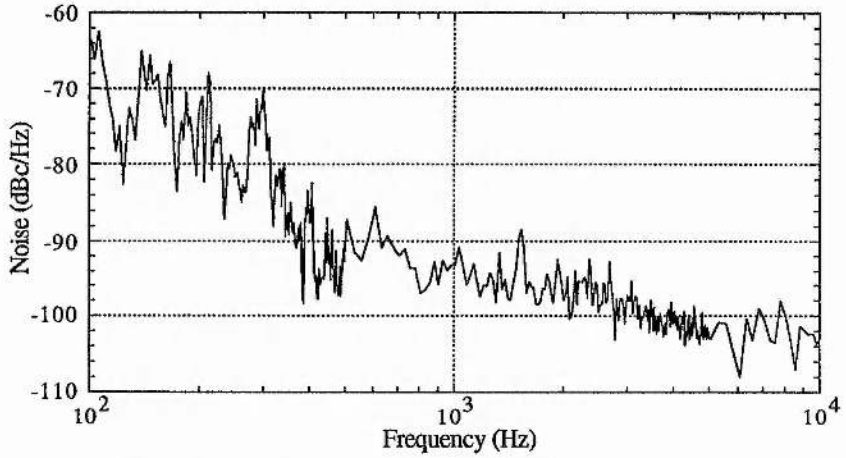


Figure 3.7b: Amplitude noise sideband of the regeneratively-initiated, self-modelocked laser locked to the 10th harmonic.

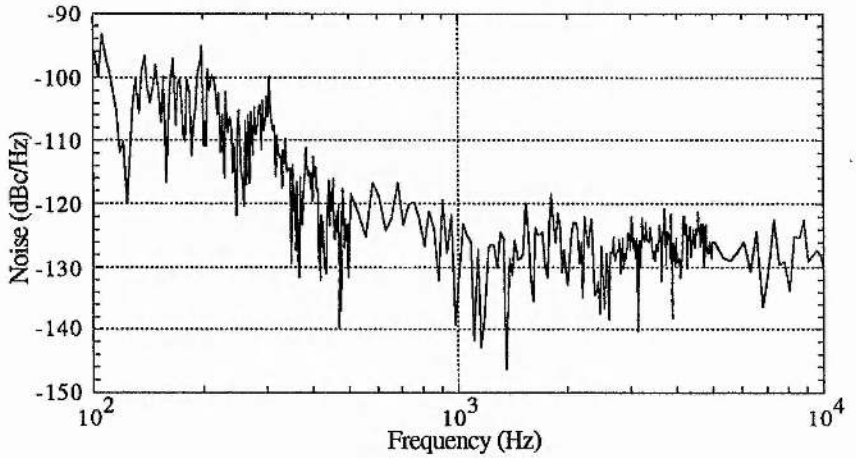


Figure 3.7c: Phase noise sideband of the regeneratively-initiated, self-modelocked laser locked to the 10th harmonic.

In a further attempt to improve the stability and noise characteristics of the regeneratively-initiated, self-modelocked Ti:$Al_2O_3$ laser output, it was decided to employ an acousto-optic modulator (as a "noise-eater") to eliminate the amplitude noise on the pump beam. The modulator was inserted into the argon-ion pump beam before the Ti:$Al_2O_3$ laser. It was then biased so as to deflect ~20% of the power out of the zeroth order and this deflected signal was used as the pump beam. The remaining power in the zeroth order was monitored using a photodiode and this signal was fed into an electronic servo loop. This signal was used to drive the acousto-optic modulator, enabling the diffraction efficiency of the modulator to be varied. When the servo loop was closed, the system acted as a "noise-eater" by varying the amount of optical power diffracted into the laser pump beam. Any amplitude fluctuations in the output of the argon-ion laser where corrected for by the modulator, keeping the Ti:$Al_2O_3$ laser pump beam at a constant level.

When the noise-eater was placed in the argon-ion beam, the Ti:$Al_2O_3$ laser did not operate properly due to beam distortion. At low pump powers, the output beam from the noise-eater was a uniform $TEM_{00}$ mode, but the Ti:$Al_2O_3$ laser was below threshold. When the pump power was increased to a reasonable operating power of ~3W, the transverse mode of the argon-ion laser beam became badly distorted. This was due to thermal lensing in the modulator material. It was therefore decided to place the noise-eater in the output beam of the Ti:$Al_2O_3$ laser. Although this will not improve the actual noise present inside the laser cavity, it will act to clean up the output of the laser, and produce a clean beam for streak camera analysis. Noise measurements was taken with the noise-eater in, and with the laser locked to the 10th harmonic. The noise power spectra are shown below in figure 3.8a for the laser fundamental frequency and 30th harmonic, at spans of 10 kHz and 1 kHz.

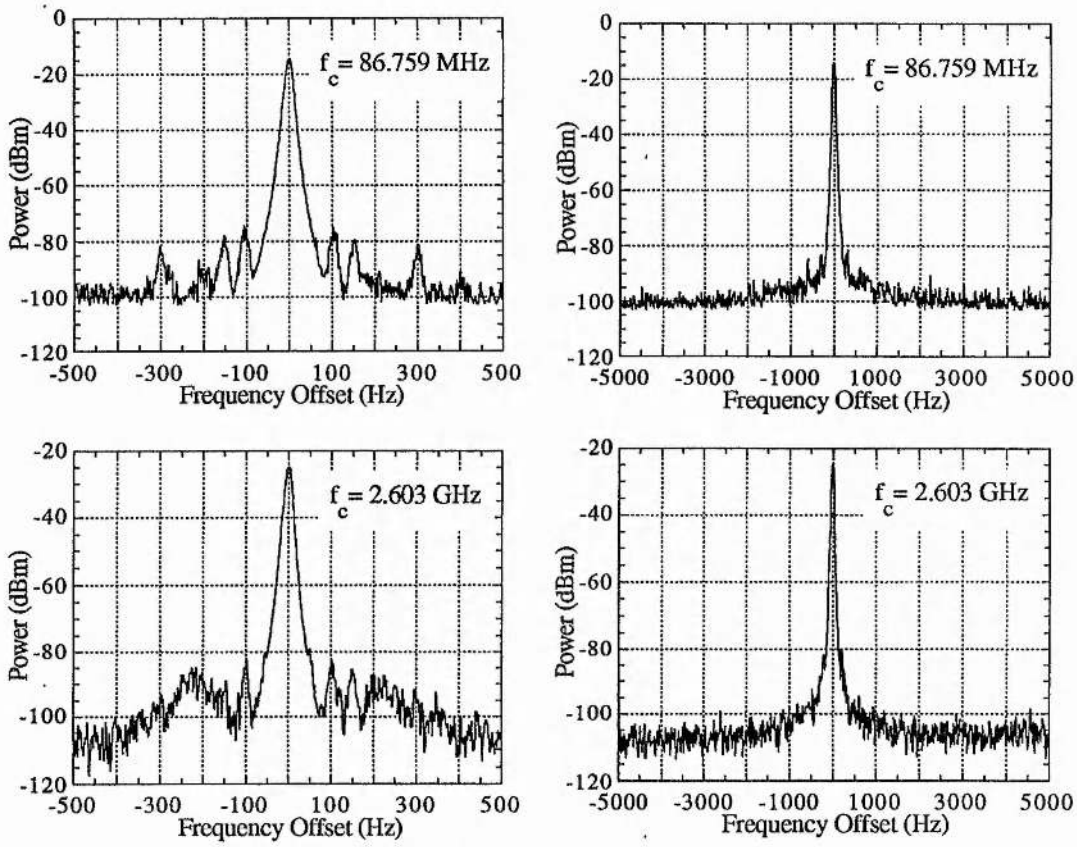


Figure 3.8a: Noise power spectra of the regeneratively-initiated, self-modelocked laser locked to the 10th harmonic with a noise-eater inserted in the output.

Figures 3.8b and 3.8c show the single-sideband amplitude noise and phase noise plots, respectively.

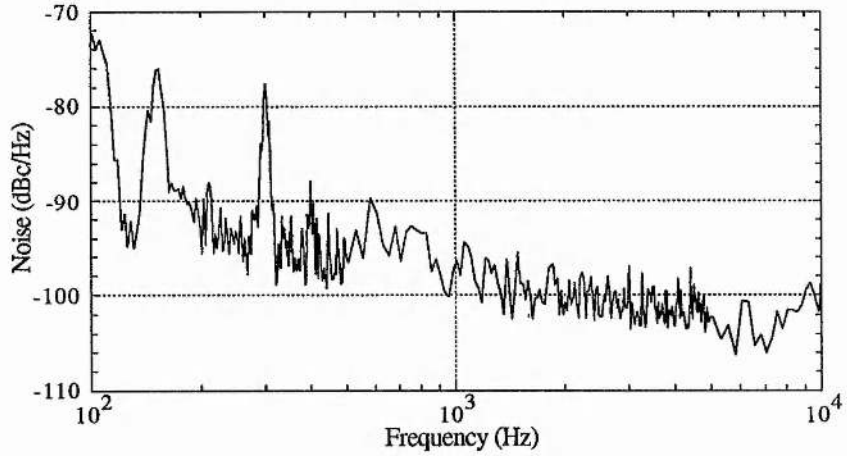


Figure 3.8b: Amplitude noise sideband from the regeneratively-initiated, self-modelocked laser with a noise-eater inserted in the output beam.

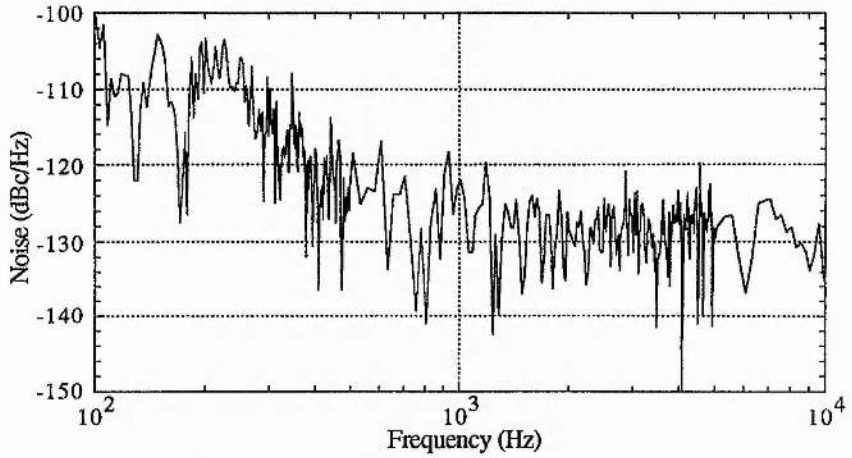


Figure 3.8c: Phase noise sideband from the regeneratively-initiated, self-modelocked laser with a noise-eater placed in the output beam.

The corresponding timing jitter figures using the fundamental and 30th harmonics were calculated to be: 174fs (50-500 Hz), 76fs (500 Hz- 5 kHz). This represents the lowest timing jitter figures ever obtained from this laser configuration. As well as the improved timing jitter figures, comparison of figures 3.7b and 3.8b shows that the noise-eater has indeed lead to a reduction in the amplitude noise on the laser output. This in turn leads to an improvement on the phase noise. This is due to the fact that the phase-lock loop will be more effective since a reduction in amplitude noise leads to a reduction in the production of amplitude-to-phase noise conversion in the balance mixer.

Table 3.1 shows a summary of the jitter figures obtained from the different phase-locked cavity configurations. It can be seen that actively stabilising the cavity repetition frequency greatly reduces the phase noise on the laser output. Also, the higher the harmonic used in the phase-lock arrangement, the greater the phase noise reduction.

| Frequency | Unlocked | Locked to 2nd Harmonic | Locked to 10th Harmonic | Locked to 10th + Noise- Eater |
|---|---|---|---|---|
| 50 - 500 Hz | 6.3 ps | 479 fs | 303 fs | 174 fs |
| 500 Hz -5 kHz | 797 fs | 154 fs | 93 fs | 76 fs |

Table 3.1: Experimental timing jitter figures for the regeneratively-initiated, self-modelocked Ti:$Al_2O_3$ laser.

From the theory developed by Haus and Mecozzi [10], we are able to calculate the expected phase noise spectra based only on the effects of quantum mechanical spontaneous emission. A consideration of how close the experimentally measured characteristics are to the quantum limit can then provide information on the success of the stabilisation technique employed. The theoretical expression for the timing jitter spectral density $S_J(f)$ of a passively modelocked laser can be obtained from equation 69 of reference 10:

$$S_J(f) = \Omega_0^2\left[\frac{4D^2}{T_R{}^2}\left(\frac{D_p}{(2\pi f)^2((2\pi f)^2+\tau_p{}^{-2})}\right)+\frac{D_t}{(2\pi f)^2}\right] \quad [3.10]$$

where: $\tau_p = \dfrac{3T_R\Omega_g{}^2\tau^2}{4g}$

$$D_p = \frac{2}{3\omega_0\tau^2}\vartheta\frac{2g}{T_R}h\upsilon$$

$$D_t = \frac{\pi^2\tau^2}{3\omega_0}\vartheta\frac{2g}{T_R}h\upsilon$$

The laser frequency f is in Hz, $T_R$ is the pulse repetition period, $\Omega_O=2\pi/T_R$ and D is the net cavity group velocity. The saturated gain is denoted by g and the gain bandwidth by $\Omega g$. $\tau$ is the 1/e pulse duration, $\omega_0$ is the intracavity pulse energy and $\theta$ is the noise enhancement factor which can be taken as unity for most four-level laser systems. This expression for the timing jitter spectral density applies to passively modelocked lasers in the absence of any timing stabilisation scheme. Thus given the appropriate laser parameters it is relatively straightforward to generate theoretical timing jitter spectra for comparison with experimental data. Figure 3.9 shows the experimentally measured phase noise spectrum and the corresponding theoretical limit which is shown as a dashed line in the case of the unlocked laser (no active stabilisation).

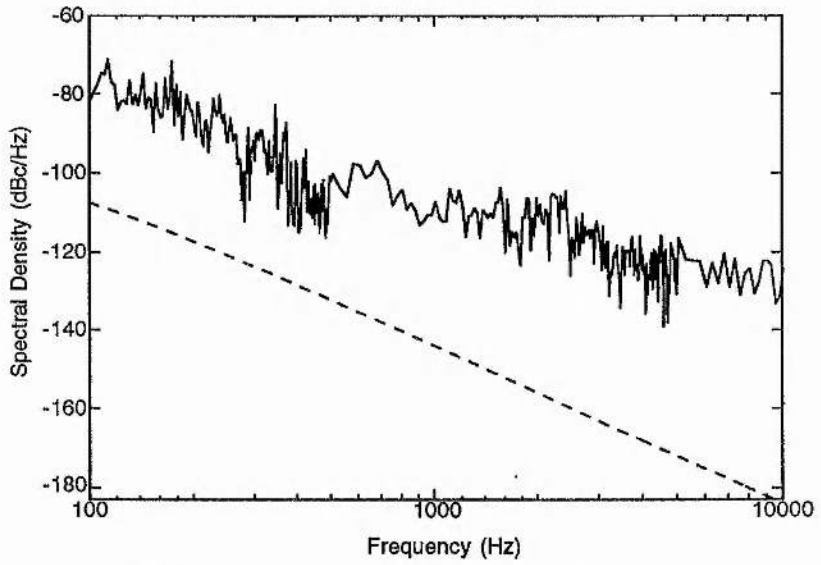


Figure 3.9: Single sideband phase noise spectrum for the unlocked, regeneratively-initiated, self-modelocked Ti:$Al_2O_3$ laser (dashed line represents the theoretical quantum limit).

The laser parameters used in the calculation of the theoretical limit were estimated to be $\lambda$=840nm, g=0.02, $\Omega_g=1.1\times10^{15}s^{-1}$, $T_R$=11.6ns, $\tau$=57fs, $\omega_o$=60nJ, $\tau_p$=1.9ms and D=500$fs^2$. It should be noted that the noise floor of the detection system did not allow a meaningful comparison between the experimental results and the theoretical limit at frequencies greater than 5 kHz. As is shown from figure 3.9, the experimentally measured noise spectrum was approximately 20 dB above the quantum limit. In terms of

rms timing jitter, the experimental results correspond to a jitter of 3.4ps (100-500 Hz) and 800fs (500-5000 Hz) while the theoretical limits are significantly lower, with values of 70fs (100-500 Hz) and 9fs (500-5000 Hz).

In the presence of active retiming of the laser pulse train, equation 3.10 is modified to give (c.f equation 108 reference 10):

$$S_J(f) = \Omega_0^2\left[\frac{4D^2}{T_R^2}\left(\frac{D_p}{((2\pi f)^2+\tau_s^{-2})((2\pi f)^2+\tau_p^{-2})}\right)+\frac{Dt}{(2\pi f)^2+\tau_s^{-2}}\right] \qquad [3.11]$$

where $\tau_s$ is the decay time of the timing fluctuations.

Figure 3.10 shows the experimentally measured phase noise spectrum and the corresponding modified theoretical quantum limit calculated using equation 3.11, which is shown as a solid line.

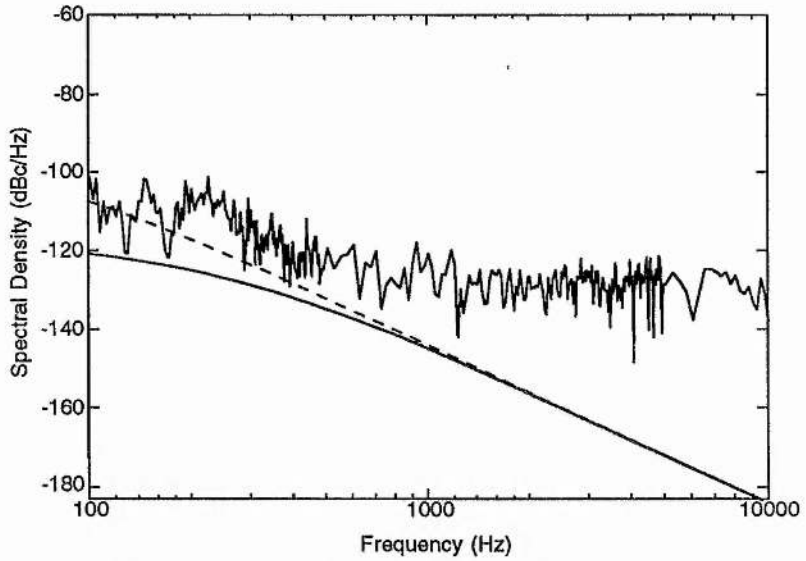


Figure 3.10: Single sideband phase noise spectrum for the phase-locked, regeneratively-initiated, self-modelocked Ti:$Al_2O_3$ laser.

In the case of the cavity frequency-locked laser system with the noise-eater inserted, the experimentally measured timing jitter figures were 150fs (100-500 Hz) and 80fs (500-5000 Hz). The corresponding quantum-limited timing jitter figures were

calculated to be: 24fs (100-500 Hz) and 7fs (500-5000 Hz). It is clear that the active cavity stabilisation scheme further reduced the phase noise spectrum by more than 20dB and the experimentally measured spectrum is comparable with the purely passively modelocked quantum limit which is shown as the dashed line.

### 3.3.2 Reduction of Phase Noise on the Hard-Aperture Self-Modelocked Ti:sapphire Laser.

To reduce the phase noise on the hard-aperture, self-modelocked Ti:$Al_2O_3$ laser, cavity length stabilisation techniques were employed as shown schematically in figure 3.11. This set-up was identical to the phase-lock loop arrangement used on the regeneratively-initiated, self-modelocked Ti:$Al_2O_3$ laser system described in section 3.3.1.

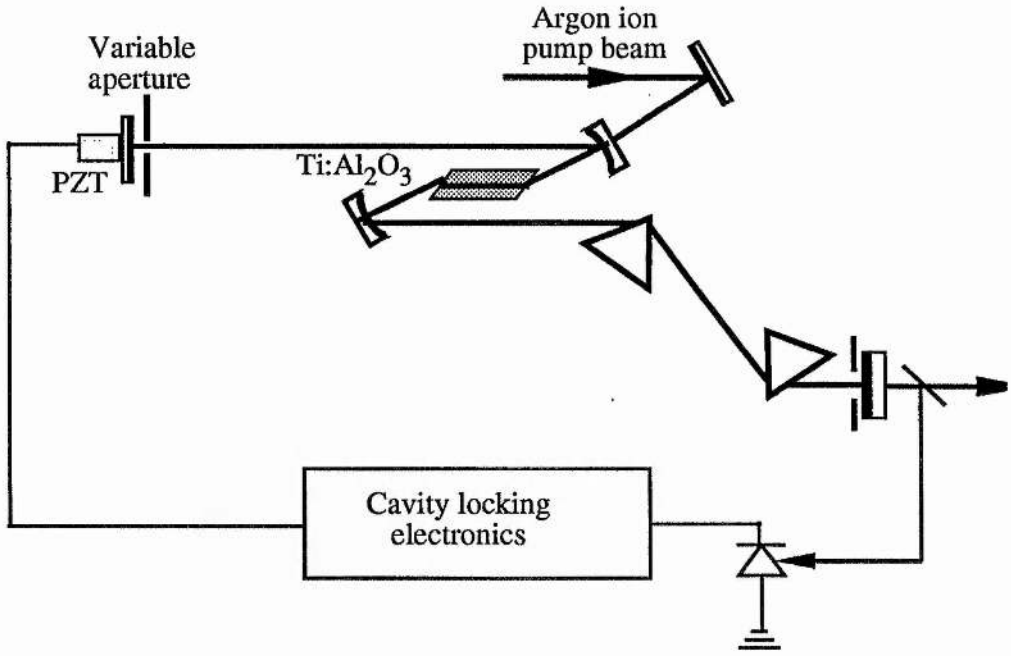


Figure 3.11: Schematic diagram of the hard-aperture, self-modelocked Ti:$Al_2O_3$ laser using cavity length stabilisation set-up.

In order to reduce the phase noise on the output of the laser, the cavity frequency was locked to that of an ultrastable reference electronic oscillator operating at ~173 MHz, the second harmonic of the cavity repetition frequency. The noise measurements for the phase-locked cavity were calculated by recording the power spectra for the fundamental and 20th harmonic. The power spectra obtained for these harmonics, for spans of 1 kHz and 10 kHz are shown below in figure 3.12a.

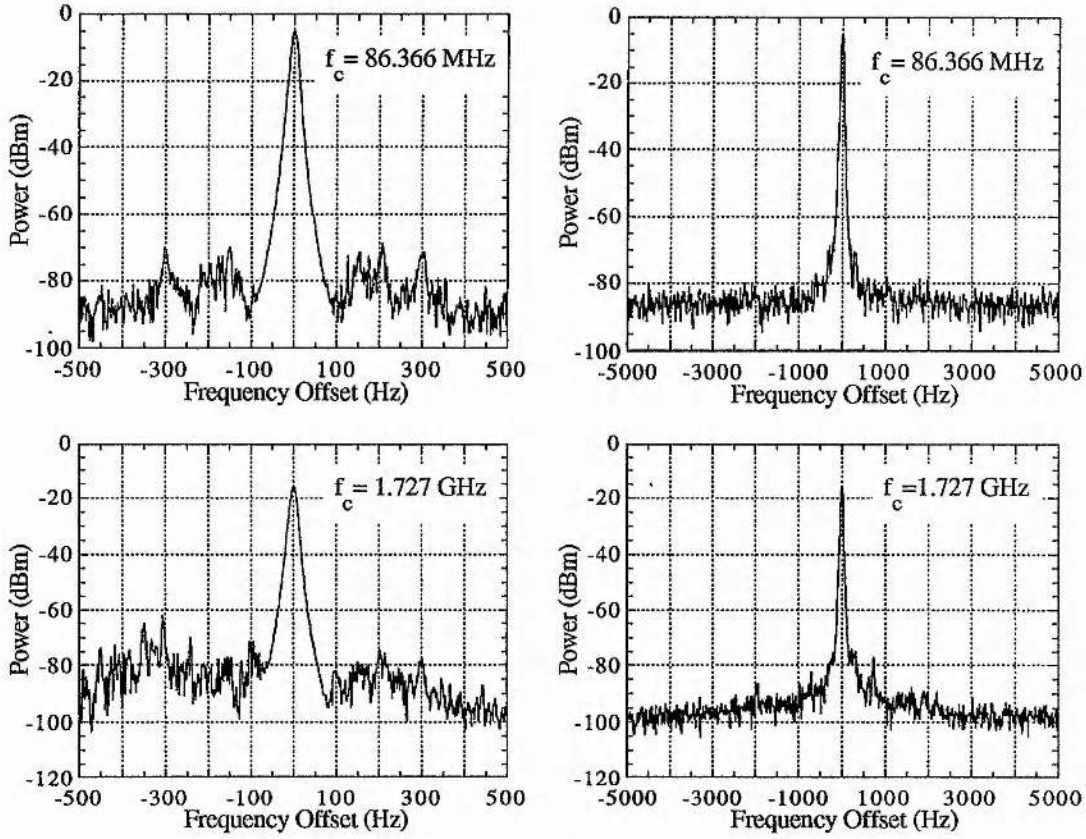


Figure 3.12a: Noise power spectra of the hard-aperture self-modelocked Ti:$Al_2O_3$ laser locked to the 2nd harmonic for the laser fundamental frequency and 20th harmonic.

Using these data, the single-sideband amplitude noise and phase noise spectra were obtained and are shown in figures 3.12b and 3.12c respectively. The corresponding pulse timing jitter figures were calculated to be: 230fs (50Hz - 500Hz) and 174fs (500Hz - 5kHz). Again, the noise on the laser output had dropped below the noise floor of the measurement system at frequencies higher than 5 kHz.

By comparison with the similar results recorded for the regeneratively-intiated self-modelocked laser (see figure 3.6b), the amplitude noise figure on the hard-aperture self-modelocked system is approximately 10dB lower. Also the phase noise sideband is reduced compared to figure 3.6c. These results are in keeping with the calculated timing jitter figures which are significantly better than the regeneratively-initiated system (479fs (500-500Hz) and 154fs (500-5000Hz)).

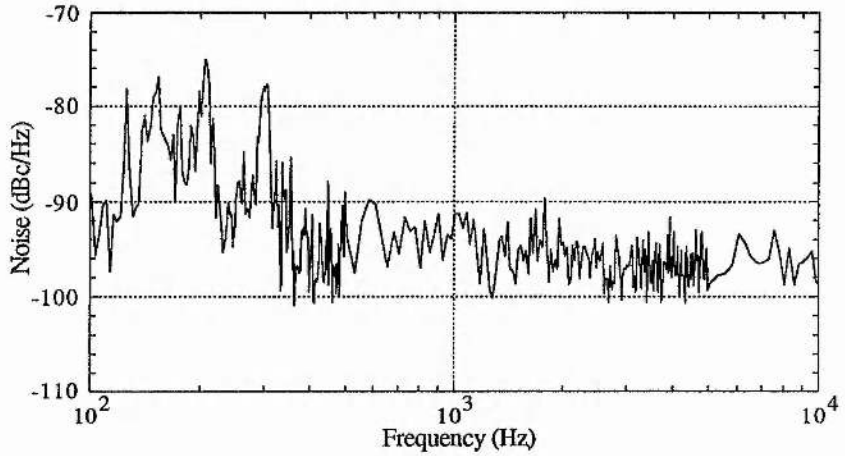


Figure 3.12b: Amplitude noise sideband of the hard-aperture self-modelocked laser locked to the 2nd harmonic.

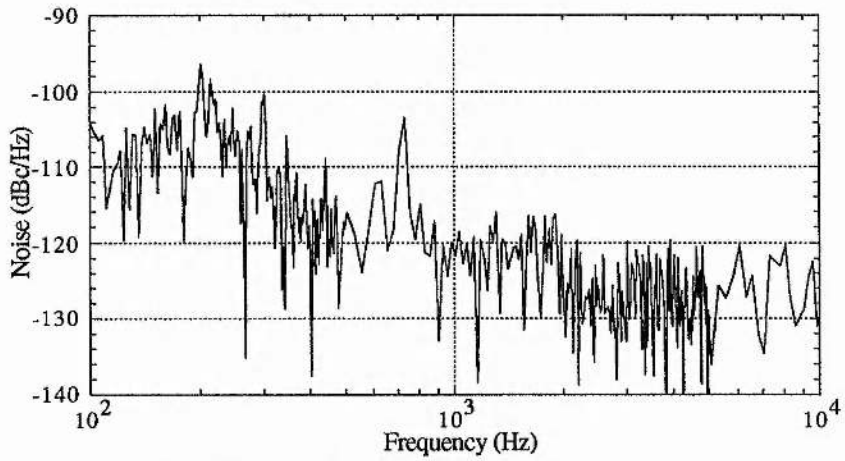


Figure 3.12c: Phase noise sideband of the hard-aperture, self-modelocked laser locked to the 2nd harmonic.

Again, to increase the sensitivity of the phase-lock loop to the timing jitter on the laser output, the 10th harmonic of the laser frequency was used to drive the mixer. When

the laser was phase-locked to the reference oscillator at the 10th harmonic, the power spectra of the fundamental laser frequency and 20th harmonic were measured and are shown below in figure 3.13a.

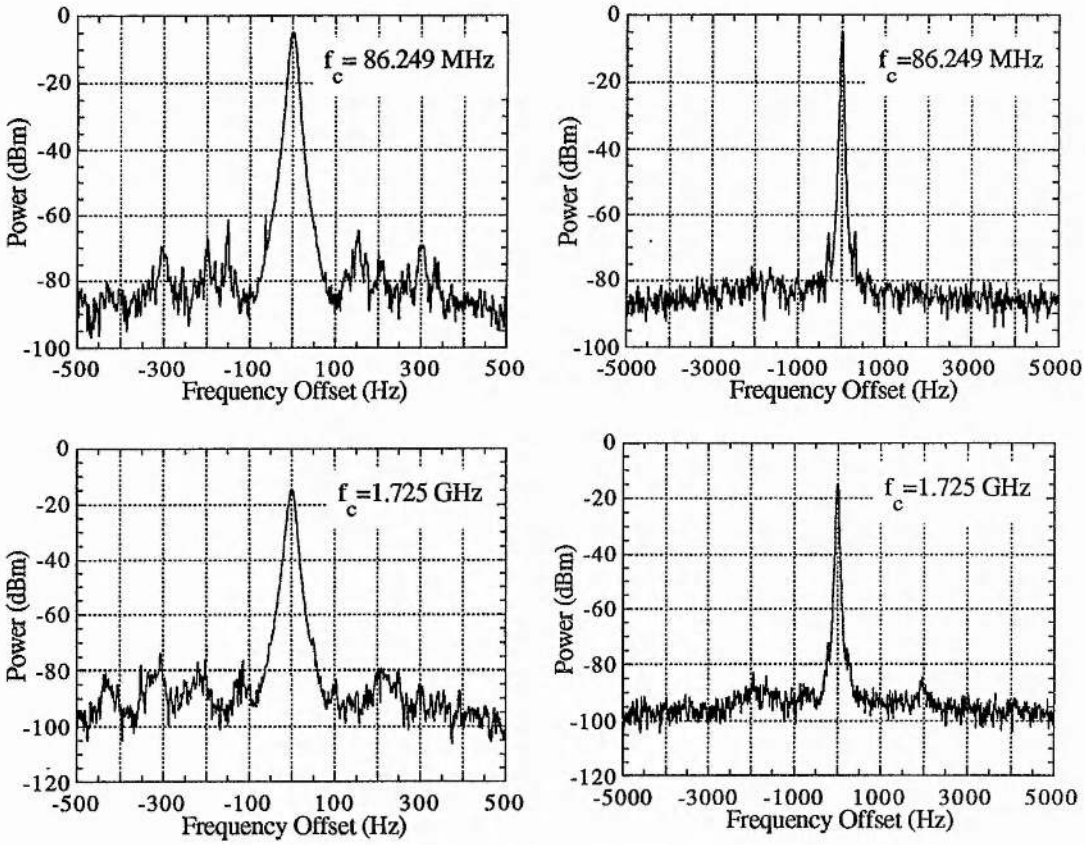


Figure 3.13a: Noise power spectra of the hard-aperture self-modelocked laser locked to the 10th harmonic, for the laser fundamental frequency and 20th harmonic.

Figures 3.13b and 3.13c show the corresponding single-sideband amplitude noise and phase noise plots. These gave a single-sideband noise spectrum corresponding to a pulse timing jitter of: 214fs (50-500Hz) and 120fs (500Hz-5kHz). Again, these timing jitter figures are significantly better than those obtained from the regeneratively-initiated, self-modelocked laser system (303fs (50-500 Hz, 93fs (500 Hz-5 kHz)).

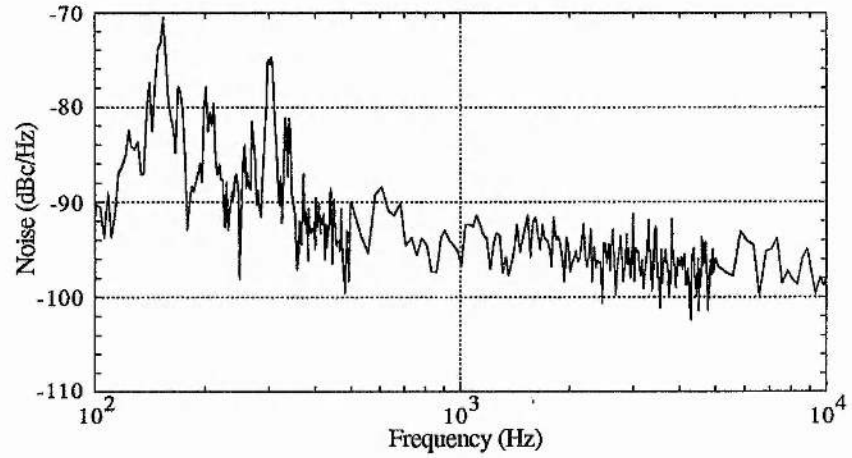


Figure 3.13b: Amplitude noise sideband for the hard-aperture, self-modelocked Ti:$Al_2O_3$ laser locked to the 10th harmonic.

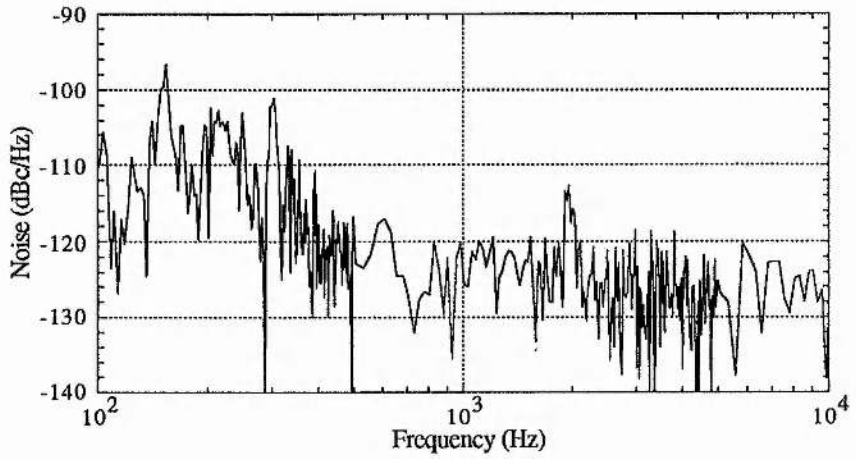


Figure 3.13c: Phase noise sideband for the hard-aperture, self-modelocked Ti:$Al_2O_3$ laser locked to the 10th harmonic.

Table 3.2 shows a summary of the timing jitter figures obtained for the different phase-lock configurations for the hard-aperture, self-modelocked Ti:$Al_2O_3$ laser.

| Frequency Band | Unlocked | Locked to 2nd Harmonic | Locked to 10th Harmonic |
|---|---|---|---|
| 50 - 500 Hz | 3.8 ps | 230 fs | 214 fs |
| 500 Hz - 5 kHz | 231 fs | 174 fs | 120 fs |

Table 3.2: Timing jitter figures for the hard-aperture, self-modelocked Ti:$Al_2O_3$ laser.

From this table it is clear that the phase noise reduction techniques have been successful and by comparison with Table 3.1 in section 3.3.1, it can be seen that the hard-aperture self-modelocked system is much more stable and less noisy than the regeneratively-initiated system.

## 3.4 Electron-Optical Streak Camera Measurements.

Despite having limiting time resolutions somewhat inferior to those of nonlinear optical techniques, electron-optical streak cameras have now become widely used for the measurement of ultrafast light phenomena. This is mainly due to their ability to directly measure the intensity profile of a light pulse, as a function of time over a wide spectral range. In applications such as the studies of modelocked lasers, optical communications, photobiology, solid-state physics and biomedical diagnostics, where the input light signal is repetitive and often very weak, synchroscan operation of a streak tube is becoming a very attractive diagnostic tool.

Up until now, the best time resolution available from an experimental streak camera is reported to be ~1ps[3], and is in the range of 2-5ps for commercially available cameras. To try and improve on these cameras, a new prototype has been designed at St. Andrews University, called Photochron V[15]. The design was carried out by

computational methods, and emphasis was directed at the different ways of minimising the physical factors which limit the temporal resolution. Recent theoretical analysis of this new streak tube has predicted a limiting timing resolution of ~500fs, but up until now an experimental temporal resolution of only 2ps has been achieved. The characterisation of previous streak tubes in synchroscan operation has shown that apart from the limiting timing resolution of the tube itself, the amplitude noise and phase noise on the laser pulse train, and intrinsic noise in the electronic circuitry used to drive the camera, also present significant limitations to its overall performance. Therefore, for a synchronously-operating streak camera to reliable operate in the femtosecond regime, it is important to use a laser system which exhibits a minimal amount of noise.

An electron-optical streak camera is also a useful tool for determining the upper limit of the timing jitter on a modelocked laser output. Because the phase noise reduction system employed on our self-modelocked Ti:$Al_2O_3$ laser systems was so successful, the measurement system was unable to accurately determine the exact timing jitter figures. However, by measuring the laser pulse duration using a streak camera it is possible to deduce the overall timing jitter on the laser. Therefore, in order to confirm the timing jitter figures previously measured from the regeneratively-initiated, self-modelocked Ti:$Al_2O_3$ laser system, the prototype Photochron V streak camera was used to measure the laser pulse duration. These measurements were also used to evaluate the temporal resolution of the camera, in an attempt to obtain a timing resolution in the sub-picosecond regime.

The laser system used was the cavity length-stabilised, regeneratively-initiated self-modelocked Ti:$Al_2O_3$ laser system previously described in section 3.3.1. For the laser pulses to arrive at the streak camera with a known seperation, an optical delay was used in the form of a glass microscope slide. This glass slide was 1.1mm thick, which provided a delay of 11ps between pulse images reflected off the front and back surfaces. The experimental set-up is shown schematically in figure 3.14. The streak images were recorded on a vidicon-based readout system (B&M Type OSA 500).

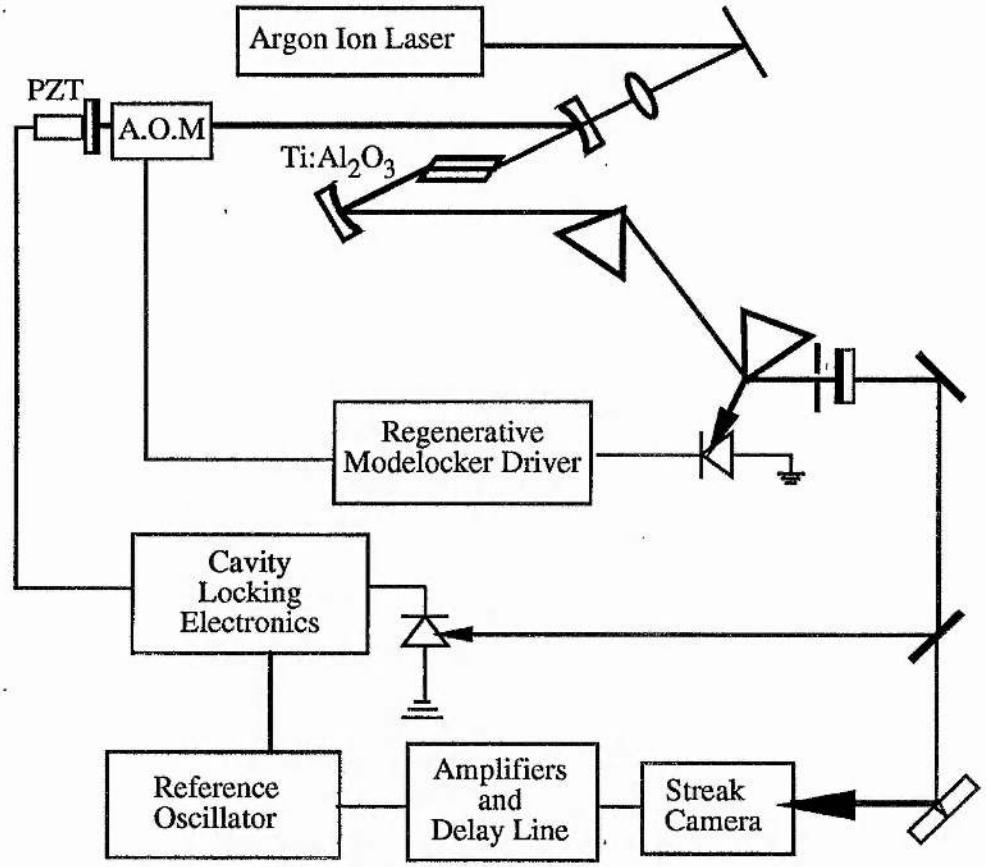


Figure 3.14: Schematic diagram showing experimental set-up for streak camera measurements.

Initially, the streak camera deflection signal was produced by an electrical signal from a tunnel diode, which was amplified using a wide band pre-amplifier followed by a narrow band, high power amplifier. This provided a deflection signal power of up to 20W. Using this scheme, temporal resolutions of 3.8ps (real-time) and 3.2ps (1ms shutter) were obtained from the streak camera . The streak camera was then driven directly from the electronic reference oscillator, rather than from the tunnel diode, and a slight improvement in the time resolution was obtained. A typical result was ~3ps (real-time) and ~2ps (1ms shutter) as shown in figures 3.15(a) and 3.15(b) respectively. These results were obtained when the pulse repetition frequency was locked to the electronic reference oscillator which was set to operate at 172.35 MHz, i.e twice the cavity frequency.

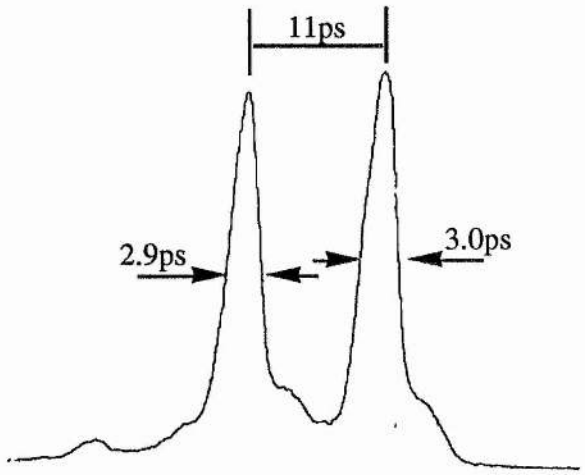


Figure 3.15a: Calibrated streak-intensity profile of a 100fs pulse from the regeneratively-initiated, self-modelocked Ti:$Al_2O_3$ laser.

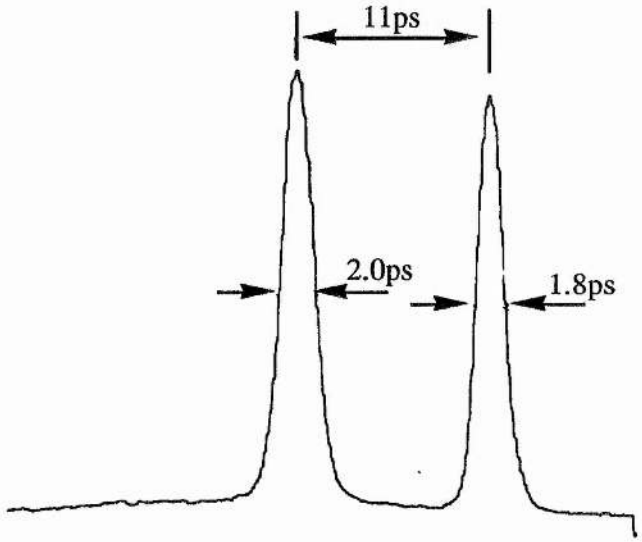


Figure 3.15b: Calibrated streak-intensity profile of a 100fs pulse from the regeneratively-initiated, self-modelocked Ti:$Al_2O_3$ laser.obtained using a 1ms shutter.

In this configuration, the signal for the cavity locking electronics was derived from the same photodiode that provided the signal for the regenerative modelocker. It was apparent that feedback from the electronic circuits in the modelocker driver was inducing noise in the mixer. Therefore, a separate fast photodiode with a low ripple power supply was used to provide a signal for the cavity locking scheme. This change resulted in a significant improvement in the overall performance of the system and

temporal resolutions of 1.5ps (real-time) and 0.9ps (1ms shutter) were achieved as shown in figures 3.16(a) and 3.16(b), respectively.

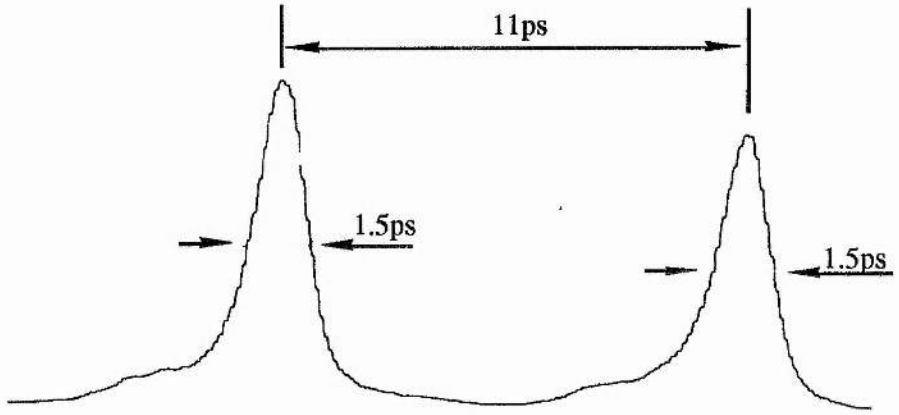


Figure 3.16a: Calibrated streak-intensity profile of a 100fs pulse from the regeneratively-initiated, self-modelocked Ti:$Al_2O_3$ laser.

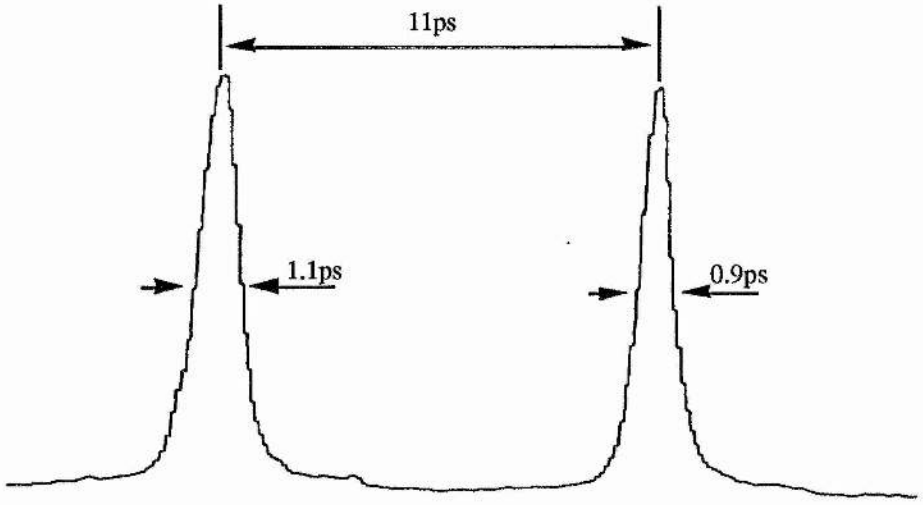


Figure 3.16b: Calibrated streak-intensity profile of a 100fs pulse from the regeneratively-initiated, self-modelocked Ti:$Al_2O_3$ laser.obtained using a 1ms shutter.

When the laser was locked to the 10th harmonic of the cavity frequency, this produced a greater reduction in the phase noise on the output pulse train. However the streak camera was unable to produce a temporal resolution better than 900fs as shown in figure 3.17.

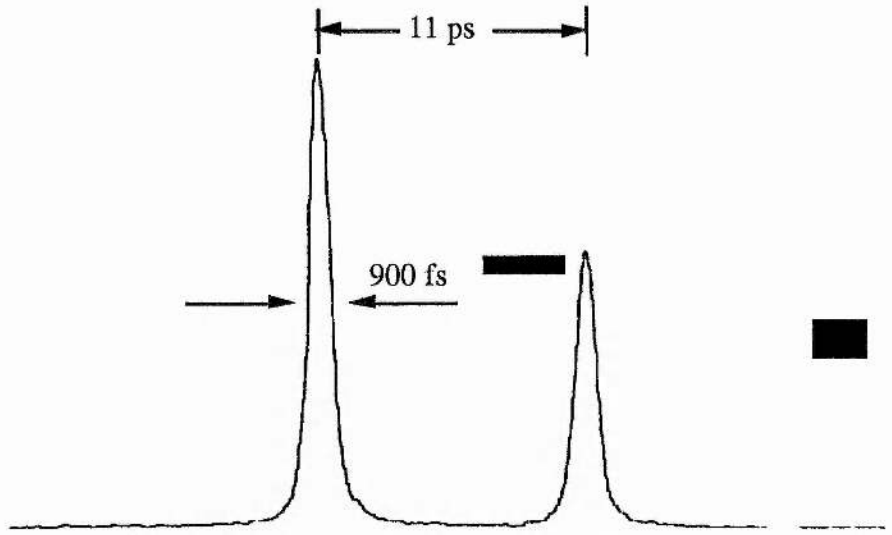


Figure 3.17: Calibrated streak-intensity profile of a 100fs pulse from the regeneratively-initiated, self-modelocked Ti:$Al_2O_3$ laser.obtained using a 1ms shutter.

This result is the best temporal resolution ever achieved from a synchronously-operating streak camera, using an argon-ion pumped Ti:$Al_2O_3$ laser system, to date.

From measurements of the maximum scan speed experimentally achievable, and the static spatial resolution of the tube, it was calculated that the limiting temporal resolution of this streak camera was 700fs (minimum spatial width of image/streak speed). This implies that the total phase noise seen by the streak camera (phase noise on laser output + electronics+ reference oscillator) was approximately 560fs. This is consistent with the experimental phase noise figures obtained for the regeneratively-initiated, self-modelocked Ti:$Al_2O_3$ laser when phase-locked to the 10th harmonic. Timing jitter figures obtained when locked to the 10th harmonic were 303fs (50-500 Hz) and 93fs (500 Hz-5 kHz) giving a total ~400fs. Although the measurement system could only measure the noise contributions up to 5 kHz, there is still noise present at higher frequencies. However, the total noise figure indicated by the streak camera measurements represents an upper-bound to the total noise present on the laser pulse train. From these measurements, we can safely deduce that the overall phase noise on the lase output is around 500fs, and is therefore not limiting the reolution of the streak camera.

## 3.5 Conclusions

In this chapter, a brief discussion of a technique for measuring the phase noise on self-modelocked lasers was given. This was followed by a description of how such a technique was applied to both the regeneratively-initiated and hard-aperture self-modelocked Ti:$Al_2O_3$ laser systems. Results have been presented that show that the phase noise on the hard-aperture self-modelocked laser system, was inherently lower than on the regeneratively-initiated counterpart. Table 3.3 below summarises the timing jitter figures measured on the different unlocked laser systems.

| Frequency | Regeneratively-initiated, self-modelocked laser | Hard-aperture, self-modelocked laser |
|---|---|---|
| 50 - 500 Hz | 6.3 ps | 3.8 ps |
| 500 Hz - 5 kHz | 797 fs | 231 fs |

Table 3.3: Summary of the timing jitter figures measured on both the unlocked regeneratively-initiated and hard-aperture self-modelocked Ti:$Al_2O_3$ laser systems.

A technique which can be generally used to reduce the phase noise on passively modelocked lasers was then discussed. This technique involved locking the laser cavity frequency to an ultrastable, electronic reference oscillator. Results were given for the reduced timing jitter figures obtained from the self-modelocked Ti:$Al_2O_3$ laser systems. It was found that locking the laser cavity to higher harmonics leads to a larger reduction in the timing jitter on the laser pulse train. For the regeneratively-initiated, self-modelocked Ti:$Al_2O_3$ laser, the lowest timing jitter figures obtained were 174fs (50-500 Hz) and 76fs (500 Hz-5 kHz). These figures were obtained when the laser cavity frequency was locked to its 10th harmonic and a noise-eater was inserted in the output

beam of the Ti:$Al_2O_3$ laser. Table 3.4 shows a summary of the timing jitter figures obtained for the different cavity configurations.

| Frequency | Locked to 2nd Harmonic | Locked to 10th Harmonic | Locked to 10th + Noise- Eater |
|---|---|---|---|
| 50 - 500 Hz | 479 fs | 303 fs | 174 fs |
| 500 Hz -5 kHz | 154 fs | 93 fs | 76 fs |

Table 3.4: Summary of the experimental timing jitter figures for the regeneratively-initiated, self-modelocked Ti:$Al_2O_3$ laser.

In the case of the hard-aperture self-modelocked Ti:$Al_2O_3$ laser system, the lowest timing jitter figures obtained were 214fs (50-500 Hz) and 120fs (500 Hz-5 kHz). These figures were measured when the laser cavity frequency was locked to its 10th harmonic. Table 3.5 shows a summary of the timing jitter figures obtained from the various frequency-locked cavity schemes.

| Frequency Band | Locked to 2nd Harmonic | Locked to 10th Harmonic |
|---|---|---|
| 50 - 500 Hz | 230 fs | 214 fs |
| 500 Hz - 5 kHz | 174 fs | 120 fs |

Table 3.5: Summary of the timing jitter figures for the hard-aperture, self-modelocked Ti:$Al_2O_3$ laser.

These results illustrate the effectiveness of the phase-noise reduction technique employed, and are the lowest timing jitter figures obtained from argon-ion pumped, self-modelocked Ti:$Al_2O_3$ laser systems to date.

In the final section of this chapter, the cavity frequency-locked, regeneratively-initiated self-modelocked Ti:$Al_2O_3$ laser was used to evaluate the temporal resolution of the Photochron V streak camera. These measurements show that the resolution of this streak camera, in synchroscan operation, was measured to be 900fs. This result is the first sub-picosecond image obtained from a synchronously-operating streak camera.

## 3.6 References.


[1] M.J.W Rodwell, D.M Bloom and K.W Weingarten "Sub-picosecond laser timing stabilisation", *IEEE J. Quantum. Electron.*, QE-25 p.817 (1989).

[2] A. Finch, Y. Liu, W.E Sleat, W. Sibbett and G. Chen "Phase noise limitations in synchroscan streak camera operation",

[3] A. Finch, W.E Sleat and W. Sibbett "Subpicosecond synchroscan operation of a Photochron IV streak camera", *Rev. Sci. Instrum.*, Vol.60 p.839 (1989).

[4] D. von der Linde "Characterisation of the Noise in Continously Operating Modelocked Lasers" *Appl. Phys. B.*, Vol.39 p.201 (1986).

[5] U. Keller, K.D Li, M.J.W Rodwell and D.M Bloom "Noise characterisation of femtosecond fiber raman soliton lasers", *IEEE J. Quantum. Electron.*, QE-25 p.280 (1989).

[6] A. Finch, X. Zhu, P.N Kean and W. Sibbett "Noise characterisation of modelocked colour-centre lasers", *IEEE J. Quantum. Electron.*, QE-26 p.1115 (1990).

[7] U. Keller, C.E Soccolich, G. Sucha, M.N Islam and M. Wegener "Noise characterisation of femtosecond color-center lasers", *Opt. Lett.*, Vol.15 p.974 (1990).

[8] J. Son, J.V Rudd and J.F Whitaker "Noise characterisation of a self-modelocked Ti:sapphire laser", *Opt. Lett.*, Vol.17 p.733 (1992).

[9] D.R Hjelme and A.R Mickelson "Theory of timing jitter in actively modelocked lasers", *IEEE J. Quantum. Electron.*, QE-28 p.1594 (1992).

[10] H.A Haus and A. Mecozzi "Noise of Modelocked Lasers", *IEEE J. Quantum. Electron.*, QE-29 p.983 (1993).

[11] M.J.W Rodwell, K.J Weingarten, D.M Bloom, T. Baer and B.H Kolner "Reduction of timing fluctuations in a modelocked Nd:YAG laser by electronic feedback", *Opt. Lett.*, Vol.11 p.638 (1986).

[12] S.B Darack, D.R Dykaar and G.T Harvey "Timing jitter stabilisation of a colliding-pulse-modelocked laser by active control of the cavity length", *Opt. Lett.*, Vol.16 p.1677 (1991).

[13] D. Cotter "Techniques for highly stable active modelocking" in *Ultrafast Phenomena IV*, D.A Auston and K.B Eisenthal, eds., New York, Springer-Verlag p.78 (1984).

[14] D.R Walker, D.W Crust, W.E Sleat and W. Sibbett "Reduction of Phase Noise in Passively Modelocked Lasers", *IEEE J. Quantum. Electron.*, QE-28 p.289 (1992).

[15] Y. Liu PhD Thesis University of St. Andrews 1992.

# Chapter 4: An All-Solid-State, Self-Modelocked Ti:Sapphire Laser.

## 4.1 Introduction.

To date, argon-ion lasers have been the most commonly used pump sources available for Ti:$Al_2O_3$ laser systems. In all-lines operation, their principal emissions which are in the 488-514nm region, give a good spectral match to the broad absorption band of titanium-doped sapphire. Although these large frame lasers can produce output powers in excess of 20W, they have the disadvantages of requiring a high current and three-phase voltage supply, along with a high pressure water supply for cooling. Such requirements make argon-ion lasers inefficient and expensive to operate and maintain. Alternatives to the commonly used argon-ion laser are arclamp-pumped, frequency-doubled Nd:YAG and Nd:YLF lasers emitting laser radiation at 532nm and 523.5nm, respectively. Modelocked versions of these lasers have been successfully used in the construction of self-starting, self-modelocked Ti:$Al_2O_3$ laser systems[1,2]. However, the output of these large frame lasers often suffers from amplitude noise which in turn affects the output and stability of the Ti:$Al_2O_3$ laser. In the construction of a highly stable, low phase noise, self-modelocked Ti:$Al_2O_3$ laser, the use of an efficient, stable and compact diode-pumped minilaser represents an attractive alternative to argon-ion lasers because of the enhanced practicality. Diode-pumped minilasers only require power supplies operating at low voltage and current ratings compared to an argon-ion laser which commands a power input of 300V at 50A. These low voltage supplies have the advantage of being easily electrically smoothed to produce low ripple outputs. The low-phase noise characteristics of an all-solid-state system has been recently demonstrated in a self-modelocked Cr:LiSAF laser directly pumped by a single self-injection-locked semiconductor laser[3]. The measured timing jitter figures for this unlocked laser are a factor of two better than the measured phase noise figures of our

low phase noise, argon-ion pumped Ti:$Al_2O_3$ laser as described in section 3.2.1. The development of all-solid-state systems will also lead to the construction of portable Ti:$Al_2O_3$ lasers which can be plugged straight into conventional mains wall sockets, instead of requiring the installation of three-phase power supplies. Although diode-pumped minilasers will not readily be able to replace argon-ion lasers for applications requiring high power Ti:$Al_2O_3$ laser systems, they have the capability of generating output powers of a few watts necessary for low power operation of self-modelocked Ti:$Al_2O_3$ lasers. However, for a laser system to be successful in replacing the argon-ion laser as a pump source for Ti:$Al_2O_3$ lasers it must be capable of producing a low amplitude ripple output in a high quality, $TEM_{00}$ beam.

The current availability of high power laser diodes emitting in the 800nm region has resulted in a renewed interest in the development of all-solid-state laser systems emitting in the green spectral region. Diode-laser-pumped systems based on Nd-doped gain media have already been widely investigated, and pulsed operation of all-solid-state Ti:$Al_2O_3$ laser systems has been reported using frequency-doubled, modelocked and Q-switched Nd:YLF[4,5] and frequency-doubled, Q-switched Nd:YAG lasers[6]. However, the relatively high oscillation threshold for continous-wave operation of Ti:$Al_2O_3$ at around 1W, has so far made diode-laser-pumping rather difficult. More recently, commercial frequency-doubled, diode-laser-pumped Nd:YAG lasers have achieved average powers suitable for pumping a cw Ti:$Al_2O_3$ laser, which had been specifically designed for low threshold operation at around 200mW[7]. However, the output power of these commercial lasers has so far been unsuitable for self-modelocked Ti:$Al_2O_3$ laser configurations.

In this chapter, the design of an all-solid-state laser suitable for pumping a self-modelocked Ti:$Al_2O_3$ laser will be described. In particular, the construction of a continous-wave, intracavity frequency-doubled diode-pumped Nd:YLF ring laser will be discussed, along with the performance characteristics of an all-solid-state, self-modelocked Ti:$Al_2O_3$ laser.

## 4.2 An All-Solid-State , Continous Wave Pump Source for Ti:Sapphire Lasers.

Compact lasers that emit a few watts of green power are attractive for display, medical and spectroscopic applications, not to mention as a potential pump source for other laser systems. Over the past ten years, new developments in high power laser diodes and new nonlinear crystals have hastened the development of efficient miniature infra-red and frequency-doubled solid-state lasers pumped by a laser diode[8-11]. Efficient harmonic generation can be attained in diode-laser pumped solid-state lasers due to their high spatial and spectral brightness. The high peak power output from Q-switched or modelocked diode-pumped lasers can be efficiently frequency doubled by a single pass through a nonlinear crystal. However, efficient frequency doubling of cw lasers requires resonant enhancement techniques.

One obvious approach to achieving efficient second harmonic generation, is to place the nonlinear crystal inside the laser cavity so as to take advantage of the high circulating powers. While the fundamental power is resonating in the cavity, the second harmonic generation is coupled out of the resonator by the nonlinear crystal. In early work at Stanford University, the nonlinear crystal MgO:$LiNbO_3$ was used to intracavity frequency-double a diode laser-pumped, cw Nd:YLF laser[12]. Second harmonic generation was also reported simultaneously by Baer[13] at Spectra Physics Inc., who demonstrated efficient intracavity doubling using the nonlinear crystal, pottasium titanium phosphate (KTP) in a diode laser-pumped Nd:YLF laser. From this work, Baer observed that this laser system suffered from large intensity fluctuations in the second harmonic output along with longitudinal mode instabilities. It was suggested that the sum-frequency generation that occurred as a result of multi-frequency operation of the laser led to these temporal instabilities in the harmonic output. This strong modulation of the second harmonic output is now referred to as the "green problem" and has severely hindered the development of cw intracavity-doubled minilasers, producing several watts of output power.

Several methods for eliminating amplitude fluctuations have therefore been developed. These methods utilize extra intracavity elements such as an etalon[14], a quarter-wave plate[15,16] or by inserting a Brewster-plate in the resonator[17]. A disadvantage of these methods is that the laser outputs are highly sensitive to the losses introduced by the insertion of extra intracavity elements. Another way of avoiding the output power instabilities inherent in intracavity second harmonic generation is by external resonant harmonic generation, first proposed and demonstrated in the late 1960's by Ashkin *et al* at Bell Laboratories[18]. The harmonic conversion efficiency is increased by generating high circulating powers in an external cavity that can be resonant at either the second harmonic or fundamental laser wavelength. However, this method requires a highly stable, narow linewidth, single frequency laser as the input source, and active stabilisation of the external cavity making the system electronically complex. The system developed by Kozlovsky *et al* [19] has combined the advantages of the single frequency nonplanar ring oscillator with the stability of a monolithic resonator fabricated onto a LBO crystal. This design offers the advantages of keeping optical elements outside the laser oscillator, independently optimising the harmonic generation process and yielding stable, low power single frequency , second harmonic output.

An alternative way of overcoming the "green problem" is to generate a single longitudinal mode. In a standing wave cavity, spatial-hole burning in the homogeneous gain medium allows several longitudinal modes to oscillate simultaneously, and high pump powers encourage this oscillation. A simple approach for obtaining single longitudinal mode operation of a laser is to reduce the length of the gain medium and cavity length so that there is only one longitudinal mode in the range of the gain spectrum[20]. Another variation is that the cavity is long enough to support several longitudinal modes but the pump power is limited to below the multi-mode operation threshold[21]. A more attractive way of generating a single longitudinal mode is in the construction of a unidirectional ring resonator[22]. By combining the unidirectional

device and the nonlinear crystal in the cavity, single frequency fundamental light can be converted into a single frequency second harmonic output.

The all-solid-state minilaser developed for use as a pump source for a self-modelocked Ti:$Al_2O_3$ laser was a diode-laser-pumped, intracavity-frequency-doubled, cw Nd:YLF ring laser. Its cavity configuration is described briefly in the following section of this chapter.

### 4.2.1 A Diode-Laser-Pumped, Intra-Cavity Frequency-Doubled, Continous-Wave Nd:YLF Ring Laser.

Neodymium-doped yttrium lithium fluoride ($Nd^{3+}$: $YLiF_4$) is an attractive alternative to the more commonly used Nd:YAG laser crystal for use in solid-state lasers, because of several beneficial optical properties. Firstly, since it is a uniaxial material one can select one of two different naturally polarised wavelengths for each transition simply by employing an intracavity polariser. Secondly, the relatively large thermal conductivity allows for efficient heat extraction, and its natural birefringence dominates thermally-induced birefringence[23,24] eliminating the thermal depolarisation problems of optically isotropic hosts like Nd:YAG. Also, weak thermal lensing in Nd:YLF provides an additional advantage over cw and modelocking operation of Nd:YAG.

Figure 4.1 illustrates a simplified energy level diagram for the $Nd^{3+}$ ion in a YLF host crystal. Stimulated emission oscillations have been realised in both the $^4F_{3/2}$ - $^4I_{11/2}$ and the $^4F_{3/2}$ - $^4I_{13/2}$ transitions of Nd:YLF by diode-laser pumping, corresponding to laser outputs at 1.05μm and 1.3μm. The peak $^4F_{3/2}$ - $^4I_{11/2}$ cross-sections are $14.2 \times 10^{-20} cm^2$ at 1.053μm (σ-polarisation) and $19.6 \times 10^{-20} cm^2$ at 1.047μm (π-polarisation). As a consequence, operation on the 1.047μm line occurs in the absence of wavelength or polarisation selective elements in the resonator at certain pump power levels.

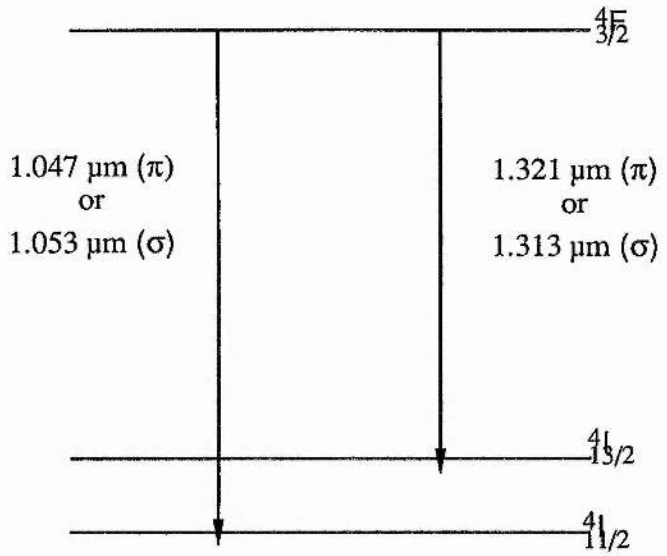


Figure 4.1: Laser transitions in Nd:YLF [25].

Studies of the optical absorption spectra of the $Nd^{3+}$ ion in YLF[26,27], have shown that there are several main absoption lines lying at 792nm, 797nm and 806nm which can be readily excited by AlGaAs laser diodes whose spectral coverage ranges from 780-860nm. These absorption lines in Nd:YLF are typically a few nanometres wide, and can therefore be well matched to the narrow emission spectrum of a laser-diode array. Because Nd:YLF is a uniaxial crystal, it exhibits strong polarisation dependent absorption and fluorescence transitions due to the anisotropic crystal field. Figure 4.2 shows the absorption spectra of Nd:YLF in the wavelength range of AlGaAs laser diodes. The σ polarised (E perpendicular to c) and π (E parallel to c) polarised spectra are shown in figures 4.2a and 4.2b respectively. The fact that the absorption cross-section of Nd:YLF is much larger for the incident light polarised parallel to the c-axis of the laser crystal, than that for the light polarised perpendicular to the c-axis of the crystal, can be considered an advantage for linearly polarised laser-diode outputs.

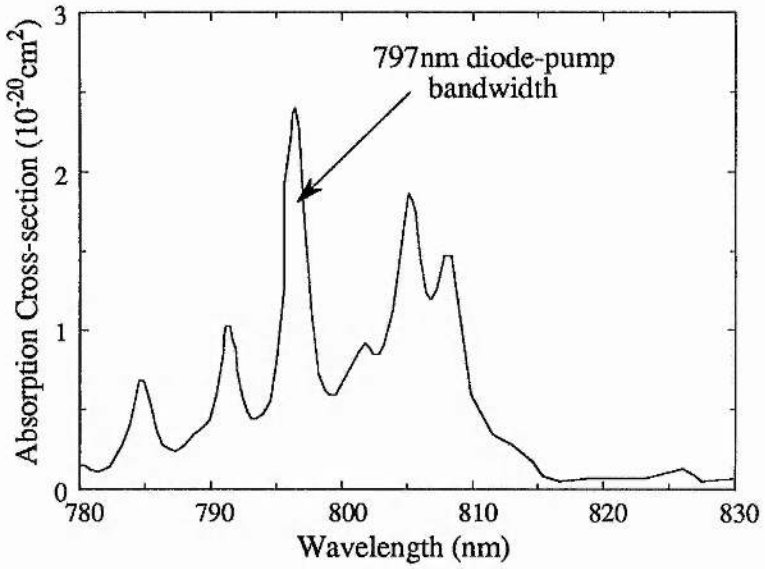


Figure 4.2a: Absorption cross-section for Nd:YLF at room temperature for light polarised perpendicular to the c-axis of the laser crystal.[28]

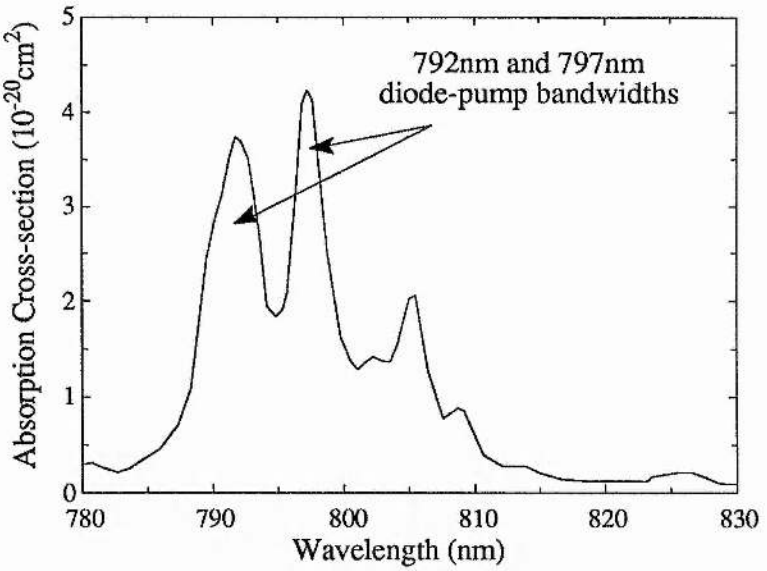


Figure 4.2b: Absorption cross-section for Nd:YLF at room temperature for light polarised parallel to the c-axis of the laser crystal.

Table 4.1 below lists some of the important laser properties of a Nd:YLF laser crystal.

| Laser Property | Value |
|---|---|
| Lasing Wavelength | 1053μm (σ) 1047μm (π) |
| Refractive Index (λ=1.06μm) | $\eta_0 = 1.4484$ $\eta_e = 1.4704$ |
| Fluorescent Lifetime | 480 μs |
| Stimulated Emission X-section | $1.8 \times 10^{-19} cm^2$ (π) $1.2 \times 10^{-19} cm^2$ (σ) |
| Thermal Conductivity | 0.06 W/cm-K |
| Melting Point | 825 °C |

Table 4.1: Important properties of Nd-doped lithium yttrium fluoride ($Nd^{3+}$:YLF).

Other advantages of Nd:YLF material in favour of diode-laser pumping, are the relatively large thermal conductivity allowing efficient non-radiative heat extraction, and weak thermal lensing effect allowing high beam quality. The thermo-mechanical properties of Nd:YLF are not as good as those of Nd:YAG. The low hardness and the inferior thermal fracture limit of this material can cause breakage in crystal mounting and catastophic damage in certain high-power end-pumping geometries.

The "green" minilaser system used as a pump source for the all-solid-state, self-modelocked Ti:$Al_2O_3$ laser was designed and constructed by Hong and Yelland at St. Andrews University[29] and is illustrated schematically in figure 4.3. The gain medium was an 18mm long prism-shaped slab of Nd:YLF. The ends of the slab were anti-reflection coated for the pump wavelength of 797nm and had high reflectivity coatings at the fundamental laser wavelength of 1047nm. The slab was pumped at each end in a novel quasi-end pumped arrangement by cw GaAlAs linear diode-laser bars operating at 797nm (Spectra Diode Labs 3460S).

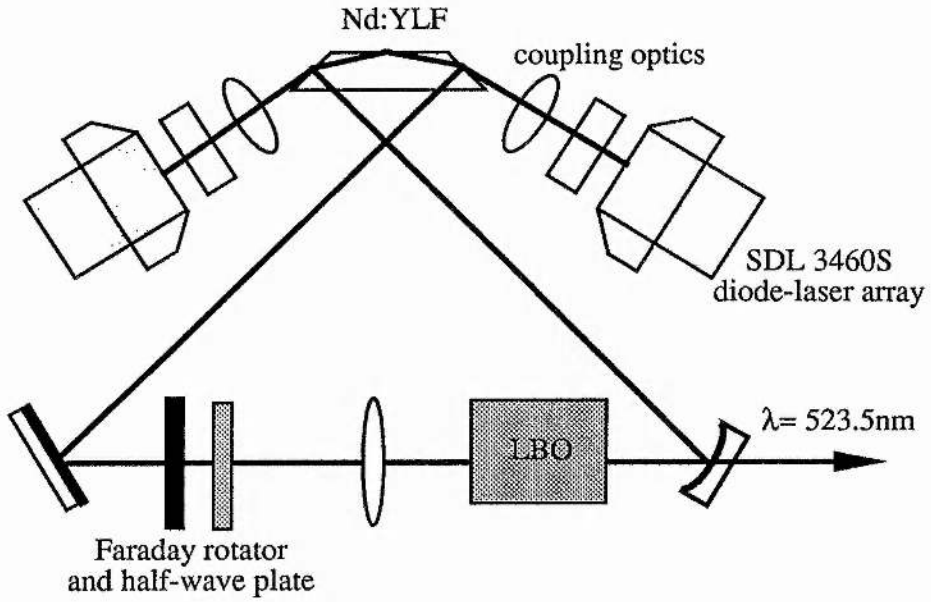


Figure 4.3: Schematic diagram of the diode laser-pumped, intracavity-doubled, cw Nd:YLF ring laser.

Each diode laser bar consisted of forty-eight 100μm emitting apertures, spaced on 200μm centres and was specified to emit 20W cw radiation at a drive current of 32A. Before installing the diode bars in the laser system, their operating characteristics were verified. The output power of the diode bar was measured as a function of the drive current and the results obtained are shown graphically in figure 4.4a. Figure 4.4b shows the peak wavelength emission of the laser-diode bar as a function of the device temperature.

The specified wavelength was 801nm at 25°C, but in practice was found to be 3nm lower at 798nm. The output wavelength of the laser diode was temperature tuned to 797nm to match the strong absoprtion band in Nd:YLF, by cooling the device to a temperature of 20.4°C. A thermoelectric cooling device (CP 2-127-06L from Thermo Electric Devices) was used to control the operating temperature of the diode laser and water cooled copper plate was used as a heat sink.

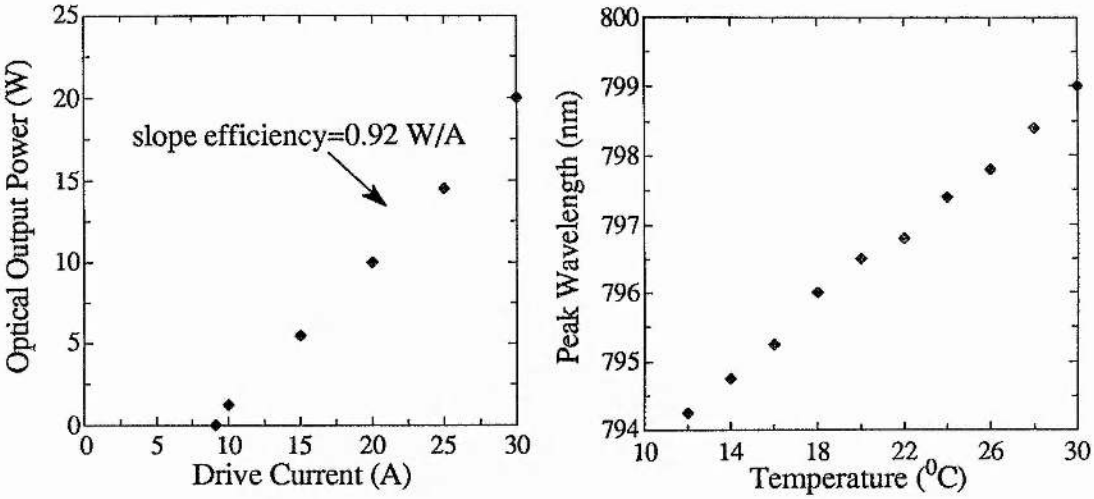


Figure 4.4 (a) diode-laser array output power characteristics and (b) diode-laser wavelength characteristics as a function of temperature.

| Parameter | SDL Specification | Measured Value | Units |
|---|---|---|---|
| Threshold | 9.0 | 9.1 | A |
| Slope Efficiency | 0.91 | 0.92 | W/A |
| Centre λ at R.T | 801 | 798 | nm |
| Wavelength Shift | 0.27-0.3 | 0.27 | nm /°C |

Table 4.2: Opeating characteristics of the diode-laser bar SDL-3460-S.

The laser output from the diode bar was foccussed into the Nd:YLF slab using a combination of a cylindrical and a spherical lens. This pumping scheme has the advantage of the high efficiencies associated with conventional end-pumped lasers, while being easily configured into a ring resonator geometry. The Faraday rotator and half-wave plate were used to ensure unidirectional operation of the ring laser. When operated unidirectionally this system produced a single longitudinal mode output at

1047nm, in a $TEM_{00}$ beam. At a diode-laser pump level of 10W, an output power of 2.2W was achieved with an output coupling of 5%.

Intracavity frequency doubling was accomplished by focussing the cavity mode to a 50μm waist inside a crystal of lithium triborate $LiB_3O_5$ (LBO) using a 50mm focal length lens. The LBO crystal was 20mm long and the faces were anti-reflection coated for both the fundamental and second harmonic wavelengths at 1047nm and 523.5nm respectively. The advantages of using LBO as the frequency-doubling crystal are related mainly to the possibility of utilising type I temperature-tuned, noncritical phase matching[30]. Also, the polarisation of the oscillating modes is not modified by the LBO crystal which is crucial in connection with Nd:YLF as it emits polarised light. The non-critical phase-matching in LBO also provides a large angular acceptance and no walk-off effect, so long crystals can be used to achieve high conversion efficiencies. In this laser system, second harmonic generation was achieved at a phase matching temperature of $160^0$C. The nonlinear crystal was housed in a temperature-stabilised oven so as to limit power fluctuations in the second harmonic output from the laser. At a total pump power of 10W, this unidirectional ring laser was capable of producing a single longitudinal mode output of up to 1W at 523.5nm, in a $TEM_{00}$ beam.

## 4.3 An All-Solid-State, Self-Modelocked Ti:$Al_2O_3$ Laser.

The all-solid-state, regeneratively-initiated, self-modelocked Ti:$Al_2O_3$ laser is shown schematically in figure 4.5, and is identical to the Ti:$Al_2O_3$ laser resonator previously described in Section 2.5.

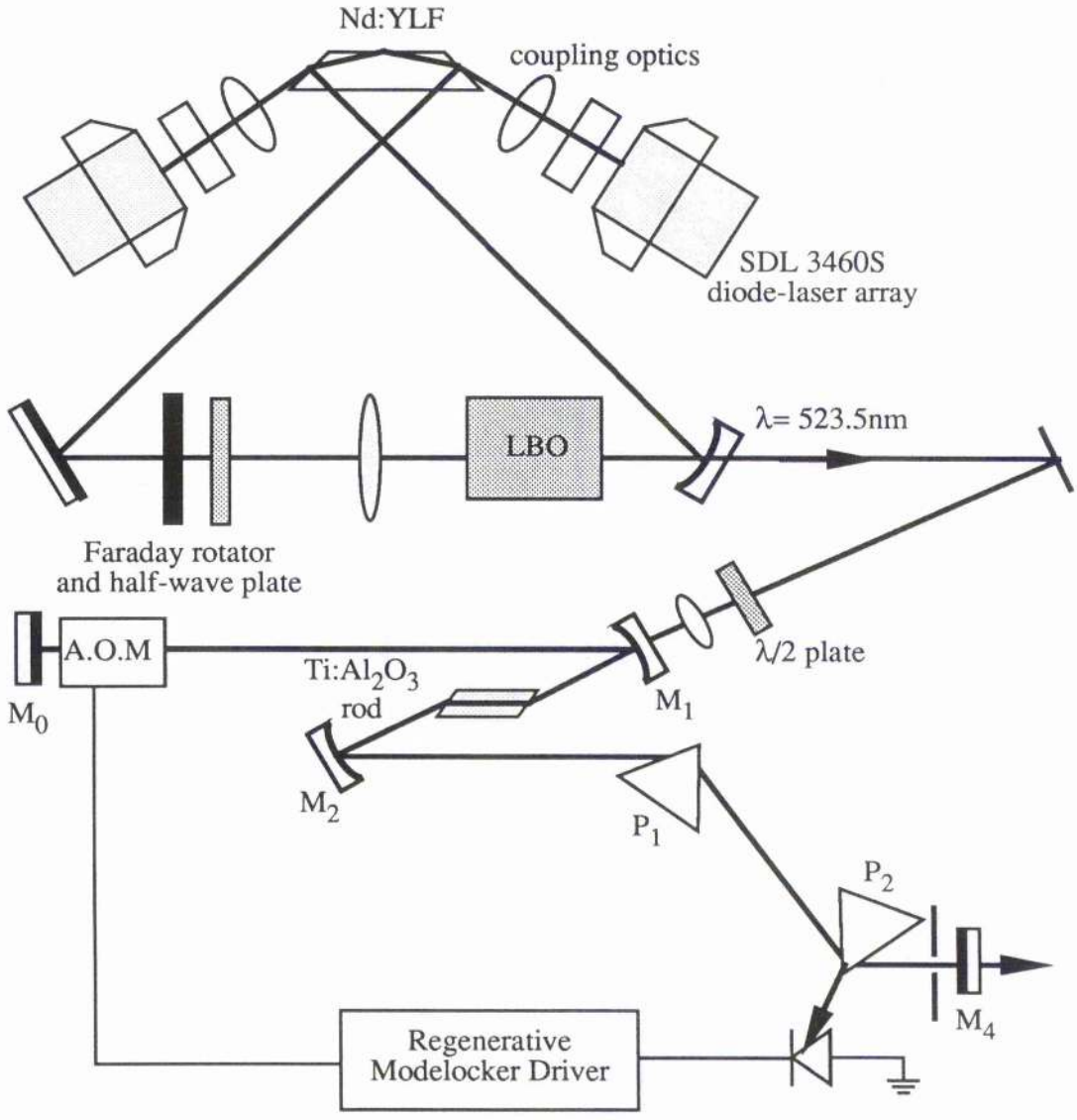


Figure 4.5: Schematic diagram of the all-solid-state, selfmodelocked Ti:$Al_2O_3$ laser cavity.

The main laser cavity was approximately 1.75m in length, and incorporated a 10mm long Brewster-angled Ti:$Al_2O_3$ rod, which had a pump absorption coefficient of 1.9 $cm^{-1}$ and a figure of merit in excess of 250. The plane output coupler $M_3$ had a transmission of 2% over the 700-850nm spectral region and the spherical mirrors $M_1$ and $M_2$ (RoC=100mm) were highly reflecting over the same wavelength range and highly transmitting for the 488-514nm $Ar^+$ pump wavelengths. Two Brewster-angled SF14 prisms, $P_1$ and $P_2$, were included for intracavity dispersion compensation and tuning was achieved using a variable slit placed between $P_2$ and $M_3$. For initiation and stabilization of the self-modelocking process, a regeneratively-driven acousto-optic modulator was located near the highly-reflecting end mirror $M_0$.

When pumped by the Nd:YLF minilaser described in section 4.3, self-modelocked operation of the Ti:$Al_2O_3$ laser was achieved. At a pumping level of approximately 700mW at 523.5nm, the self-modelocked Ti:$Al_2O_3$ laser produced an average output power of approximately 20mW at a centre wavelength near 806nm. The pump power threshold for cw laser oscillation was measured to be approximately 400mW, with a threshold for self-modelocked operation at 500mW. The pulses from the laser were recorded using a real-time autocorrelator that provided both intensity and interferometric autocorrelations. The spectral data were recorded using a monochromator and a linear CCD array. The pulse duration was typically 110fs (assuming a $sech^2$ intensity profile) and the pulse repetition rate was approximately 86 MHz. Figure 4.6 shows intensity and interferometric autocorrelation data, and spectral data for the self-modelocked Ti:$Al_2O_3$ laser when producing 110fs pulses. The spectral bandwidth was measured to be ~9.2nm and this corresponds to a duration-bandwidth ~0.46. This indicates that the pulse duration was slightly greater than the transform-limit ($\Delta\tau\Delta\upsilon$= 0.32) under these self-modelocking conditions. The interferometric autocorrelation trace further indicates that the pulses were not significantly frequency-chirped.

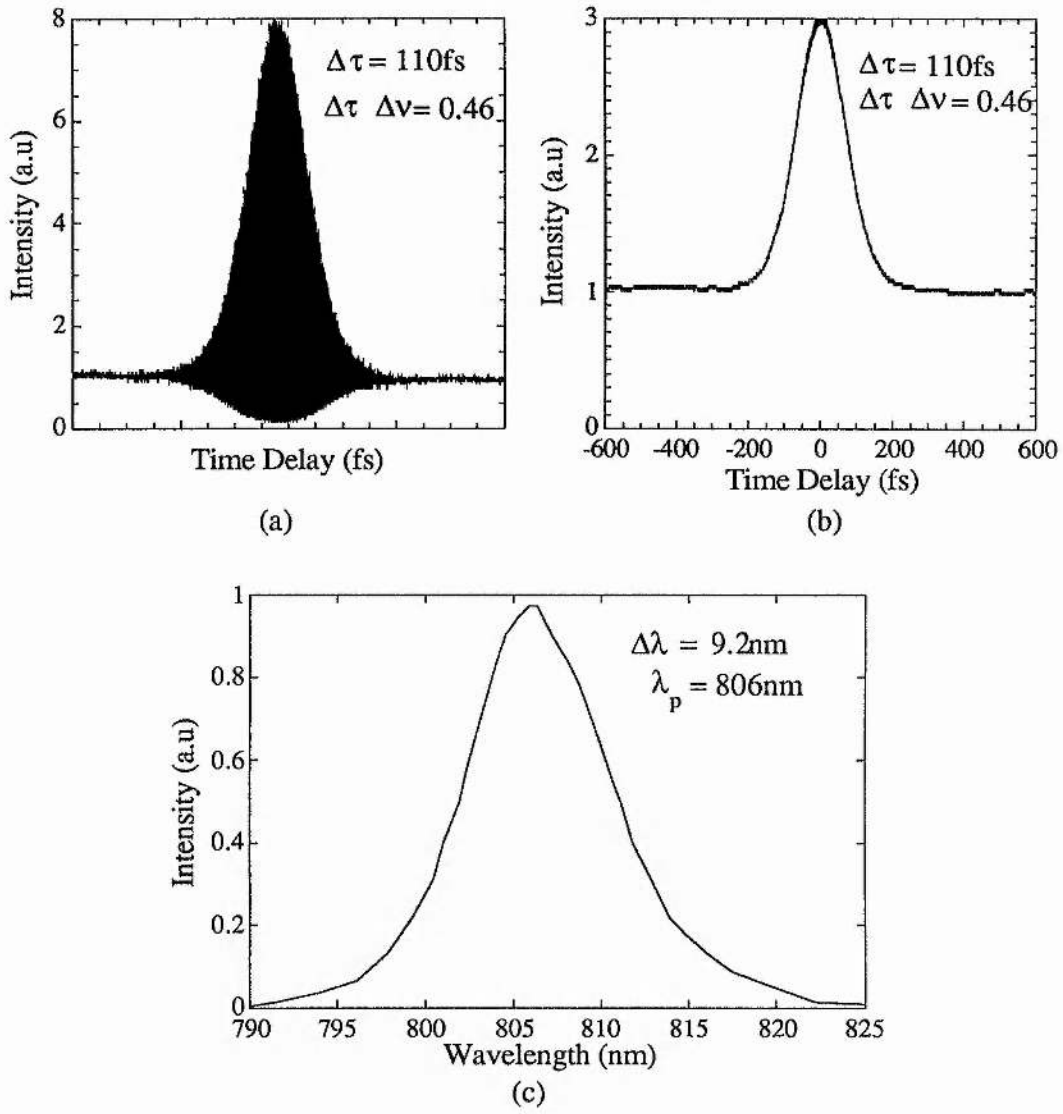


Figure 4.6: (a) Interferometric and (b) intensity autocorrelation profiles and (c) spectrum of the output of the all-solid-state, self-modelocked Ti:$Al_2O_3$ laser.

The maximum output power available from the Nd:YLF minilaser was ~1W. However, due to losses in beam collimating and steering optics, only a maximum of 700mW was available at the Ti:$Al_2O_3$ laser crystal. Because this power level was close to the oscillation threshold of the self-modelocked Ti:$Al_2O_3$ laser system, optimisation of the output pulse duration and stabilisation of the pulse train proved difficult.

## 4.4 Conclusions.

In this chapter, the construction of an all-solid-state, self-modelocked Ti:$Al_2O_3$ laser system has been described. The pump laser was a diode-laser-pumped, intracavity frequency doubled, cw Nd:YLF ring laser. When operated unidirectionally, this laser was capable of producing powers of up to 1W at 523.5nm in a $TEM_{00}$ mode output. At pumping levels of 700mW, the self-modelocked Ti:$Al_2O_3$ laser was capable of generating ultrashort pulses of 110fs in duration at a repetition rate of 86 MHz. These pulses had an average power of 20mW and were centred at a wavelength around 806nm.

For such a system to replace an argon-ion-pumped, self-modelocked Ti:$Al_2O_3$ laser, the development of an all-solid-state pump source producing output powers greater than 1W is required. Since this work was completed, commercial diode-pumped minilaser systems have become available which boast high output powers in the green spectral region, suitable for pumping self-modelocked Ti:$Al_2O_3$ lasers. One such laser is the Lightwave Corp. Model 240 system based on an intracavity frequency doubled Nd:YAG laser, which is specified to produce a low noise continous-wave output at power levels approaching 2W at 532nm. A more recent development is the Spectra Physics Millenia system which is based on an intracavity frequency-doubled Nd:$YVO_4$ laser and has a specified continous-wave output of up to 5W at 532nm, with less than 0.1% rms noise. Unlike previous laser systems which rely on single frequency operation to overcome the "green" problem, this system was deliberately designed to operate with 100's of oscillating modes. Because there are 100's of modes oscillating and not just a few, the mode-beating produced is so fast, that it will not affect the operation of a Ti:$Al_2O_3$ lasers. The development of these systems means that there is now a serious alternative to small frame argon-ion lasers for the construction of low phase noise, all-solid-state, self-modelocked Ti:$Al_2O_3$ lasers.

## 4.5 References.


[1] F. Krausz, M.E Fermann, T. Brabec, P.F Curley, M. Hofer, M.H Ober, Ch. Spielmann, E. Wintner and A.J Schmidt "Femtosecond Solid State Lasers", *IEEE J. Quantum. Electron.*, QE-28 p.2097 (1992).

[2] C.W Siders, E.W Gaul, M.C Downer, A. Babin and A. Stephanov, "Self-starting, 30fs Ti:sapphire laser synchronously-pumped by a pointing-stabilised Nd:YAG laser", in *Conference in Lasers and Electro-Optics* Vol.8 of 1994 OSA Technical Digest Series (Optical Society of America Washington D.C 1994) paper CThI10.

[3] M.P Critten, D. Burns, J.M Evans, K. Lamb, C. Yelland and W. Sibbett "All-solid-state femtosecond $Cr^{3+}$:LiSAF lasers pumped at 532nm and 670nm", *J. Modern Optics* (1996). (accepted for publication).

[4] G.T Maker and A.I Ferguson "Ti:sapphire laser pumped by a frequency doubled diode pumped Nd:YLF laser", *Opt. Lett .*, Vol.15 p.375 (1990).

[5] G.P.A Malcolm and A.I Ferguson "Ti:sapphire laser pumped by a frequency-doubled diode-pumped Nd:YLF laser", *Opt. Commun.*, Vol.82 p.299 (1991).

[6] T.R Steele, D.C Gerstenberger, A. Drobshoff and R.W Wallace "Broadly tunable high power operation of an all-solid-state titanium-doped sapphire laser system", *Opt. Lett.*, Vol.16 p.399 (1991).

[7] J. Harrison, A. Finch, D.M Rines, G.A Rines and P.F Moulton "Low-threshold, cw, all-solid-state Ti:$Al_2O_3$ laser", *Opt. Lett.*, Vol.16 p.581 (1991).

[8] S.R Chinn "Intracavity Second Harmonic Generation in a Nd: pentaphospate Laser", *Appl. Phys. Lett.*, Vol.29 p.176 (1976).

[9] T. Baer and M.S Kierstead in *Digest of Conference on Lasers and Electro--Optics* (Optical Society of America, Washington, D.C 1985) paper ThZZ1.

[10] B. Zhou, T.J Kane, G.J Dixon and R.L Byer "Efficient, frequency-stable laser-diode-pumped Nd:YAG laser", *Opt. Lett.*, Vol.10 p.62 (1985).

[11] T.Y Fan, G.J Dixon and R.L Byer "Efficient GaAlAs diode-laser-pumped operation of Nd:YLF at 1.047μm with intracavity doubling to 523.6nm", *Opt. Lett.*, Vol.11 p.204 (1986).

[12] T.Y Fan, G.J Dixon and R.L Byer "Efficient GaAlAs diode-laser-pumped operation of Nd:YLF at 1.047μm with intracavity doubling to 523.6nm", *Opt. Lett.*, Vol.11 p.204 (1986).

[13] T. Baer "Large-amplitude fluctuations due to longitudinal mode coupling in diode-pumped intracavity-doubled Nd:YAG lasers", *J. Opt. Soc. Am. B.*, Vol.3 p.1175 (1986).

[14] T. Baer "Large-amplitude fluctuations due to longitudinal mode coupling in diode-pumped intracavity-doubled Nd:YAG lasers", *J. Opt. Soc. Am. B.*, Vol.3 p.1175 (1986).

[15] M. Oka and S. Kubota "Stable intracavity doubling of orthogonal linearly polarised modes in diode-pumped Nd:YAG lasers", *Opt. Lett.*, Vol.13 p.805 (1988).

[16] L.Y Liu, M. Oka, W. Wiechmann and S. Kubota "Longitudinally diode-pumped continous wave 3.5W green laser", Opt. Lett., Vol.19 p.189 (1994).

[17] H. Nagai, M. Kume, I. Ohta, H. Shimizu and M. Kazumura "Low-noise operation of a diode-pumped intracavity-doubled Nd:YAG laser using a Brewster plate", *IEEE J. Quantum. Electron.*, QE-28 p.1164 (1992).

[18] A. Ashkin, G.D Boyd, J.M Dziedzic "Resonant optical second harmonic generation and mixing", *IEEE J. Quantum. Electron.*, QE-2 p.109 (1966).

[19] W.J Kozlovsky, C.D Nabors and R.L Byer "Second-harmonic generation of a continous-wave diode-pumped Nd:YAG laser with an externally resonant cavity", *Opt. Lett.*, Vol.12 p.1014 (1987).

[20] J. J Zayhowski and A. Mooradian, "Single frequency microchip Nd lasers", *Opt. Lett.*, Vol.14 p.24 (1989).

[21] C. Pederson, P.L Hansen, T. Skettrup and P. Buchhave, "Diode-pumped single frequency Nd:$YVO_4$ laser with a set of coupled resonators", *Opt. Lett.*, Vol.20 p.1389 (1995).

[22] A.J Alfrey "Simple 1 micron ring laser oscillators pumped by fibre-coupled laser diodes", *IEEE J. Quantum. Electron.*, QE-30 p.2350 (1994).

[23] H. Vanherzeele, "Thermal lensing measurement and compensation in a cw modelocked Nd:YLF laser", *Opt. Lett.*, Vol.13 p.369 (1988).

[24] G. Cerullo, S. De Silverstri and V. Magni "High efficiency, 40W cw Nd:YLF laser with large $TEM_{00}$ mode", *Opt. Commun.*, Vol.93 p.77 (1992).

[25] W. Koechner, "Solid-state Laser Engineering", Third Edition, *Springer Verlag* p.61 (1993).

[26] A.L Harmer, A. Linz and D.R Gabbe, "Fluorescence of $Nd^{3+}$ in Lithium Yttrium Fluoride", *J. Phys. Chem. Solids*, Vol.30 p.1483 (1969).

[27] T.M Pollak, W.F Wing, R.J Grasso, E.P Chicklis and H.P Jenssen, "CW laser operation of Nd:YLF", *IEEE J. Quantum. Electron.*, QE-18 p.159 (1982).

[28] J.R Ryan and R. Beach "Optical absorption and stimulated emission of Neodymium in yttrium lithium fluoride", *J. Opt. Soc. Am. B.*, Vol.9 p.1883 (1992).

[29] K. Lamb, D.E Spence, J. Hong, C. Yelland and W. Sibbett "All-solid-state, self-modelocked Ti:sapphire laser", *Opt. Lett.*, Vol.19 p.1864 (1994).

[30] C. Chen, Y. Wu, A. Jiang, B. Wu, G You, R. Li, and S. Lin "New nonlinear-optical crystal: $LiB_3O_5$", *J. Opt. Soc. Am. B* Vol.6 p.616 (1989).

# Chapter 5: An All-Solid-State, Self-Modelocked Cr:LiSAF laser.

## 5.1 Introduction

The laser material $Cr^{3+}$:$LiSrAlF_6$ (Cr:LiSAF) has many properties similar to Ti:sapphire (Ti:$Al_2O_3$) crystals. The bandwidth and tuning range are comparable and therefore both crystals are capable of producing tunable, ultrashort pulses in the near-infrared spectral region. Apart from the fact that Cr:LiSAF is also an attractive solid-state alternative to the previously used dye lasers for the production of ultrashort pulses, certain material characteristics mean that it is now being looked at as an attractive alternative to Ti:$Al_2O_3$ for many applications. A comparison of some key optical properties of Ti:$Al_2O_3$ and Cr:LiSAF are listed below in Table 5.1.

| Material | Ti:$Al_2O_3$ | Cr:LiSAF |
|---|---|---|
| Pump Band $\lambda$ ($\mu$m) | 0.45 - 0.6 | 0.40 - 0.75 |
| Emission Cross-section $\sigma$ ($10^{-19}cm^2$) | 3.8 | 0.48 |
| Upper-state Lifetime $\tau$ ($\mu$s) | 3.2 | 67 |
| Fluorecence Peak (nm) | 780 | 830 |
| Tuning Range (nm) | 660 - 1180 | 760 - 920 |
| $\sigma\tau$ ($10^{-19}cm^2\mu s^{-1}$) | 12.16 | 32.16 |

Table 5.1: Optical properties of Ti:$Al_2O_3$ and Cr:LiSAF laser materials.

Unlike Ti:$Al_2O_3$, the relatively long upper state lifetime of Cr:LiSAF and the excellent overlap of its absorption bands with the emission bands of xenon flashlamps, makes Cr:LiSAF a good candidate for flashlamp[1] pumping. For continuous-wave laser operation, a longitudinal pumping scheme using another laser source must be employed, and Cr:LiSAF has been successfully pumped by argon-ion[2], krypton-ion[3], and alexandrite[4] laser systems. However, its most attractive feature is that due to its absorption bands in the red spectral region, Cr:LiSAF permits direct diode-pumping by the new generation of laser diodes[5]. Also, since the product $\sigma\tau$ is inversely proportional to the oscillation threshold power of a laser system, Cr:LiSAF should exhibit an inherently lower oscillation threshold than Ti:$Al_2O_3$. Again, this is an attractive advantage in the application of diode-laser based pump sources as replacements for conventional high power ion-laser systems.

Self-modelocked operation of Cr:LiSAF laser systems, was first demonstrated using mainframe argon-ion[6] and krypton-ion[7] lasers operating at 488 and 647nm respectively, as the pump sources. However, the use of diode lasers as pump sources for solid-state gain media is a much more attractive alternative to mainframe ion laser systems. Diode lasers are much more convenient because they consume only modest quantities of electrical power, can be air-cooled and are compact, reliable and inherently stable. Progress in direct diode pumping of Cr:LiSAF has to date been restrained by the performance of suitable GaInP/AlGaInP laser diodes at ~670nm[8].

An alternative approach to direct-diode pumping of Cr:LiSAF is the use of diode-pumped Nd:YLF minilasers. Unlike diode lasers which exhibit poor beam quality and low brightness, minilasers have the advantage of producing good, diffraction-limited output beams. Pulses as short as 30ps have been generated from an actively modelocked all-solid-state Cr:LiSAF laser, which used the output of a cw Nd:YLF minilaser doubled from 1319nm to 659nm[9] as the pump source. Unfortunately, the 1319nm line of Nd:YLF is relatively weak, and therefore high powers, in the order of several watts, cannot be generated when frequency doubling to 659nm.

Our minilaser system utilises the strong 1.047μm line of Nd:YLF frequency doubled to 532nm. Unfortunately, this wavelength region is in the trough of the absorption curve of Cr:LiSAF (see figure 5.2). Fortunately, an advantageous property of Cr:LiSAF is that there is no reduction of crystal quality at the higher doping levels[10]. Pumping at this wavelength is therefore made possible by the use of highly-doped material, an approach in parallel with the 752nm IR "wing-pumping" scheme previously reported, which utilised AlGaAs laser diode arrays[11] as the pump lasers.

In this chapter, a brief outline will be given of the spectroscopic characterstics of various $Cr^{3+}$-doped laser crystals, including Cr:LiSAF. This will be followed by a description of the construction and self-modelocked operation of an all-solid-state Cr:LiSAF laser.

## 5.2 Spectroscopic Characteristics of Cr-doped Laser Materials.

The $Cr^{3+}$ ion has been observed to lase in a variety of host materials and is historically significant since the first laser was demonstrated using chromium-doped sapphire (ruby) by Maiman in 1960[12]. Since then, researchers have been successful in developing a variety of solid-state laser gain media which utilise chromium as the active ion. A selection of hosts materials and their optical properties are shown below in Table 5.2.

| Host Material | Name | Peak lasing Wavelength (nm) | Slope Efficiency | Reference |
|---|---|---|---|---|
| $Be_3Al_2(SiO_3)_6$ | Emerald | 768 | 64 | [13] |
| $LiCaAlF_6$ | LiCAF | 780 | 54 | [14] |
| $BeAl_2O_4$ | Alexandrite | 752 | 51 | [15] |
| $LiSrAlF_6$ | LiSAF | 825 | 36 | [16] |
| $ScBeAlO_4$ | Scalexandrite | 792 | 30 | |
| $ScBO_3$ | Borate | 843 | 29 | [3] |
| $Gd_3Sc_2Ga_3O_{12}$ | GSGG | 785 | 28 | [17] |
| $Y_3Sc_2Al_3O_{12}$ | GSAG | 784 | 19 | [18] |
| $SrAlF_5$ | Pentafluoride | 932 | 15 | [19] |
| $Mg_2SiO_4$ | Fosterite | 1235 | 1 | [20] |

Table 5.2: Optical data for various Cr-doped laser materials.

There are several reasons as to why the $Cr^{3+}$ ion has been seen to oscillate in such a variety of hosts. Firstly, the trivalent oxidation state is resistant to both oxidation and reduction. This means that there is good flexibilty in the host materials that can accomodate the $Cr^{3+}$ ion, and in the atmosphere in which such materials can be grown. Secondly, the $Cr^{3+}$ impurity tends to be incorporated into octahedronal sites and will therefore exclusively occupy the octahedronal sites in a host material in which other kinds of sites are also present. Thirdly, the lowest excited state of $Cr^{3+}$ is resistant to nonradiative decay processes, thereby rendering the luminescent quantum yield unity at room temperature. In short, this means that because the $Cr^{3+}$ impurity ion has a tendency to be incorporated into many hosts with the required oxidation state and nearest-neighbour enviroment, the possibility of achieving laser action is greatly enhanced compared to the prospects expected for other transition-metal ions.

In tunable $Cr^{3+}$ lasers, ions excited into the $^4T_2$ state by pumping in the red absorption band and into the $^4T_1a$ state by pumping in the blue absorption bands, have a laser transition to excited vibrational states of the $^4A_2$ ground level.

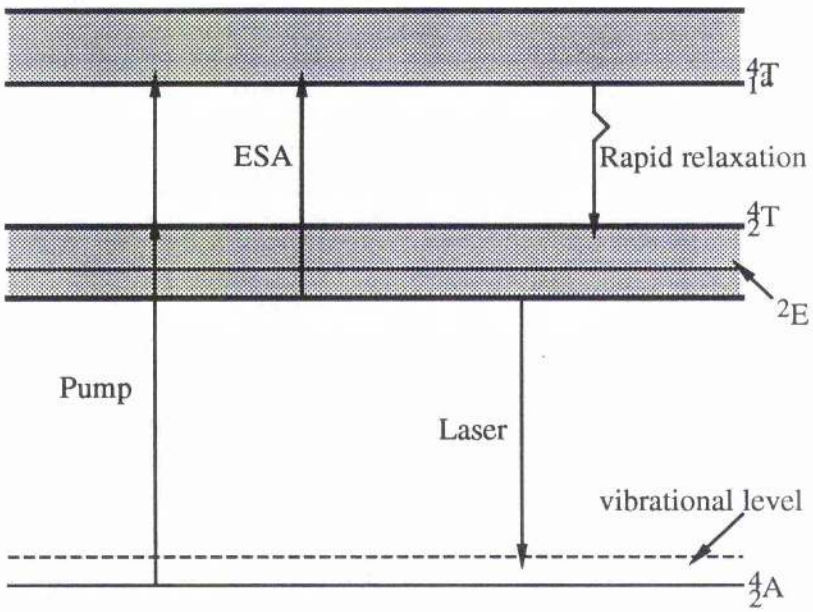


Figure 5.1: Energy level diagram for "low-field" $Cr^{3+}$ host materials.

This scheme requires crystals in which the $^4T_2$ state in its relaxed lattice configuration is lower in energy than the $^2E$ state and such crystals are called "low-field" $Cr^{3+}$ hosts. Unfortunately, excited state absorption (ESA) is shown to originate from the upper laser and is an intrinsic process that reduces the efficiency of Cr-doped laser gain materials. The severity of ESA is inherent to the structure of the host crystal and has been shown to be negligible in some crystals such as alexandrite[21] and LiCAF[22]. Figure 5.1 shows the electronic transitions involved for optical pumping, optical gain and excited state absorption (ESA) in "low-field" $Cr^{3+}$ hosts.

Apart from excited state absorption, the presence of other loss mechanisms such as parasitic impurities and defect absorptions, has been shown to greatly degrade the performance and efficiency of certain Cr-doped laser gain media. These problems are particularly prevalent in the host materials GSGG[23], $SrAlF_5$[24] and fosterite[21]. Also, the generation of pump-induced colour-centres in the gallium-based garnet host media, means that these materials tend to be inefficient as laser gain media.

One of the most successful "low-field" $Cr^{3+}$ host materials is lithium strontium aluminium fluoride, LiSAF. Figure 5.2, shows the absorption spectra for Cr:LiSAF for both $\pi$ (E parallel to c-axis) polarisation and $\sigma$ (E perpendicular to c-axis) polarisation.

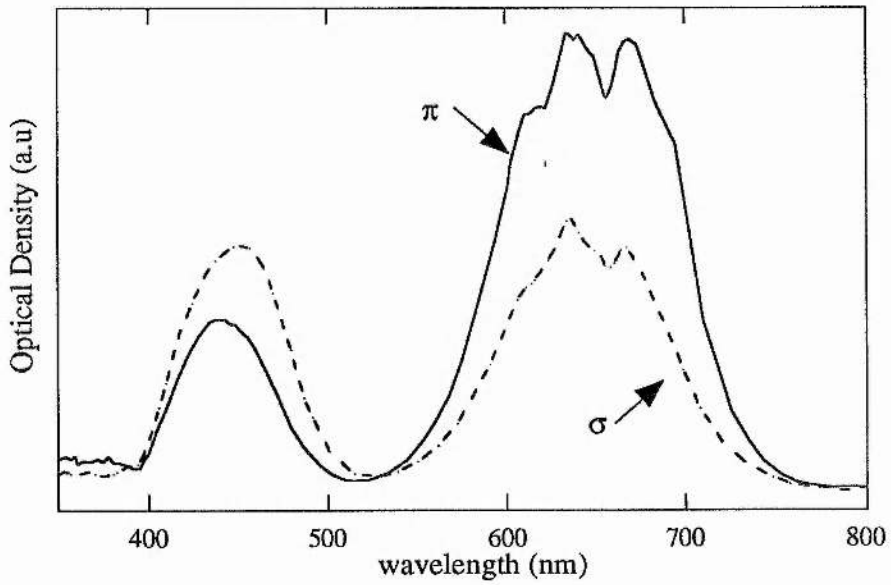


Figure 5.2: Measured absorption spectra of Cr:LiSAF[25].

The absorption band centred around 450nm is due to the $^4A_2$-$^4T_1a$ transition and the band centred around 650nm is the $^4A_2$-$^4T_2$ transition. These absorption features are typical of what is seen for most "low-field" Cr-doped materials and are characteristic of the $3d^3$ electronic configuration of the $Cr^{3+}$ ion. These absorption bands in the blue and red spectral regions leave a transparent region in the green which gives these crystals their characteristic emerald green colour.

For the work reported in this chapter, the optical pumping of Cr:LiSAF was in the green spectral region at 514 and 532nm. It can be seen from figure 5.3, that this wavelength region is at the very lowest point of the absorption curve. Fortunately, the use of recently available, highly-doped crystals permits pumping at such a low absorption cross-section.

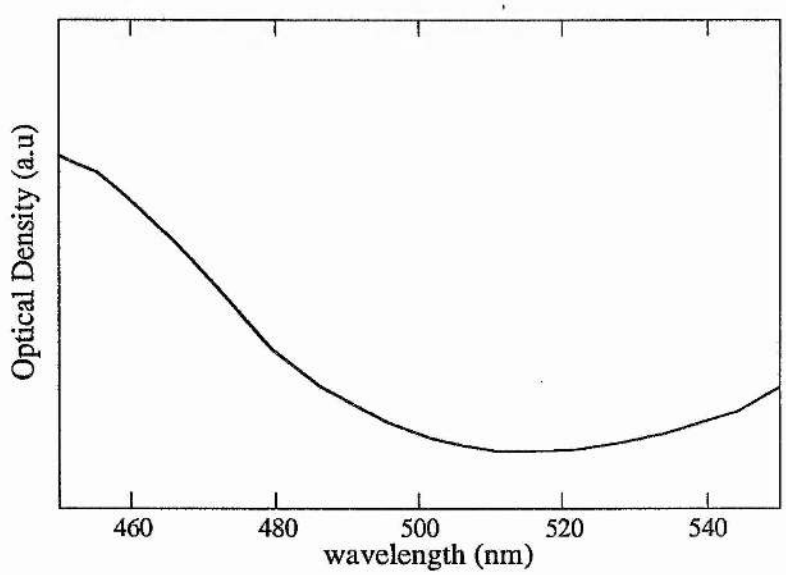


Figure 5.3: Absorption spectra of Cr:LiSAF from 450-550nm.

The emission spectrum which is due to the $^4T_2$-$^4A_2$ transition is shown in figure 5.4. From this diagram it can be seen that the emission band is shifted away from the main absorption peak of Cr:LiSAF, with only the lowest wavelengths of emitted light being reabsorbed by the crystal.

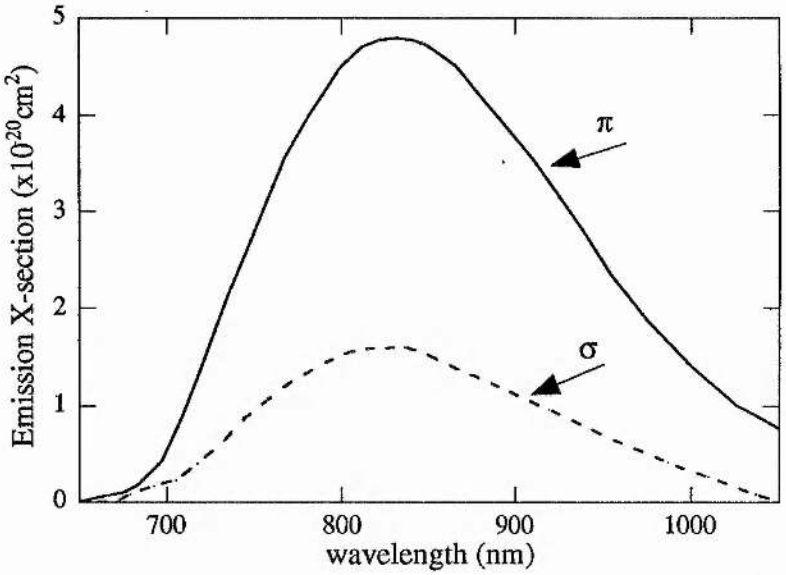


Figure 5.4: Emission Cross-section spectra of Cr:LiSAF[26].

The emission spectrum also suggests that the tuning range of Cr:LiSAF should extend from about 680-1000nm. However, the tuning range of Cr:LiSAF is limited at the short wavelength side to by $Cr^{3+}$ ground-state absorption, and at the high wavelength side by the effects of ESA which are not negligible in Cr:LiSAF. The upper-state lifetime of Cr:LiSAF is 67μs and has been shown to be independent of temperature from 20-300K[3] meaning that non-radiative decay from the upper laser level is of no consequence at these temperatures. However, work performed by Stalder *et al* [27] has shown that at temperatures above 343K (70°C), the emission lifetime of Cr:LiSAF decreases dramatically due to the tunnelling of ions between the excited vibrational states of the upper and lower laser levels. For efficient laser operation, it is therefore vital that the temperature of the laser gain medium should not exceed this value. Important properties of Cr:LiSAF as an effective laser gain medium are listed in Table 5.3.

| Properties | Values at 300K |
|---|---|
| Refractive Index, n | 1.4 |
| Nonlinear Refractive Index, $n_2$ | $1.5 \times 10^{-20}$ $m^2W^{-1}$ |
| Peak Absorption Cross-section, $\sigma_{abs}$ | ~$6 \times 10^{-20}$ $cm^2$ |
| Peak emission Cross-section, $\sigma_{em}$ | ~$5 \times 10^{-20}$ $cm^2$ |
| Peak absorption wavelength | 650 nm |
| Peak emission wavelength | 830 nm |
| Upper state lifetime, $\tau_p$ | 67 μs |

Table 5.3: Important characteristics of Cr:LiSAF.

Although Cr:LiSAF has many advantages as a laser medium over Ti:sapphire, there are also a few major disadvantages. The fracture toughness and thermal conductivity of Cr:LiSAF are considerably lower than the values measured for Ti:sapphire. This leads to an increase in the possibility of mechanical failure at high pump powers, and to adverse thermal effects.

## 5.3 An All-Solid-State, Self-Modelocked Cr:LiSAF Laser.

The laser cavity configuration is similar to the all-solid-state, regeneratively-initiated, self-modelocked Ti:$Al_2O_3$ laser described previously in chapter 4. The gain medium was a 12mm long slab of Cr:LiSAF with a $Cr^{3+}$ doping level of 10%, and the plane-parallel crystal facets were anti-reflection coated at 850nm to reduce cavity losses. The laser crystal was incorporated in a 1.7m long resonator having optics that were coated in the 800-900nm spectral range. The output coupling transmission was 1.5%, and two SF14 prisms were inserted for intracavity dispersion compensation. For initiation and stabilisation of the self-modelocking process, a regeneratively-driven acousto-optic modulator was placed near the highly-reflecting end mirror. The laser cavity is illustrated schematically in figure 5.5.

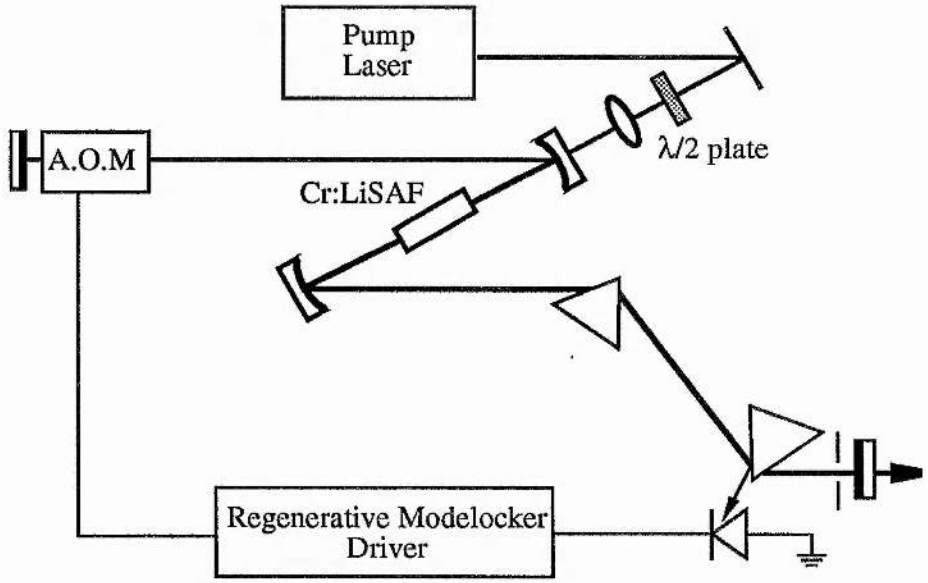


Figure 5.5: Schematic diagram of self-modelocked Cr:LiSAF laser.

The all-solid-state pump laser was a continuous-wave, diode-laser pumped, intracavity frequency-doubled Nd:YLF ring laser, which was used to pump the all-solid-state, self-modelocked Ti:$Al_2O_3$ laser described in chapter 4. The cavity configuration of this laser is again illustrated schematically in figure 5.6.

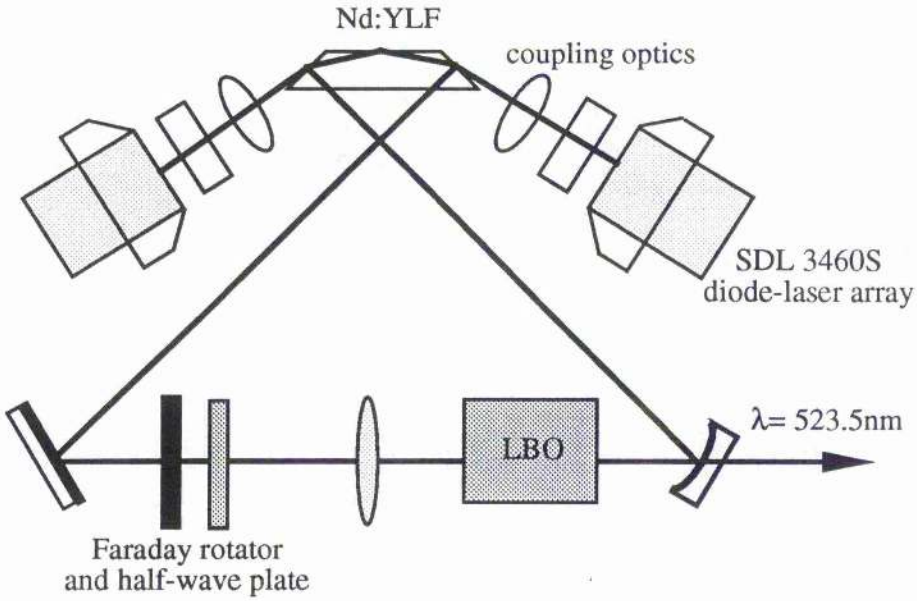


Figure 5.6: Schematic diagram of the diode laser-pumped, intracavity-doubled, cw Nd:YLF ring laser.

At a total diode-laser pump power of ~10W, this unidirectional Nd:YLF ring laser was capable of producing a single longitudinal mode output of up to 1W at 523.5nm, in a $TEM_{00}$ beam. Again, due to losses in the beam collimating and beam steering optics, only a maximum of 700mW was available at the Cr:LiSAF laser crystal.

The cw threshold of the all-solid-state, Cr:LiSAF laser system was measured to be ~150mW with an output coupling of 1.5%. When self-modelocked, this laser produced 90fs pulses at a repetition rate of ~86 MHz, and a wavelength centred around 860nm. At pump power level of ~500mW, an average output power of 30mW was obtained. Intensity and interferometric autocorrelation data (see figure 5.7a and 5.7b) indicate that the pulses were of 90fs duration and contained minimal frequency chirp. The measured spectral data (see figure 5.7c) implied a pulse bandwidth of 9.8nm. This corresponds to a duration-bandwidth product of ~0.36, indicating that the pulses are approximately transform-limited under these self-modelocking conditions (assuming $sech^2$ pulse profile).

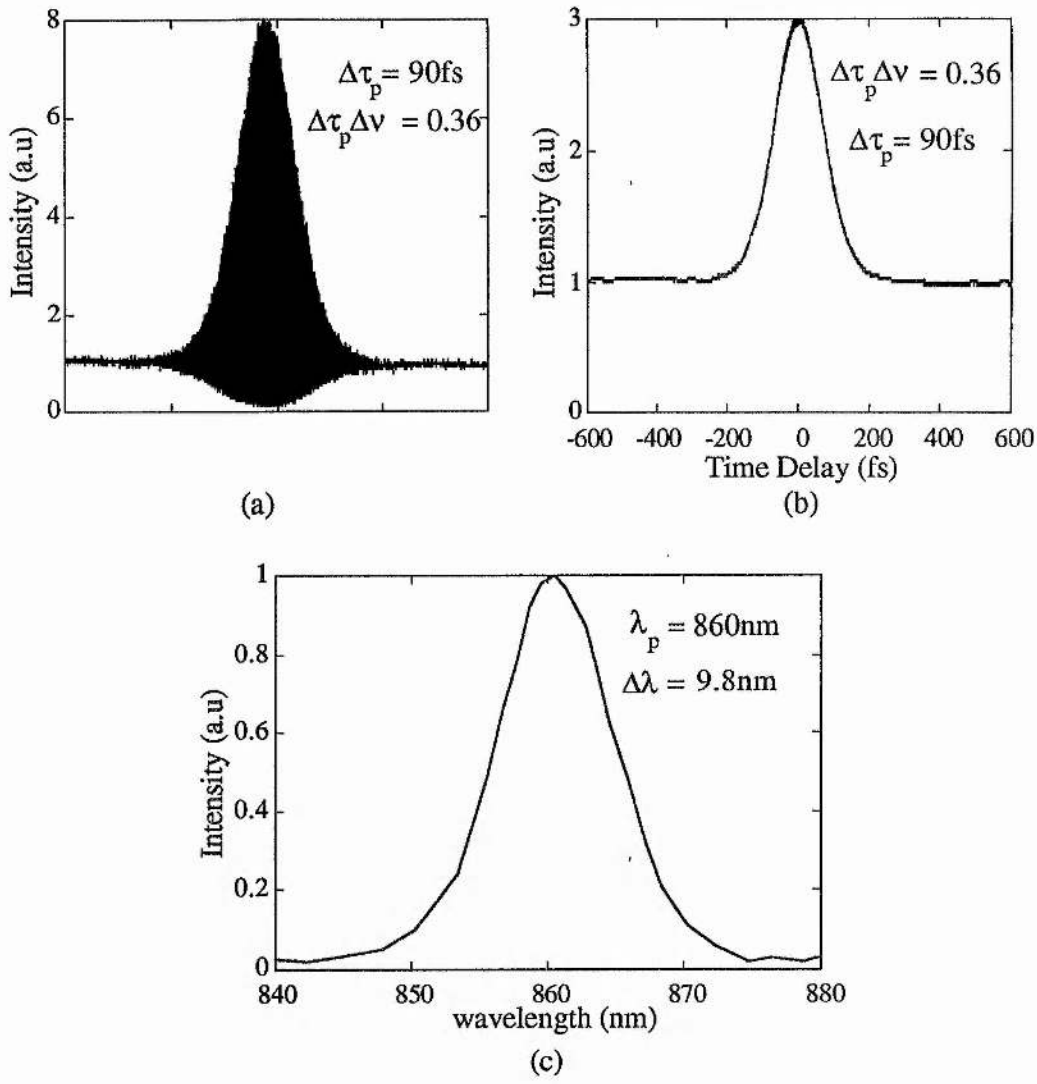


Figure 5.7: (a) Interferometric (b) intensity autocorrelation data and (c) spectral data of the output of the all-solid-state, self-modelocked Cr:LiSAF laser.

However, green pumping of the Cr:LiSAF crystal confirmed that the material suffers from thermal problems at high pump powers due to low thermal conductivity. Also, the anti-reflection coatings on the crystal faces easily became damaged at pump power levels ≥ 1W. In order to minimise degradation in the laser efficiency due to adverse thermal effects, the laser crystal was mounted on a heat-sink cooled by a peltier-effect cooler. The laser power transfer characteristics were measured at various heat-sink temperatures and the results are shown graphically in figure 5.8. These results show that at pump power levels >1.2W, the laser cw output suffered badly from

thermally-induced roll-off. Further cooling would of course enable pumping at higher power levels, unfortunately cooling to temperatures < 13°C introduced condensation problems.

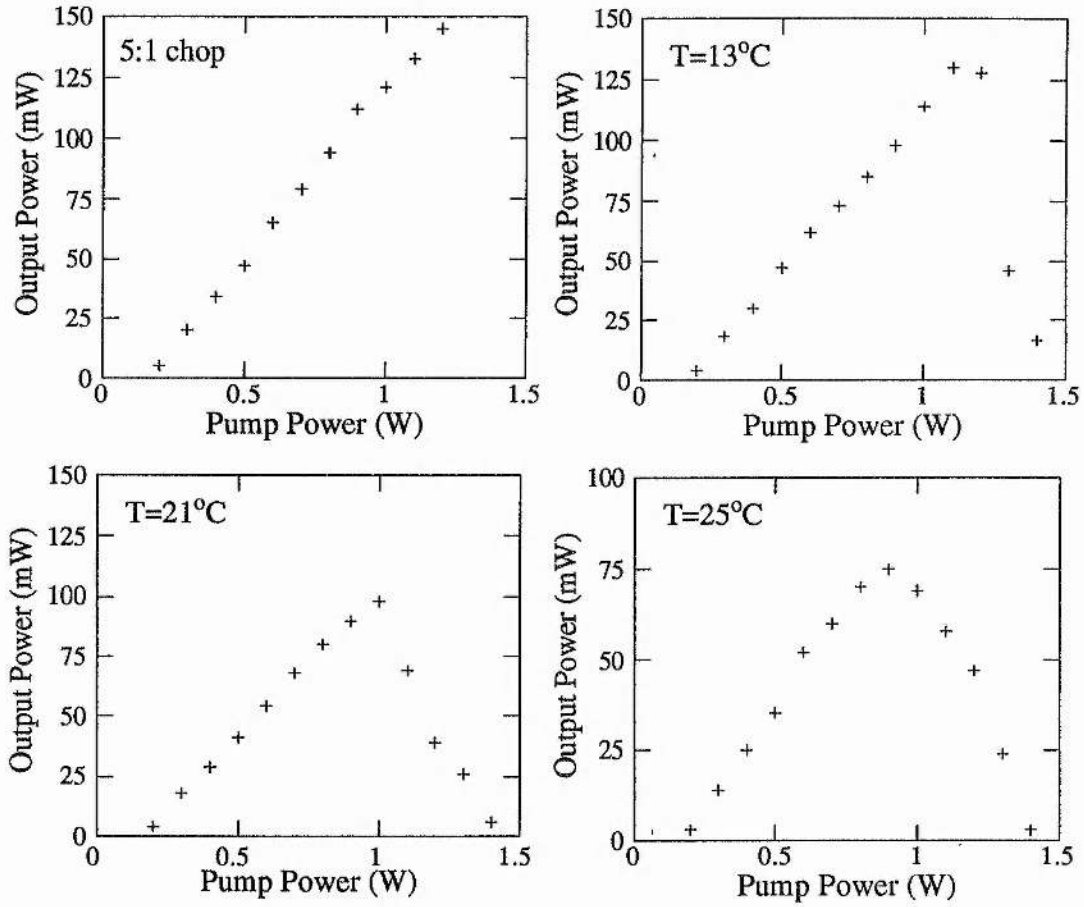


Figure 5.8: Cw output power versus input pump power at various crystal temperatures.

In an attempt to overcome the adverse effects introduced by the anti-reflection coatings on the plane-cut laser crystal, a 14mm-long Brewster-angled Cr:LiSAF rod was incorporated into the laser cavity shown in figure 5.5. This crystal was doped with 22% $Cr^{3+}$ giving ~95% absorption at pump wavelengths around 514nm. This cw threshold power of this laser was measured to be ~170mW. To minimise any thermal problems, the crystal mount was electronically cooled to ~13°C and the cw laser output was a steady 60mW at a pump power of 800mW. The output power was measured to be 15% higher when the pump beam was chopped with a 5:1 duty cycle, therefore thermal effects were not entirely eliminated. Due to the humidity levels in the

laboratory enviroment, there arose the problem of condensation at these low temperatures, therefore pure nitrogen gas was passed over the top of the crystal to keep the surrounding atmosphere dry.

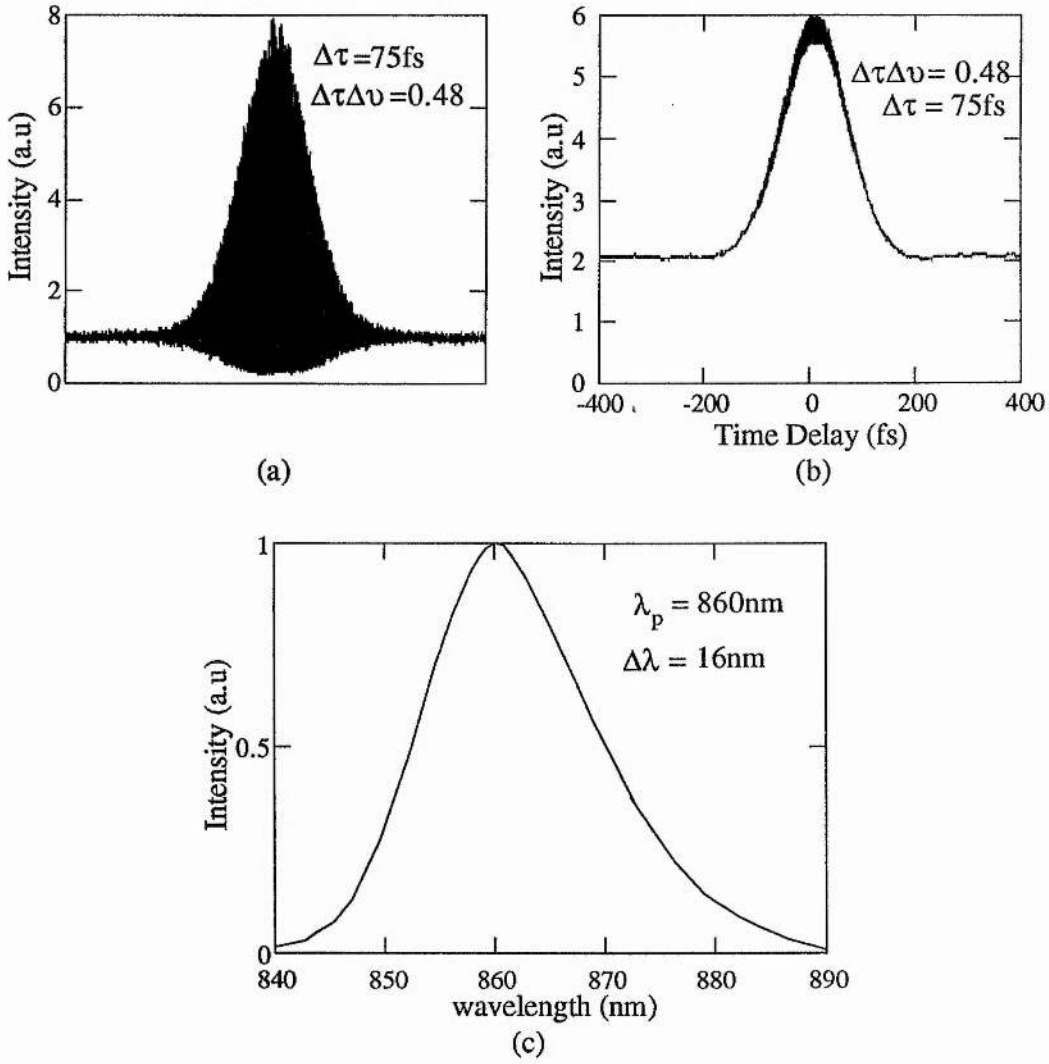


Figure 5.9: (a) Interferometric (b) intensity autocorrelation and (c) spectral data for the output pulses from the self-modelocked Brewster-angled Cr:LiSAF laser.

When pumped at levels of ~800mW, this laser produced at self-modelocked output of 75fs, with an average power of 30mW. The self-modelocking threshold was measured to be ~650mW. The output characteristics of this laser are illustrated above in figure 5.9. The intensity and interferometric auotcorrelation data show that the duration of the pulses are ~75fs. The spectral data implies a bandwidth of ~16nm, giving a duration-

bandwidth product of 0.48. This value implies that the pulses contain excess frequency chirp. However, this is not evidence of excess frequency chirp in the interferometric autocorrelation. The spectrum obtained was asymmetric and it was therefore difficult to ascertain a true spectral bandwidth. The appearance of such asymmetry may have been due to excess pumping of the laser.

## 5.4 Conclusions.

In this chapter an introduction into the optical properties of the $Cr^{3+}$ ion has been given along with the laser characteristics of $Cr^{3+}$-doped LiSAF. The construction and operation of an all-solid-state, self-modelocked Cr:LiSAF laser has also been described. This laser was capable of producing 90fs pulses with an average output power of 30mW, at a pump power level of ~500mW.

It has been shown that although Cr:LiSAF exhibits a lower oscillation threshold than Ti:sapphire, it suffers from quenching of laser action at modest operational temperatures, and mechanical failure at pump powers above 1.5W. This means that as a source of ultrashort pulses in the near-infrared at modest output powers, it has not been shown to be superior to Ti:sapphire systems. However, improvements in the output power and spectral brightness of laser diodes have now led to the construction of efficient, compact self-modelocked Cr:LiSAF lasers pumped directly by diode lasers[28]. This now means that compact, reliable all-solid-state Cr:LiSAF laser systems operating at low output powers, are now becoming a reality.

## 5.5 References.


[1] M. Stalder, B.H.T Chai and M. Bass "Flashlamp pumped Cr:LiSrAlF$_6$ laser", *Appl. Phys. Lett.*, Vol.58 p.216 (1991).

[2] N.H Rizvi, P.M.W French and J.R Taylor "Generation of 33fs pulses from a passively modelocked Cr3+:LiSrAlF$_6$ laser", *Opt. Lett*, Vol.17 p.1605 (1992).

[3] S.A Payne, L.L Chase, L.K Smith, W.L Kway and H.W Newkirk Laser performance of LiSrAlF$_6$:$Cr^{3+}$", *J. Appl.Phys.*, Vol.66 p.1051 (1989).

[4] D.J Harter, J. Squier and G. Mourou "Alexandrite-laser-pumped $Cr^{3+}$:LiSrAlF$_6$", *Opt. Lett.*, Vol.17 p.1512 (1992).

[5] R. Scheps, J.F Myers, H.B Serreze, A. Rosenberg, R.C Morris and M. Long "Diode-pumped Cr:LiSrAlF$_6$ laser", *Opt. Lett.*, Vol.16 p.820 (1991).

[6] J.M Evans, D.E Spence W. Sibbett, B.H.T Chai and A. Miller "50fs pulse generation from a self-modelocked Cr:LiSrAlF$_6$ laser", *Opt. Lett*, Vol. 17 p.1447 (1992).

[7] A. Miller, P. LiKamWa, B.H.T Chai and E.W Van Stryland "Generation of 150fs tunable pulses in Cr:LiSrAlF$_6$", *Opt. Lett.*, Vol.17 p.195 (1992).

[8] Q. Zhang, G.J Dixon, B.H.T Chai and P.N Kean "Electronically tuned diode-laser-pumped Cr:LiSAF laser", *Opt. Lett*, Vol.17 p.43 (1992).

[9] M.J.P Dymott, I.M Botheroyd, G.J Hall, J.R Lincoln and A.I Ferguson "All-solid-state actively,modelocked Cr:LiSAF laser", *Opt.Lett* ., Vol.19 p.634 (1994).

[10] S.A Payne, L.L Chase, L.J Atherton, J.A Caird, W.L Kway, M.D Shinn, R.S Hughes and L.K Smith *Solid-State Lasers,* SPIE Conf. Series Vol.1223 p.84 (1990).

[11] S.A Payne, W.F Krupke, L.K Smith, W.L Kway, L.D DeLoach and J.B Tassano "752nm wing-pumped Cr:LiSAF laser", *IEEE J. Quantum. Electron.*, QE-28 p.1188 (1992).

[12] T.H Maiman *Nature* Vol.187 p.493 (1960).

[13] S.T Lai "Highly efficient emerald laser", *J. Opt. Soc. Am. B.*, Vol.4 p.1286 (1987).

[14] S.A Payne, L.L Chase, H.W Newkirk, L.K Smith and W.F Krupke, "LiCaAlF$_6$:$Cr^{3+}$: A promising new solid-state laser material", *IEEE. J. Quantum. Electron.*, QE-24 p.2243 (1988).

[15] S.T Lai and M.L Shand "High efficiency cw laser-pumped tunable alexandrite laser", *J. Appl. Phys.*, Vol.54 p.5642 (1983).

[16] S.A Payne, L.L Chase, L.K Smith, W.L Kway and H.W Newkirk "Laser performance of LiSrAlF$_6$:$Cr^{3+}$", *J. Appl. Phys.*, Vol. 66 p.1051 (1989).

[17] B. Struve and G. Huber "Laser performance of Cr3+:GdScGa garnet", *J. Appl. Phys.*, Vol.57 p.45 (1985).

[18] J. Drube, B. Struve and G. Huber "Tunable room-temperature cw laser action in $Cr^{3+}$:GdScAl garnet", *Opt. Commun.*, Vol.50 p.45 (1984).

[19] H.P Jenssen and S.T Lai "Tunable laser characteristics and spectroscopic properties of SrAlF$_6$:Cr", *J. Opt. Soc. Am. B.*, Vol.3 p.115 (1986).

[20] V. Petricevic, S.K Gayen, R.R Alfano, K. Yamagishi, H. Anzai and Y. Yamaguchi "Laser action in chromium-doped forsterite", *Appl. Phys. Lett.*, Vol.52 p.1040 (1988).

[21] M.L Shand, H.P Jenssen"Temperature-dependence of the excited-state absorption of alexandrite", *IEEE J. Quantum. Electron.*, QE-19 p.480 (1983).

[22] H.W.H Lee, S.A Payne and L.L Chase "Excited state absorption of $Cr^{3+}$ in $LiCaAlF_6$ - effects of asymmetric distortions and intensity selection rules", *Phys. Rev. B.*, Vol.39 p.8907 (1989).

[23] S.E Stokowski, M.H Randles and R.C Morris "Growth and characterisation of large Nd, Cr-GSGG crystals for high average power slab lasers", *IEEE. J. Quantum. Electron* QE-24 p.934 (1988).

[24] J.A Caird, W.F Krupke, M.D Shinn P.R Staver and H.J Guggenheim, in Advances in Laser Science-I edited by W.C Swalley and M. Lapp (AIP, New York 1986).

[25] J.M Evans PhD Thesis, University of St. Andrews 1993.

[26] L.L Chase and S. Payne Optics and Photonics News p.16 August 1990.

[27] M. Stalder, M. Bass and B.H.T Chai "Thermal quenching of fluorescence in chromium-doped fluoride laser crystals", *J. Opt. Soc. Am. B* ., Vol.9 p.2271 (1992).

[28] D. Burns, M.P Critten and W. Sibbett "A low threshold all-solid-state, femtosecond Cr:LiSAF laser" *Opt. Lett* .. accepted for publication.

# Chapter 6: A self-modelocked Ti:$Al_2O_3$ laser operating at 1.053μm.

## 6.1 Introduction:

Successful operation of a tunable laser system capable of producing picosecond and sub-picosecond pulses at 1μm is interesting for a number of applications. In particular, the performance of Nd:glass chirped pulse amplification systems used to generate ultrashort, high energy pulses, can be significantly improved by introducing such a source as a master oscillator[1,2].

Until now, sub-picosecond pulses with the highest energies have been extracted from solid-state amplifier media such as Nd:glass. However, in order to amplify short pulses, three basic requirements have to be met. Firstly, the bandwidth of the amplifying medium must be large enough to accommodate the full spectrum of the short pulse. Secondly, to efficiently extract the energy stored in the amplifier, the fluence of the short pulse has to be near the saturation fluence of the amplifier medium and thirdly, the intensity within the amplifier must remain below the critical level at which nonlinear effects become significant. Nd:glass has a bandwidth greater then 20nm and should therefore be capable of supporting pulses as short as 100's of femtoseconds. Unfortunately, amplifying a 1ps pulse to the saturation fluence of Nd:glass creates a power density far above the critical level of the amplifier. This leads to the onset of nonlinear effects such as self-focussing which distorts the spatial and temporal profiles of the pulses and can also lead to catastrophic damage of the amplifier. These high power levels therefore mean inefficient energy extraction. Chirped pulse amplification (CPA) was first introduced in 1985[3] as a reliable technique to amplify short pulses to the saturation levels required, while maintaining moderate power levels within the amplifier.

In CPA, a long optical pulse is deliberately produced by stretching a short, low energy pulse in a single mode optical fibre. The pulse is linearly chirped in the fibre due to group velocity dispersion and self-phase modulation effects. The stretched pulse is then amplified and subsequently recompressed by a double grating pair. Amplifying the stretched pulse rather than the compressed pulse allows for higher energies to be achieved before self-focussing occurs. It has been shown that amplification does not appear to effect the chirp linearity of the pulse, therefore the pulses can be fully recompressed.

Using CPA, picosecond pulses generated by modelocked Nd:YAG and Nd:YLF lasers have been amplified in Nd:glass to powers in the order of a joule, producing peak powers up to 30 TW[4-8]. However, the shortest pulse duration available from these systems has been limited by spectral narrowing during the amplification process[9]. In order to achieve shorter, higher energy pulses it is therefore necessary to eliminate this spectral narrowing in the regenerative amplifier. This has been achieved by replacing the Nd:glass regenerative amplifier with Ti:$Al_2O_3$ tuned to match the peak of Nd:glass at 1.053μm[10-12].

Ti:$Al_2O_3$ is an excellent amplifier material because of its high energy storage capacity, long upper level lifetime and high thermal conductivity. Despite its low gain at 1.053μm, Ti:$Al_2O_3$ is still suitable for the amplification of picosecond and femtosecond pulses up to the mJ level since the saturation fluence of Ti:$Al_2O_3$ is comparable to that of Nd:glass at these long wavelengths. Also, the spectrum of a free-running Ti:$Al_2O_3$ regenerative amplifier is 6 times the width of Nd:glass, hence short pulses can be successfully amplified without experiencing any spectral narrowing[13].

To produce ultrashort high energy pulses in the order of 100's of femtoseconds, pulses 10's of picoseconds long generated from a Nd:YLF oscillator have to be spectrally broadened in an optical fibre before undergoing the amplification process. However, these systems are unable to produce high energy pulses with durations shorter than 1ps. Due to the broad bandwidth of Ti:$Al_2O_3$ which extends from 690-1160nm, self-modelocked Ti:$Al_2O_3$ lasers are capable of producing 100fs pulses at

1.053μm, and are now being considered as master oscillators for high power TW systems[14,15].

In this chapter, the construction of a compact all-solid-state, self-modelocked Ti:$Al_2O_3$ laser is examined. In particular, the generation of ultrashort pulses at 1.053μm for the purpose of a master oscillator for a Ti:sapphire/Nd:glass power chain, is the key motive for this work.

## 6.2 A Self-Modelocked Ti:$Al_2O_3$ Laser Operating at ~1μm.

The basic laser cavity configuration is shown schematically in figure 6.1. The laser cavity was approximately 1.1m long and was symmetric around a 10mm long, Brewster-angled rod of titanium-doped sapphire which had a pump absorption coefficient of 2.3 $cm^{-1}$ (Crystal Systems). The folding section consisted of spherical mirrors $M_1$ and $M_2$ with a radius of curvature of 100mm and were highly reflecting over the spectral region 980 - 1100nm and highly transmitting for the 532nm pump wavelength (LaserOptik). Mirror $M_3$ and $M_4$ were output couplers and highly reflecting end mirrors respectively. The pump beam was focussed into the Ti:$Al_2O_3$ rod with a 100mm focal length lens. For the initial investigation, the Ti:$Al_2O_3$ laser was pumped with a Spectra-Physics argon-ion Model 2030 laser at 514nm. The free-running wavelength of this Ti:$Al_2O_3$ oscillator was 993nm.

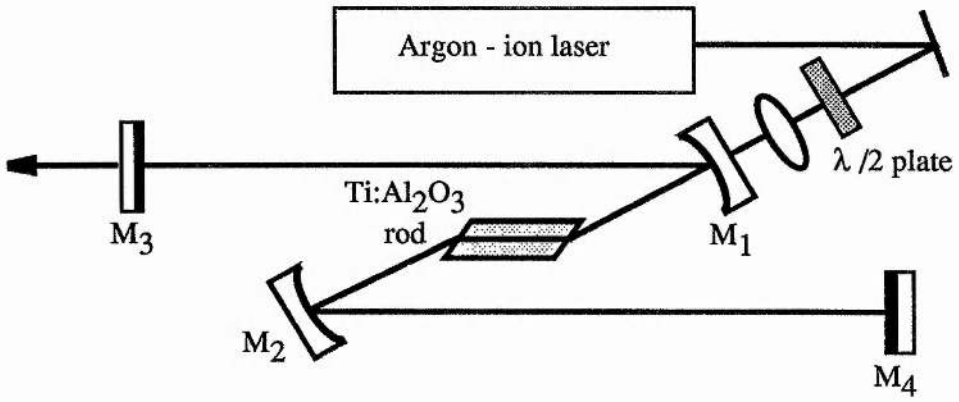


Figure 6.1: Schematic diagram of basic laser cavity configuration.

The cw output power of the Ti:$Al_2O_3$ laser was measured as a function of input pump power for a range of output couplers. Figure 6.2 shows the measured slope efficiencies of this laser for the different output couplers.

Using equation 2.2, and the power characteristics measured from this laser, we calculated an intrinsic slope efficiency $\eta_0$=17% and a total passive loss L = 0.7%. This means that the loss per pass due to the Ti:$Al_2O_3$ crystal and the other cavity mirrors is 0.35%.

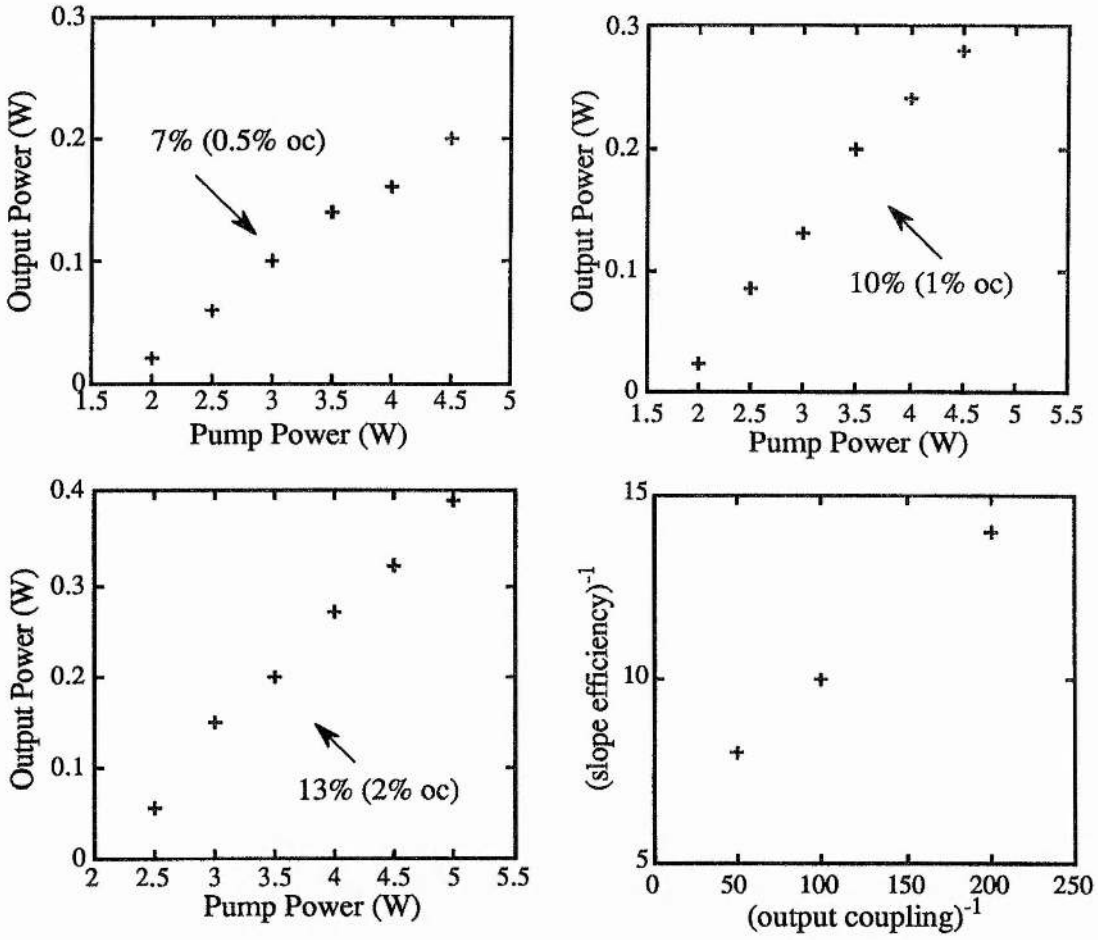


Figure 6.2: Incident pump power versus cw output power for various output coupling.

The cw output of the Ti:$Al_2O_3$ laser was tuned continuously across the bandwidth of the mirrors, which were coated to have high reflectivity from 980 - 1100nm. A SF14 prism was placed in one arm the of the laser cavity as a dispersive

element. Output spectra were measured with an output coupling of 0.5% at pump powers of 5W and 7W and these results are shown below in figures 6.3 and 6.4.

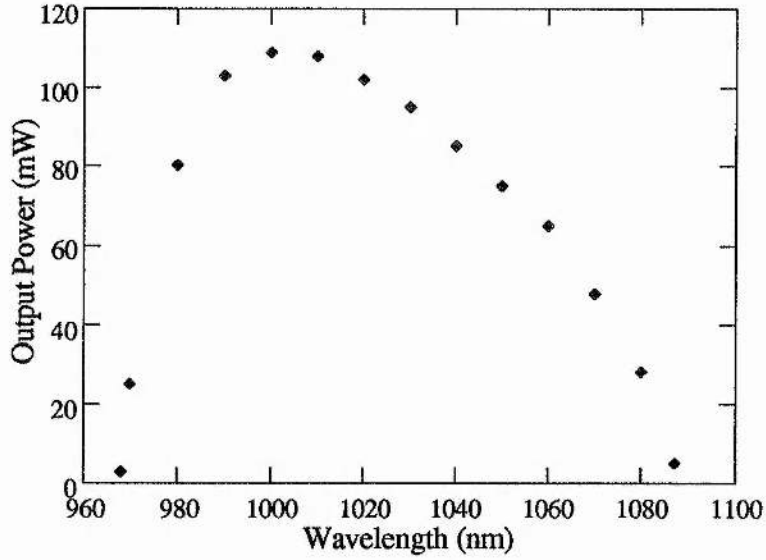


Figure 6.3: Output power versus wavelength for a cw Ti:$Al_2O_3$ laser at 5W pump power.

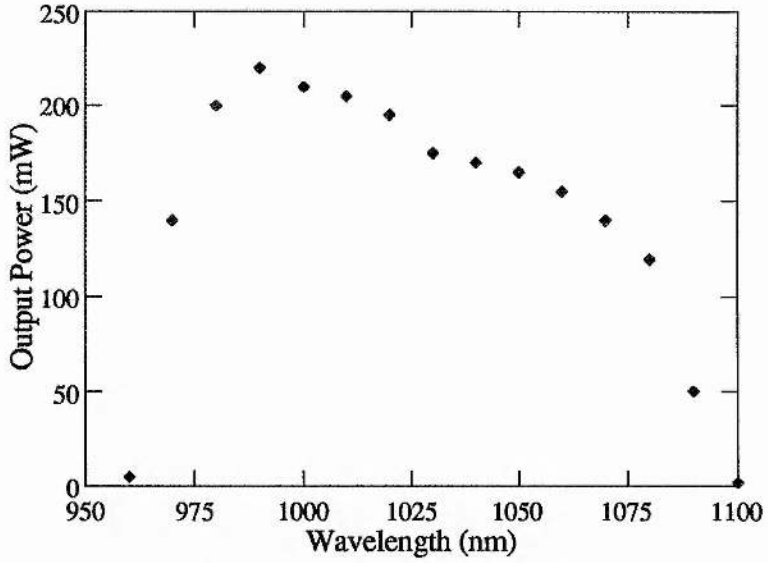


Figure 6.4: Output power versus wavelength for the cw Ti:$Al_2O_3$ laser at 7W pump power.

From these plots it can be seen that the cw output powers obtained at 1053nm were 70mW and 160mW respectively. The sharp cut-offs at both 960nm and 1100nm

were due to the spectral limits of the mirror coating. The long wavelength cut-off at 1100nm is also due to the edge of the $Ti:Al_2O_3$ fluorescence spectrum. It was observed that the laser threshold power for cw operation at 1053nm was -3.5W for an output coupling of 0.5%. These results indicate that for the successful construction of an all-solid-state $Ti:Al_2O_3$ oscillator operating at 1053nm, the pump source must be capable of producing a cw output power of ≥4W.

In order to investigate the self-modelocked operation of this $Ti:Al_2O_3$ laser, the cavity was extended to approximately 1.8m in length and an acousto-optic modulator and SF14 prism sequence were inserted into the cavity. The self-modelocked cavity configuration is illustrated schematically in figure 6.5.

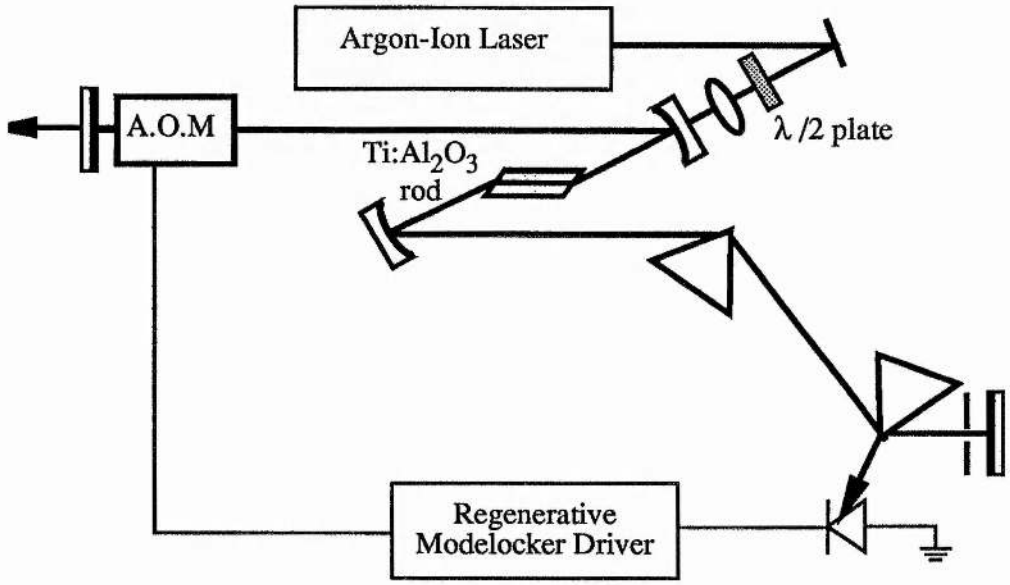


Figure 6.5: Schematic diagram of a modelocked $Ti:Al_2O_3$ laser cavity.

At pumping levels of ~5W and an output coupling of 1%, the $Ti:Al_2O_3$ laser generated 100fs pulses, with an average output power of 30mW. When the laser was allowed to oscillate freely in an optimised cavity, the self-modelocked output wavelength was measured to be 1μm. These results are shown below in figure 6.6. Figures 6.6a and 6.6b show the intensity and interferometric autocorrelation data measured for these pulses, respectively. Figure 6.6c shows the spectral data for a 100fs pulse and indicates a spectral bandwidth of 11nm centred around 1005nm. From these

data, the duration-bandwidth product was calculated to be 0.34, implying that these pulses were transform-limited under these self-modelocking conditions.

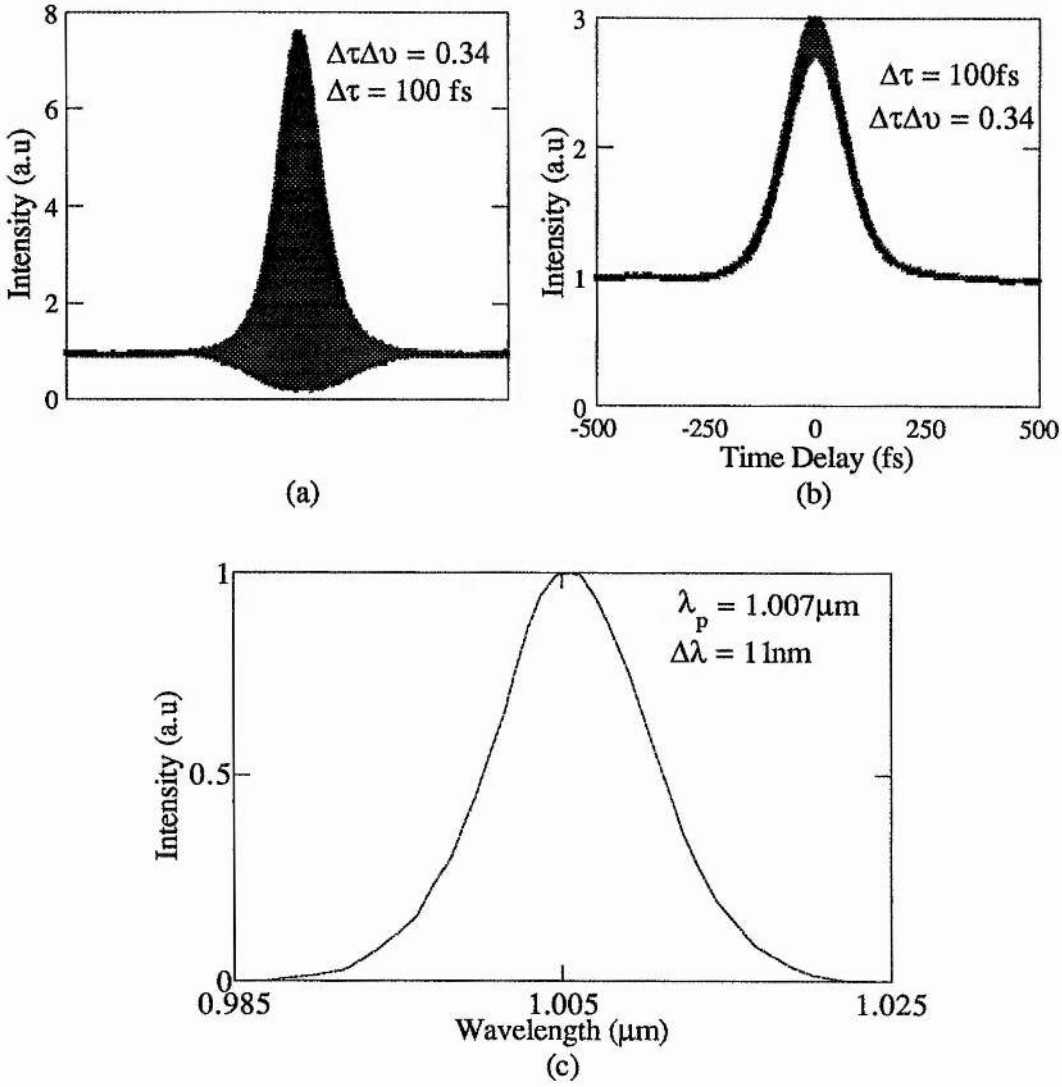


Figure 6.6: (a) Interferometric autocorrelation (b) intensity autocorrelation data and (c) spectral data for the output of the self-modelocked Ti:$Al_2O_3$ laser operating at 1μm.

With the aid of a vertical slit placed next to the highly reflecting end mirror, the self-modelocked Ti:$Al_2O_3$ laser was tuned across its spectral bandwidth to 1053nm. For a pump power of ~5W and an output coupling of 1%, this laser produced 30mW, 140fs pulses at a wavelength of 1053nm. The output characteristics of the laser at this wavelength are shown below in figure 6.7. Figures 6.7a and 6.7b show the interferometric and intensity autocorrelation data measured for these output pulses.

Figure 6.7c shows the measured spectral data giving a pulse spectral bandwidth of 9nm, centred around 1053nm. From these data, the calculated duration-bandwidth product was again 0.34, indicating that these pulses were transform-limited under these self-modelocking conditions.

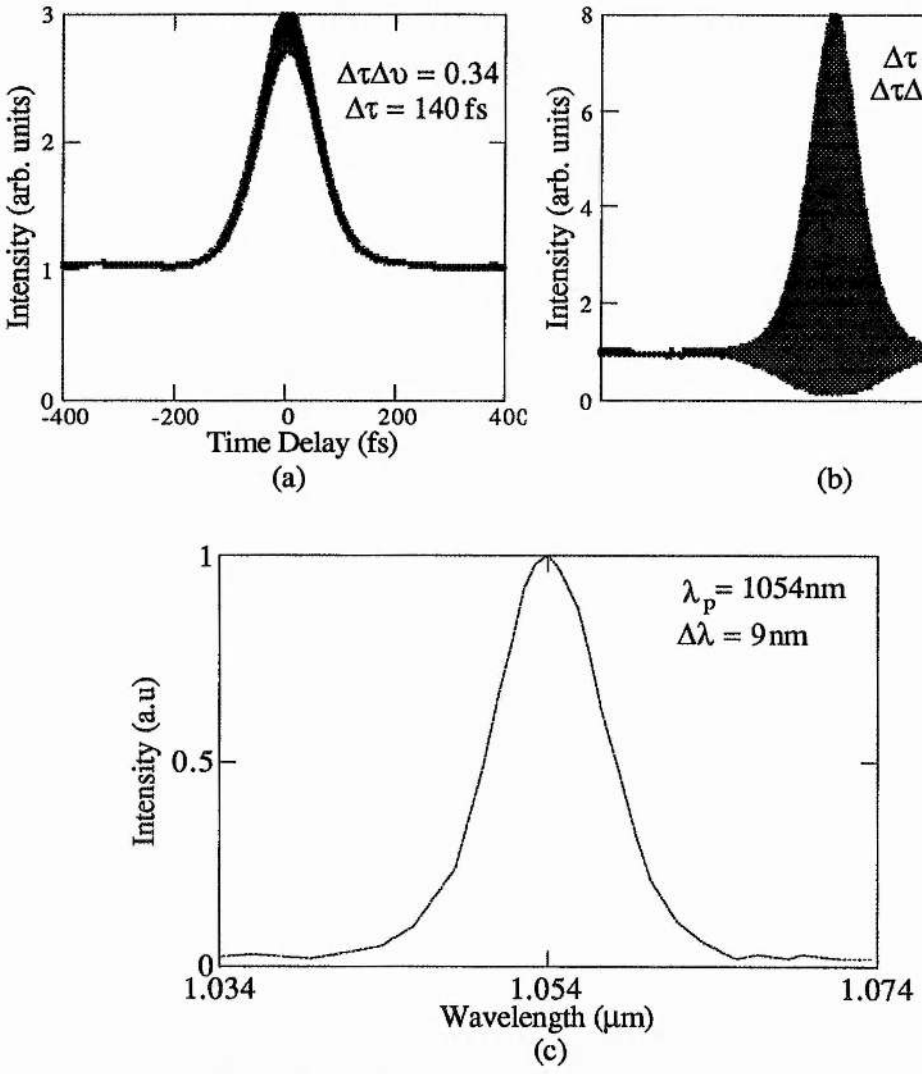


Figure 6.7: (a) Interferometric autocorrelation (b) intensity autocorrelation data and (c) spectral data from the output pulses from a self-modelocked Ti:$Al_2O_3$ laser operating at 1.053μm.

From these results obtained for self-modelocked operation, it can be seen that the construction of a similar all-solid-state laser system requires a pump source producing a cw output power of ~5W.

Conventionally, losses from the surface of the laser crystal are minimised by cutting the crystal faces at the Brewster angle. However, this has the effect of increasing the pump and cavity mode waists by a factor equal to the refractive index of the material. In an attempt to decrease the oscillation threshold of the Ti:$Al_2O_3$ laser, by decreasing the mode waists inside the crystal, a cavity configuration incorporating a plane-cut gain medium was constructed. For the short, basic laser cavity illustrated in figure 6.1, the cavity mode waist in the plane-cut rod was calculated to be 28μm. The variation of mode waist over the length of the crystal is shown below in figure 6.8.

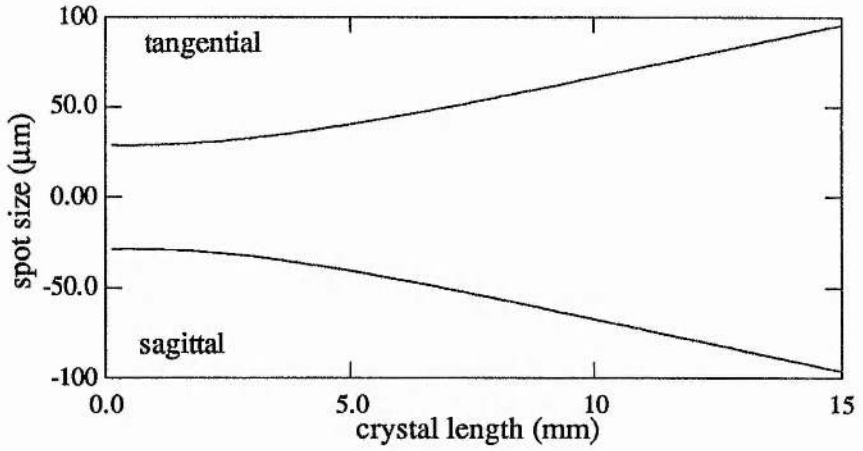


Figure 6.8: Beam waist inside the plane-cut Ti:$Al_2O_3$ laser rod.

In the case of the brewster-angled rod, the laser mode is elliptical in shape with radii 30μm and 52μm, leading to a mode area twice as large as the mode area in the plane-cut rod. Figure 6.9 shows the variation of the mode waist over the length of the Brewster-cut laser rod.

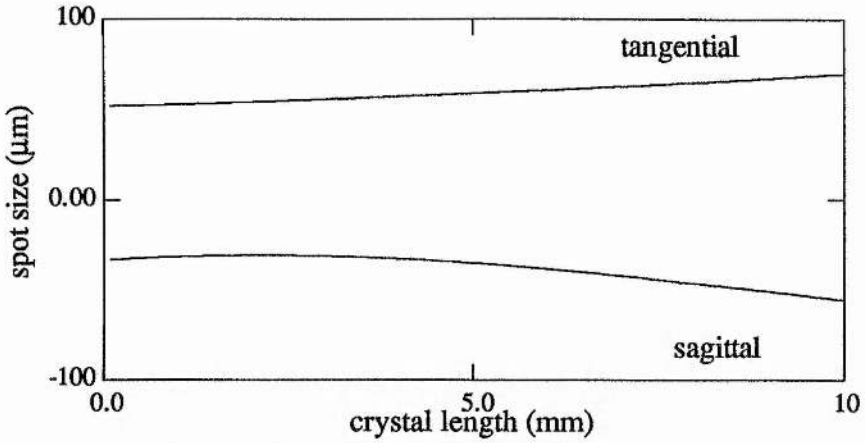


Figure 6.9: Beam waist inside the brewster-cut Ti:$Al_2O_3$ laser rod.

Because the threshold power varies with the area of the cavity mode, we would expect the tighter the cavity mode waist inside the crystal, the lower the oscillation threshold power, assuming a good mode-match between pump and cavity modes. However, although the mode waist is tighter in the plane rod, the rate of change of mode waist over the length of the crystal is much larger, therefore an average mode radius has to be considered.

To predict the reduction in oscillation threshold by using a plane-cut rod, the cavity was modelled using the results already obtained for the short laser cavity incorporating the Brewster-cut rod. Assuming no extra losses introduced into the cavity by replacing the Brewster rod with an identical plane rod (i.e perfect anti-reflection coatings at both the pump and laser wavelengths), the oscillation threshold was calculated to be ~1.2W with a 1% output coupler at a wavelength of 1000nm. For an output coupling of 1%, the oscillation threshold with the Brewster rod was measured experimentally to be ~1.8W at 1000nm as shown in figure 6.2. Data were obtained from the model, for the threshold values and slope efficiences of the plane rod as a function of excess loss introduced into the cavity, such as realistic coating losses on the crystal faces. The results are shown graphically in figure 6.10, were the dotted line represents the oscillation threshold and slope efficiency of the brewster-angled rod.

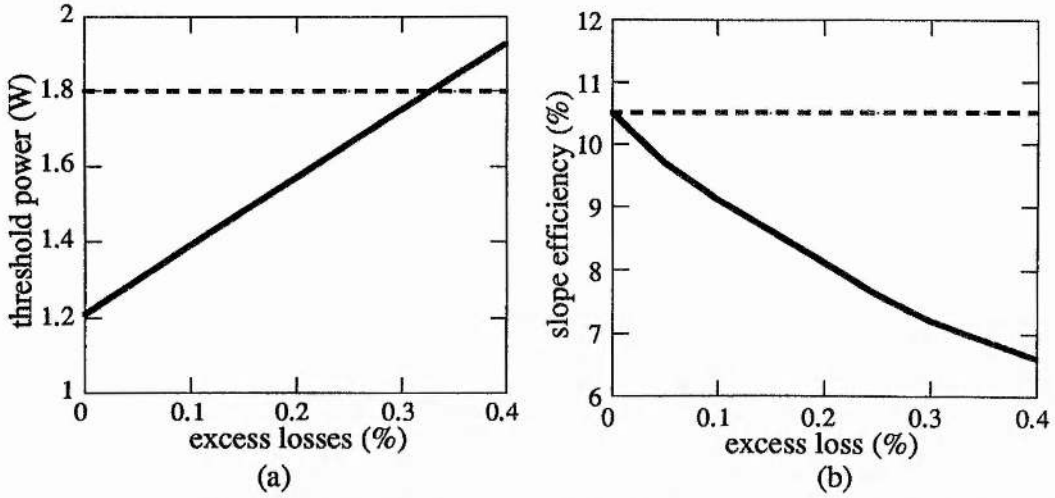


Figure 6.10: (a) Graph of threshold power of plane rod versus excess cavity losses, and (b) graph of the slope efficiency of the plane rod versus excess cavity loss.

These results show that if the total losses due to the anti-reflection coatings on the plane rod exceed ~0.3% per pass, then no reduction in oscillation threshold is gained in using a plane rod over a brewster rod. These results were also obtained at a laser wavelength of 1000nm where the emission cross-section is ~0.3 times the peak emission cross-section. At 1053nm, the cavity mode waists increase very slightly in the rod leading to a marginal increase in threshold. However, the emission cross-section at 1053nm, is only 0.16 times the peak emission cross-section (see figure 6.11).

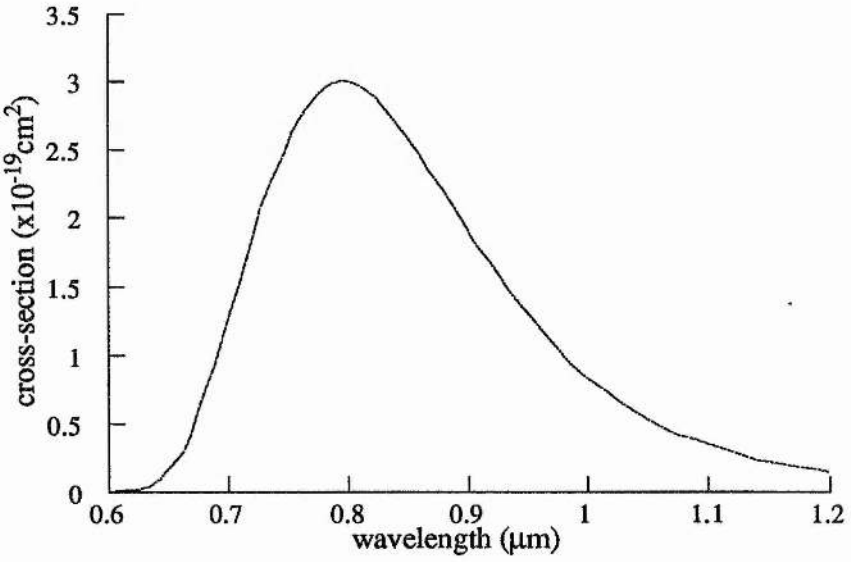


Figure 6.11: Stimulated emission cross-section of Ti:$Al_2O_3$ for π polarisations.[16]

From our model, it was calculated that this effect in a Brewster-cut rod leads to an increase in threshold from ~1.8W to ~3.2W, which has been experimentally verified in this work for an output coupling of 1%. It would therefore be expected that a similar increase in threshold power would be observed in a laser incorporating the plane-cut, rod when tuning the laser output from 1000nm to 1053nm (i.e from 1.2W to 2.1W).

A laser cavity was constructed with a 15mm long plane-cut Ti:$Al_2O_3$ laser crystal which had a pump absorption coefficient of 2.3$cm^{-1}$, and a FOM in excess of 300 (Union Carbide). The cavity was symmetric about the gain medium and the cavity was approximately 1.1m in length. The basic cw laser cavity configuration is identical to the configuration used in the case of the brewster-angled rod (see figure 6.1). The ends of the laser rod were anti-reflection coated for the laser oscillation wavelength of 1053nm. A 7% reflection loss of the pump radiation was measured at the front surface of the laser crystal. However, this loss may be significantly reduced by anti-reflection coating the ends of the rod for the pump wavelength.

Input power versus output power characteristics were measured for various output couplings and the data obtained are shown below in figure 6.12 at an output wavelength of 1000nm (the pump power was measured at the entrance of the pump focussing lens and has not been corrected for the 7% reflection loss).

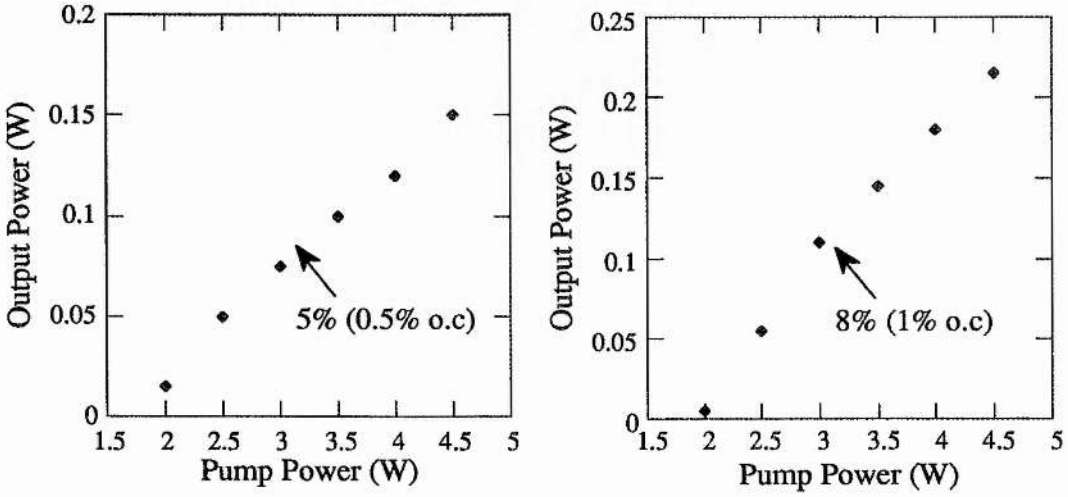

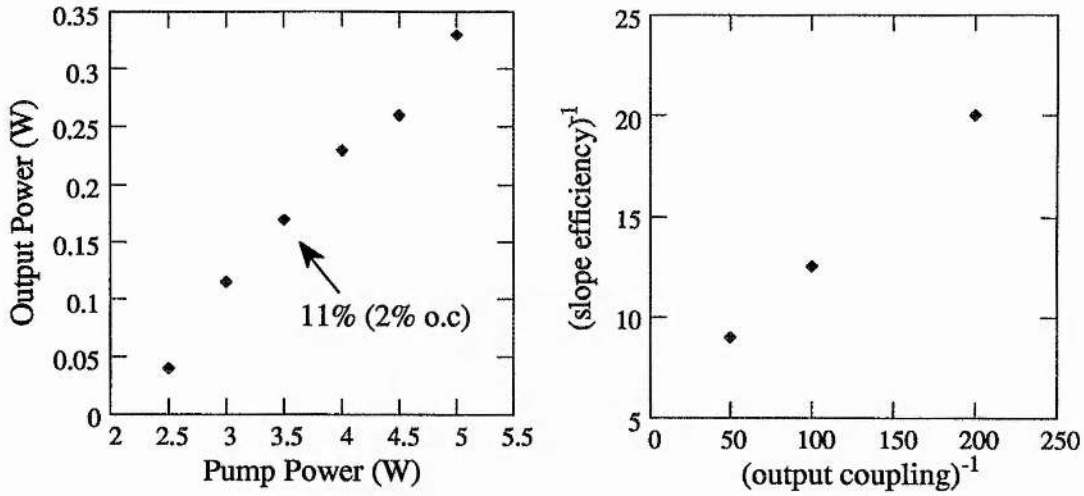


Figure 6.12: Incident pump power versus cw output power for the plane-cut laser rod.

From these data, the intrinsic slope efficiency of this laser was calculated to be 19%, giving a total passive loss per pass due to the coated crystal and the cavity mirrrors of 0.7%. The total passive losses measured in the case of the brewster rod was 0.35%, and since the cavity mirrors used in both cases are identical, this means that the coatings on the crystal have introduced an excess loss per pass of 0.35%. This excess loss due to the coatings and the loss of pump power due to reflection from the front surface of the crystal means that a reduction in oscillation threshold was not observed. For an output coupling of 1%, the oscillation threshold was measured to be ~2W which was the threshold power predicted from the model in figure 6.10a when an excess loss of 0.35% was present.

In order to observe the expected low threshold power characteristics of a laser incorporating a plane-cut rod it is therefore necessary to obtain very high quality, low loss anti-reflection coatings for both the laser oscillation wavelength and the pump laser wavelength. However, the possibility of coating a laser rod with multiple anti-reflection coatings and limiting the excess loss introduced by these coatings to below 0.3% per pass, does not appear to be possible.

## 6.3 Conclusions.

In this chapter, the development and construction of an argon-ion pumped, regeneratively-initiated, self-modelocked Ti:$Al_2O_3$ laser operating at the long wavelength limit of the laser bandwidth has been described. This laser was capable of generating 100fs pulses at 1000nm, with an average power of 30mW at a pumping level of 5W. By the use of a variable slit, this laser was tuned out to 1053nm, and results are shown for 140fs pulses at 1053nm, with an average power of 30mW. The possibilty of constructing an all-solid-state Ti:$Al_2O_3$ system operating at 1053nm, for use as a master oscillator for a Nd:glass power chain has also been discussed. From this work it has been observed that the powers required to produce a usable output from a self-modelocked Ti:$Al_2O_3$ laser at 1053nm is ~5W. Recently, commercial devices have become available which are capable of generating 5W of cw power at 532nm from an all-solid-state laser system (Spectra Physics Millennia). It is therefore possible that such a system could replace the argon-ion laser as a pump source for Ti:$Al_2O_3$ lasers in the near future.

## 6.4 References.


[1] C. Rouyer, E. Mazataud, I. Allias, A. Pierre, S. Seznec, G. Mourou and A. Migus "Generation of 50TW femtosecond pulses in a Ti:sapphire/ Nd:glass chain", *Opt. Lett.*, Vol.18 p.214 (1993).

[2] Y. Beaudoin, C.Y Chien, J.S Coe, J.L Tapie and G. Mourou "Ultrahigh-contrast Ti:sapphire/ Nd:glass TW laser system", *Opt. Lett.*, Vol.17 p.865 (1992).

[3] D. Strickland and G. Mourou "Compression of amplified chirped optical pulses", *Opt.Commun.*, Vol.56 p.219 (1985).

[4] M. Ferray, L.A Lompre, O. Gobert, A. L'Huillier, G. Mainfray, C. Manis, A. Sanchez and A.S Gomes "Multi-TW picosecond Nd:glass laser system at 1053nm", *Opt. Commun.*, Vol.75 p.278 (1990).

[5] C. Sauteret, D. Husson, G. Thiell, S. Seznec, S. Gary, A. Migus and G. Mourou "Generation of 20-TW pulses of picosecond duration using chirped-pulse amplification in a Nd:glass power chain", *Opt. Lett.*, vol.16 p.238 (1991).

[6] F. G Patterson, R. Gonzales and M.D Perry "Compact 10-TW, 800fs Nd:glass chain", *Opt. Lett.*, Vol.16 p.1107 (1991).

[7] Y.H Chuang, D.D Meyerhofer, S. Augst, H. Chen, J. Peatross and S. Uchida "Suppresion of the pedestal in a chirped pulse amplification laser", *J. Opt. Soc.Am.B.*, Vol.8 p.1226 (1991).

[8] K. Yamakawa, C.P.J Barty, H. Shiraga and Y. Kato "Generation of high-energy picosecond laser pulses with a high contrast ratio by chirped pulse amplification", *IEEE J. Quantum. Electron.*, QE-27 p.288 (1991).

[9] J. Coe, P. Maine, P. Bado "Regenerative amplification of picosecond pulses in Nd:YLF - gain narrowing and gain saturation", *J. Opt. Soc. Am. B.*, Vol.5 p.2560 (1988).

[10] J. Squier, F. Salin, G. Mourou and D. Harter "100fs pulse generation and amplification in Ti:$Al_2O_3$", *Opt. Lett.*, Vol.16 p.324 (1991).

[11] J.D Kmetec, J.J Macklin, J.F Young "0.5-TW, 125fs Ti:sapphire laser", *Opt. Lett.*,Vol.16 p.1001 (1991).

[12] A. Sullivan H. Hamster, H.C Kapteyn, S. Gordon, W. White, H. Nathel, R.J Blair and R.W Falcone "Multi-TW, 100fs laser", *Opt. Lett.*, Vol.16 p.1406 (1991).

[13] F. Salin, C. Rouyer, J. Squier, S. Coe and G. Mourou "Amplification of 1ps pulses at 1.053μm in a Ti:$Al_2O_3$ regenerative amplifier", *Opt. Commun.*, Vol.84 p.67 (1991).

[14] C. Rouyer, E. Mazataud, I. Allias, A. Pierre, S. Seznec, C. Sauteret, G. Mourou and A. Migus "Generation of 50-TW femtosecond pulses in a Ti:sapphire/ Nd:glass chain", *Opt. Lett.*, Vol.18 p.214 (1993).

[15] J. Squier, F. Salin, S. Coe, P. Bado and G. Mourou "Characteristics of an actively-modelocked 2ps Ti:sapphire laser operating in the 1μm wavelength regime", *Opt. Lett.*, Vol.16 p.85 (1991).

[16] J. Squier, F. Salin, S. Coe, P. Bado and G. Mourou "Characteristics of an actively-modelocked 2ps Ti:sapphire laser operating in the 1μm wavelenth regime", *Opt. Lett.*, Vol.16 p.85 (1991).

# Chapter 7: General Conclusions.

The work described in this thesis has been concerned with the development of tunable, femtosecond laser systems exhibiting low threshold powers for both continuous-wave and self-modelocked laser operation. The development of both self-modelocked Ti:$Al_2O_3$ lasers and self-modelocked Cr:LiSAF lasers has been discussed, although most of the work has concentrated on the development of Ti:$Al_2O_3$ laser systems.

Since its first demonstration by Moulton in 1982, the Ti:$Al_2O_3$ laser has become the most popular source of laser radiation in the near-infrared spectral region. One of its most striking features is its tuning range from 660-1180nm, giving a bandwidth of over 400nm, which extends well beyond that of any dye compound and has the potential of producing pulses as short as 4fs. The broad absorption peak of titanium-doped sapphire around 500nm makes the conventional argon-ion laser an obvious pump source for this laser material. However, the use of an efficient, stable and compact all-solid-state laser is an extremely attractive alternative to the current high power pump lasers. Until recently, the development of all-solid-state Ti:$Al_2O_3$ lasers has been held back by the relatively high cw oscillation threshold powers of Ti:$Al_2O_3$ lasers, and by the low output powers from all-solid-state "green" lasers. To date pulsed operation of Ti:$Al_2O_3$ lasers has been reported using frequency-doubled modelocked and Q-switched Nd:YLF and Nd:YAG lasers. Continuous-wave operation of an all-solid-state Ti:$Al_2O_3$ laser has also been reported that had been specifically designed for low threshold operation at 200mW.

In the early days, one of the major problems in the construction of efficient Ti:$Al_2O_3$ lasers was that the laser performance was impaired by the presence of a weak residual infra-red absorption that peaks around 820nm, causing the laser to re-absorb its emitted radiation. This residual infrared absorption has been shown to be due to the presence of $Ti^{3+}$-$Ti^{4+}$ pairs within the crystal, which are formed during the crystal growth process. Growth of titanium-doped sapphire has been achieved using various growth techniques such as the heat-exchanger method (HEM) and the Czochralski

method. Unlike all the other growth techniques, HEM is a non-moving method which leads to the production of high quality laser crystals containing no lattice distortions. Also using this method, the titanium ions are formed in the lattice predominantly as $Ti^{3+}$ ions as the crystal boule is grown under a vacuum or a controlled atmosphere. In moving growth techniques such as the Czochralski method, lattice distortionds can only be minimised but not avoided. These growth techniques also favour the production of $Ti^{4+}$ ions under their oxidisng system and further treatment of these crystals is required to convert the $Ti^{4+}$ ions back to $Ti^{3+}$ ions to improve the crystal quality. This has been achieved by annealing the crystals at high temperatures in a reducing atmosphere, such as an Ar-$H_2$ mixture.

Although the HEM technique inherently produces high quality laser crystals, recent improvements in annealing techniqes have now shown that crystals grown by either technique are of a comparable high optical quality. Over the fast 5 years there has been great progress in crystal growth techniques leading to the production of high quality laser crystals exhibiting low residual infra-red absorption along with the possibility of relatively high dopant concentrations. This in itself has aided the development of efficient Ti:$Al_2O_3$ lasers, exhibiting low loss and low threshold powers.

In chapter 2, the construction and continuous-wave operation of a Ti:$Al_2O_3$ laser was discussed. This laser incorporated a 10mm-long Brewster-angled Ti:$Al_2O_3$ laser crystal with a pump absorption coefficient of $1.9cm^{-1}$. The lowest threshold power achieved was ~350mW in a cavity with no output coupling loss. This crystal was then replaced by a crystal with a slightly higher dopant level. The pump absorption coefficient was $2.3cm^{-1}$, and this laser demonstrated a continuous-wave, laser oscillation threshold of ~230mW.

Results were also presented for a regeneratively-initiated self-modelocked Ti:$Al_2O_3$ laser. At a pump power of ~2W, this laser was capable of generating ultrashort pulses of typically 85fs in duration, with an average power of 110mW at 840nm. This laser was also capable of generating pulses of typically 100fs in duration at pump levels as low as 500mW. The demonstration of self-modelocked operation at such low pump

powers, means that the development of an all-solid-state, self-modelocked Ti:$Al_2O_3$ laser now looks possible.

This laser system relied on an acousto-optic modulator to initiate and stabilise self-modelocked operation, although the laser was capable of generating stable pulse trains for periods of hours with the modulator disconnected. However, self-modelocked operation could easily be disrupted by external perturbations in the laboratory enviroment, and the modulator was required to again initiate self-modelocked operation. The requirement of the regeneratively-driven modulator adds to the complexity and the overall size of the laser system. In a move towards compact and portable laser systems, it would therefore be an advantage not to have to rely on any actively-driven electronic components.

One such alternative system is a hard-aperture, self-modelocked Ti:$Al_2O_3$ laser. Results were presented for the operation of a hard-aperture, self-modelocked Ti:$Al_2O_3$ laser which routinely produced 150mW, 80fs pulses at pumping levels of ~3W. This laser system was also capable of producing 100fs pulses at pump power levels as low as 1.5W. Unfortunately, the self-modelocking threshold was found to be higher than the regeneratively-initiated Ti:$Al_2O_3$ laser, meaning that it was not such a good candidate for the developement an all-solid-state Ti:$Al_2O_3$ laser system.

Chapter 3 compared the phase-noise characteristics of both the regeneratively-initiated, self-modelocked Ti:$Al_2O_3$ laser and the hard-aperture self-modelocked Ti:$Al_2O_3$ laser. The development of modelocked lasers with very low phase noise characteristics is important in applications such as electro-optic sampling, time-domain spectroscopy and synchronous streak camera measurements. Results show that the hard-aperture, self-modelocked system was inherently less noisy than the regeneratively-initiated system. The timing jitter figures (phase noise) were measured to be 6.3ps (50-500Hz) and 797fs (500Hz-5kHz) for the regeneratively-initiated laser, and 3.8ps (50-500Hz), 231fs (500Hz-5kHz) for the hard-aperture, self-modelocked laser. Details of a phase-noise reduction technique were described and this technique was applied to both of the self-modelocked Ti:$Al_2O_3$ laser configurations. This technique which was based on cavity

length stabilisation, reduced the total timing jitter on the output pulse trains to values as low as 300fs at freqeuncies below 5 kHz. These results illustrate the effectiveness of the phase-noise reduction technique employed, and are the lowest timing jitter figures reported from an argon-ion-pumped, self-modelocked Ti:$Al_2O_3$ laser.

Low phase noise optical sources have direct applications for use in conjunction with synchronously-operating streak cameras having femtosecond resolution. Research into the development of high resolution streak cameras has been ongoing at St. Andrews for many years, and has led to the production of the Photochron V streak tube. The low phase noise, self-modelocked Ti:$Al_2O_3$ laser was used to evaluate the temporal resolution of this streak tube, and a streak pulse profile with a resolution of 900fs was successfully obtained. Work is ongoing in this area to improve the camera resolution in order to achieve a temporal resolution of the order of 500fs.

In the construction of a highly-stable, low phase noise, self-modelocked Ti:$Al_2O_3$ laser, for use in conjunction with high resolution streak cameras, the use of an efficient, stable and compact diode-laser-pumped minilaser represents an attractive alternative to argon-ion lasers. Diode-pumped minilasers only require power supplies operating at low voltage and current ratings compared to an argon-ion laser which command a input power of 300V at 50A. Low voltage power supplies have the advantage of being more easily smoothed to produce low ripple outputs. The low phase noise characteristics of an all-solid-state laser system has been recently demonstrated at St. Andrews, in a self-modelocked Cr:LiSAF laser directly pumped by a single self-injection locked semiconductor laser. The measured timing jitter figures for this unlocked laser was a factor of two better than the measured phase noise figures of the argon-ion pumped Ti:$Al_2O_3$ laser described in section 3.2.1.

The development of all-solid-state pump sources for Ti:$Al_2O_3$ lasers should not only lead to lower phase noise systems, but also to the construction of portable Ti:$Al_2O_3$ lasers systems. Such systems could be plugged straight into conventional mains wall sockets, instead of requiring the installation of three-phase power supplies along with high pressure water required for cooling. In chapter 4, the operation of an all-solid-state,

self-modelocked Ti:$Al_2O_3$ laser is described. The pump laser was a continuous-wave, intracavity frequency-doubled, diode-laser pumped Nd:YLF ring laser. When operated unidirectionally, this laser was capable of producing powers of up to 1W at 523.5nm in a $TEM_{00}$ mode output. At a pumping level of 700mW, the self-modelocked Ti:$Al_2O_3$ laser was capable of producing 110fs pulses with an average output power of 20mW and were centred at a wavelength around 800nm.

Although the output power of this Nd:YLF ring laser was sufficient to pump this Ti:$Al_2O_3$ laser, for such a system to replace an argon-ion pumped, self-modelocked Ti:$Al_2O_3$ laser, the development of an all-solid-state pump source producing output powers greater than 1W is required. Since this work was completed, commercial diode-pumped minilaser systems have become avilable which boast output powers in the green spectral region, suitable for pumping self-modelocked Ti:$Al_2O_3$ lasers. One such laser is the Lightwave Corp. Model 240 system based on an intracavity frequency-doubled Nd:YAG laser, which is specified to produce a low noise, continuous wave output at power levels approaching 2W. A more recent and encouraging development is the Spectra Physics Millenia system which is based on a diode laser-pumped intracavity frequency-doubled Nd:$YVO_4$ laser, and has a specified continuous-wave output of up to 5W, with less than 0.1% rms noise. The development of these systems means that there is now a serious all-solid-state alternative to small frame argon-ion lasers as pump sources for self-modelocked Ti:$Al_2O_3$ lasers.

In chapter 5, the construction of an all-solid-state, self-modelocked Cr:LiSAF laser was described. Cr:LiSAF has a bandwidth and tuning range comparable to titanium-doped sapphire, however the longer upper-state lifetime and smaller emission cross-section means that it has an inherently lower oscillation threshold. Many research groups are therefore now looking at Cr:LiSAF as an alternative to Ti:$Al_2O_3$ lasers. One of the most attractive features of Cr:LiSAF is that it possesses an absorption band in the red spectral region, permitting direct diode-pumping by the new generation of laser diodes. Workers at St. Andrews have successfully developed an all-solid-state, self-

modelocked Cr:LiSAF laser pumped by a single red laser diode, and are now developing an all-solid-state, self-modelocked Cr:LiSGAF laser.

As well as an absorption band in the red, Cr:LiSAF also exhibits a weak absorption band in the green spectral region. Fortunately, an advantageous property of LiSAF is that there is no apparent reduction in crystal quality at high dopant levels. Pumping in the green spectral region is therefore made possible by the use of good quality, highly doped material. Results were presented for an all-solid-state, self-modelocked Cr:LiSAF laser pumped by the continuous-wave, intracavity-frequency doubled Nd:YLF ring laser described in chapter 4. This laser system was capable of producing 90fs pulses with an average output power of 30mW, at a pump power of 500mW.

Although Cr:LiSAF has been shown to have a lower threshold than titanium-doped sapphire, it also suffered from quenching of laser action at modest operational temperatures, and mechanical failure at pump powers above 1.5W. This means that green-pumped Cr:LiSAF lasers, as a source of ultrashort pulses in the near-infrared at modest output powers, have not been shown to be superior to Ti:$Al_2O_3$ laser systems.

In chapter 6, a self-modelocked Ti:$Al_2O_3$ laser operating at 1053nm was described. Successful operation of a tunable laser system capable of producing sub-picosecond pulses at 1μm is interesting for a number of applications. In particular, the performance of Nd:glass chirped pulse amplifications systems used to generate ultrashort, high energy pulses can be significantly improved by introducing such a source as a master oscillator. Due to the broad bandwidth of Ti:$Al_2O_3$ which extends out to 1180nm, self-modelocked Ti:$Al_2O_3$ lasers are capable of producing 100fs pulses at 1053nm, and are now being considered as master oscillators for high power TW systems.

Results were given for a self-modelocked Ti:$Al_2O_3$ laser operating at 1053nm. This laser was capable of producing 140fs pulses with an average output power of 30mW, at a pumping level of 5W. Compared to commercial laser systems such as the Spectra Physics Tsunami Ti:$Al_2O_3$ laser, which requires 10W of pump power to generate

ultrashort pulses at wavelengths as long as 1053nm, this laser has been shown to have a relatively low self-modelocked threshold. Work is ongoing in this area to reduce the threshold power of this laser in order to construct an all-solid-state, self-modelocked Ti:$Al_2O_3$ laser operating at 1053nm. Although a pump power requirement of 5W initially sounds like an unrealistic prospect for an all-solid-state laser system, the Spectra Physics Millenia system is now a possible pump source. Such recent developments now mean that the production of a 1053nm, all-solid-state, self-modelocked Ti:$Al_2O_3$ laser is now possible.

# Publications

## Karen Oppo (nee Lamb)

### Journal Publications.

"Nearly quantum-limited timing jitter in a self-modelocked Ti:sapphire laser."
D.E Spence, J.M Dudley, K. Lamb, W.E Sleat, W. Sibbett.
Optics Letters Vol.19 No.7 p481-483 (1994).

"All-solid-state, self-modelocked Ti:sapphire laser."
K. Lamb, D.E Spence, J. Hong, C. Yelland, W. Sibbett.
Optics Letters Vol.19 p184 (1994).

"All-solid-state femtosecond Cr3+:LiSAF lasers pumped at 532nm and 670nm."
M.P Critten, D. Burns, J.M Evans, K. Lamb, C. Yelland and W. Sibbett.
Journal of Modern Optics (accepted for publication) 1996.

### Conference Publications.

"All-solid-state, femtosecond Ti:sapphire laser."
K. Lamb, D.E Spence, J. Hong, C. Yelland, W. Sibbett in *Conference on Lasers and Electro-Optics* , Vol.8 of OSA Technical Digest Series (Optical Society of America, Washington D.C 1994) paper CWI3.

"A self-modelocked Ti:sapphire laser pumped by a frequency-doubled Nd:YLF minilaser."
K. Lamb, D.E Spence, J. Hong, C. Yelland, W. Sibbett in Ultrafast Phenomena IX, Springer Series in Chemical Physics Vol.60 eds. P.F Barbara, W.H Knox, G.A Mourou, A.H Zewail.paper MA4.

"An all-solid-state, femtosecond Cr:LiSAF laser pumped at 532.5nm."
K. Lamb, M.P Critten, C. Yelland, J. Hong, D. Burns, W. Sibbett in *European Conference on Lasers and Electro-Optics*, of Technical Digest Series (Optical society of America, Washington D.C 1994) paper CPD1.1.

"A low-phase noise, all-solid-state, self-modelocked Ti:sapphire laser."
K. Lamb, D. Burns, M.P Critten, C.Yelland, W.E Sleat and W. Sibbett in Technical Digest of the Twelfth UK National Quantum Electronics Conference Southampton, 1995 paper 4-4.

## Acknowledgements.

I would like to thank my supervisor, Professor Wilson Sibbett, for his support and guidance throughout this project. I am also indebted to Dr. Bill Sleat for his "magic touch" with all things electronic, particularly when it comes to operating a streak camera. I would also like to thank David Spence for dragging me kicking and screaming through my first year at St. Andrews, and the rest of the W-squad for putting up with my massive mood swings. In particular I would like to thank Matthew "KABOOM" Critten for his help with the care and management of the laser crystals, and to David Burns for his artistic input in producing the title page of this thesis. So that no-one is left out, I would like to thank David, Yueping, David, Johnny, Robert, John, Derryck, Hong, Carl, Zhang, Gareth, David, Peter, Gordon, Cate and Zoe for being a friend and a reliable drinking partner.

I would like to thank my husband, Gian-Luca, for his support, encouragement and faith, and for driving from Glasgow to St. Andrews nearly every weekend for over three years. Without you, I would probably have gone insane.

This work was funded by the Engineering and Physical Sciences Research Council.

The End